THE CENTRAL REGIONS
OF
SERSIC-PASTORIZA GALAXIES

T.P. PRABHU

Thesis submitted to the
Madurai University
for the Degree of
Doctor of Philosophy

INDIAN INSTITUTE OF ASTROPHYSICS
January 1979

Certificate from Supervisor

I certify that the thesis entitled "THE CENTRAL REGIONS OF SERSIC-PASTORIZA GALAXIES" by T.P. Prabhu is a record of research carried out by him at the Kodaikanal, Kavalur and Bangalore units of the Indian Institute of Astrophysics. I declare that the thesis has not previously formed the basis for the award of any Degree, Diploma, Associateship, Fellowship or similar title. It contains an account of observations made by the candidate, of the central regions of a family of spiral galaxies that show the hot spot phenomenon, and of his inference therefrom.

(M.K.V. Bappu)
Director
Indian Institute of Astrophysics

ACKNOWLEDGEMENTS

The work contained in this thesis was entirely carried out at the Indian Institute of Astrophysics, Kodaikanal, Kavalur and Bangalore. All the observations were obtained with the 102cm reflector at Kavalur.

The work would not have materialized if not for the valuable suggestions, able guidance and constant encouragement by Dr. M.K.V. Bappu, at every stage. The auxilliary equipments used in the observations were all designed by him.

Mr. A.T. Charles rendered all the help required in the construction and testing of the equipments.

I am grateful to Mr. K.K. Scaria for equiping the photography laboratory where all the photographic reductions were made.

Mr. A.M. Batcha typed the entire thesis. Mr. S. Muthukrishnan, Mr. Sampath Kumar and Jayakumar prepared all the diagrams. The copies were made by Mr. R. Krishnamoorthy and Mr. Monnappa.

Mr. R. Krishnamoorthy, Mr. A.K. Pati and Mr. A.M. Batcha kept up late hours to tackle the problems of final presentation. Mr. and Mrs. R. Krishnamoorthy bound the thesis. I am indebted to each of these individuals.

Finally, I express my thanks to all my colleagues at the Institute who took a keen interest in my work and rendered every help that was sought.

Bangalore-34
Dt.30-1-1979

(T.P. Prabhu)

CONTENTS

CONTENTS

CONTENTS

CONTENTS

--

SUMMARY

Apart from the sustained interest in the enhanced forms of activity in the nuclei of galaxies, other classes of phenomena occurring in the central regions of galaxies have also drawn considerable interest. One such aspect of investigations of the central regions of galaxies is the system of 'hot spots' described originally by Morgan. Though some enthusiasm was derived at least once from the speculation that these are the results of a split due to explosive activity in the nucleus, the spectroscopic evidences obtained by the Burbidges and others proved that the hot spots are simply giant HII complexes.

Sersic and Pastoriza broadened the definition of this class of phenomena observed in the central regions of galaxies to include bright amorphous formations as well. The purpose of the present investigations is to test whether the objects from the lists of Sersic and Pastoriza form a homogeneous class, and to derive parameters which assist in understanding their structure and content.

We begin with a brief over view of the principle of superposition of quasi-independent subsystems in galaxies in Chapter 1. We will also describe some of the classification schemes describing the central regions of galaxies.

Following Morgan's operational approach, we show in Chapter 2 that the central regions of galaxies listed by Sersic and Pastoriza are morphologically intermediate between the normal and Seyfert galaxies. We will also compile an additional list of similar central formations based on the descriptions published by various authors. The correlation of the occurrence of such 'perinuclear formations' with the morphology of the parent galaxies is also investigated.

The techniques of observation and of reduction are presented. They include direct and filter photography, and spectroscopy with a narrow as well as a wide slit. The techniques used in obtaining equal intensity contours are also presented.

A morphological classification of the central regions of 50 galaxies from the lists of Sersic and Pastoriza is proposed in Chapter 4. The classes range from the elliptical appearance of 'ϵ' types, through the formations with bright distinct hot spots ('σ') to the irregular pattern of hot spots of low surface brightness ('ζ'). Some correlations with the types of the parent galaxy are also investigated.

The surface photometric data is presented in Chapter 5 in terms of the equal intensity contours in the integrated light ($\lambda\lambda$4000-8700) for 27 galaxies from the finding list. The equivalent luminosity profiles have been presented for all these galaxies.

The blue-infrared colour distribution across the nucleus and the 'perinuclear formation' have been presented in Chapter 6 for one galaxy of type ϵ (NGC 210) and for five of class σ (NGC 613, 1097, 1365, 1808 and 2903). The nucleus appears reddest in all the cases. The perinuclear formations of class ϵ possess neutral colour with respect to the main body of the galaxy. The hot spots of formations of class σ are generally redder than the main body of the galaxy though a few hot spots are distinctly bluer. The perinuclear regions of NGC 1808 are the reddest among the galaxies investigated. The nucleus of NGC 2903 has been discovered on our infrared photographs.

The mean profiles for different classes of formations have also been computed in Chapter 6, and appear similar to each other in all the cases except in the class η . The formations of class η have a lower luminosity gradient than the other classes. A small difference noticed in class σ could be due to the existence of discrete hot spots.

A method has been described in Chapter 7 for obtaining the emission line rotation curves of galaxies using spectrograms with a wide slit. The dispersed image can be compared with an undispersed image in the same emission line to evaluate the distortion due to the velocity field. The latter can then be calculated. The method is demonstrated with a dispersed image of the central regions of NGC 5236 in the emission lines of H_α and [NII] λ 6584. Since an undispersed image was not available, a profile in the integrated light has been used after subtracting an estimated profile of the nucleus which is expected to be a bright continuum source especially in the red. The results are presented only as an illustration while necessary observations are planned for the future.

The conclusions presented in Chapter 8 recognize that the formations in the central regions of the galaxies examined, are a single class of phenomenon if class ι is excluded. The hot spots are possibly formed by a burst of star formation and evolve from class σ towards class ϵ. While the σ stage provides an opportunity to study the distribution and motion of gas in the central regions of galaxies, the ϵ stage enables the study of the structures of the central stellar subsystems.

CHAPTER 1

THE CENTRAL REGIONS OF GALAXIES

The discovery of galaxies is a fairly recent event in the history of science despite the fact that the 'great nebula in Andromeda', a naked-eye galaxy, was known even to the Arabs. Further, little attention has been paid to the central regions of galaxies even though the spectra of galaxies usually represent only the bright central parts. Investigations of the central regions of galaxies are vital to several problems of extragalactic research including the formation and evolution of galaxies. A study of the central regions of galaxies assists in building up the chain of events leading to the higher forms of activity as in the nuclei of Seyfert, N and the radio galaxies as well as the quasi-stellar and related objects. It is, therefore, not too optimistic a statement to make that the central regions may provide clues to the formation and sustenance of spiral arms in galaxies with discs.

We summarize in the present chapter the important concepts which have broadened our outlook and the principal lines of investigation which have contributed much to our familiarity of the central regions of galaxies.

1.1 Coexistence of Different Subsystems in a Galaxy

Beginning with Baade's (1944) recognition of Population I (disc) and Population II (halo), it has become increasingly evident that a galaxy is constituted of several quasi-independent subsystems. Other examples of such subsystems are that of the globular clusters, the lobes of radio galaxies, and nuclear jets in galaxies like M 87 and NGC 3561. These subsystems have characteristics independent of the rest of the galaxy except for the dynamical interaction. This phenomenon of superposition of sub-systems (Ambartsumian, 1961) is one of the fundamental observational facts to be explained by any theory attempting to reveal the processes involved in the formation and the evolution of galaxies.

All the subsystems of a galaxy are more or less concentric. The region of congruence of the centres of all the subsystems is also the region of maximum density and intensity. We refer to this region as the central part or the central region of a galaxy, following Ambartsumian (1971). Different subsystems can be recognized in the central regions of galaxies as will be discussed in the next section.

1.2 Subsystems in the Central Regions of Galaxies

The term 'nucleus' has been used in the past variously and at times ambiguously to denote the main body of a galaxy, the central bulge or lens, as well as the compact subsystems that are several orders of magnitude smaller in spatial extent. It would be worthwhile to consider the problems of semantics in order to avoid confusion. We follow the terminology given below while dealing with the observations in the optical region. This terminology has been adopted mainly from the ideas expressed by Ambartsumian on various occasions (Ambartsumian 1961, 1971; Morgan et al 1971).

(a) Nucleus: Structures presenting a starlike or almost starlike image superposed on the central region of maximal intensity, on photographs of moderate resolution (1-3 arcsec) obtained with ground-based telescopes.

(b) Perinuclear formation: Most of the galaxies show a more extended subsystem roughly centred on the nucleus, with typical extents of several seconds of arc to a few tens of seconds of arc. A nucleus may not be very conspicuous when superposed on a bright perinuclear formation.

This latter subsystem appears as a shoulder in the luminosity profiles, especially evident in Seyfert galaxies (Morgan et al. 1971). The perinuclear formation will be considered in greater detail throughout the rest of this work.

Since our definitions are based on resolution, they may still have some residual ambiguities dependent on distances to the objects under investigation. We are, however, restricting ourselves to the brighter of the Shapley-Ames galaxies outside the local group and mostly beyond the nearest groups. For a typical distance of a few tens of megaparsecs, a nucleus would have an upper limit on its size of a few hundred parsecs and may include substructures of much smaller scales like the ones observed as the nuclei of nearby galaxies (M32: 2pc; M31: 15pc; M33: 17pc). The nucleus would thus be a collective term for all these subsystems.

The distinction between the nucleus and the perinuclear formation would be obliterated as we approach distances of $\sim$ 100 Mpc and this may be considered a limit for ground-based telescopes in the study of the perinuclear formations.

Millimeter and radio observations, not being limited by the atmospheric effects, reach a resolution of 10^{-4} arcsec using intercontinental base-lines in the very long base-line interferometry (VLBI) technique. Compact sources of different spatial extents have been discovered in the central regions of different galaxies. Using the VLBI procedure. The 7AU+200AU source of 3.8 cm wavelength at the centre of our galaxy and the 1200 AU radio source in the nucleus of M81 are near the lower end of the linear sizes observed. Several ellipticals, radio galaxies, and quasars show a prominent 'radio nuclus' of a few tenths to a few units of parsecs, while the spirals generally possess compact sources ranging from a few tenths to a few kiloparsecs in extent (Ekers, 1978). The need to recognize different classes of events possibly operating at different spatial scales is obvious. It is also desirable to devise an unambiguous terminology of classification. But this will not be attempted here since our major concern would be the structure of the optical nucleus and the perinuclear formations.

1.3 Classification and Description of Central Regions of Galaxies

Even though no classification scheme has been devised for the central regions of galaxies based on the relative importance of the nucleus and the perinuclear formations relative to the outer regions of galaxies, yet different degrees of central condensations have been noted. The earliest attempt to describe the central regions of galaxies systematically is due to Morgan (1958, 1959). Morgan classified 915 galaxies into 7 concentration classes a, af, f, fg, g, gk and k in increasing order of central concentration of light. The terminology is derived from a correlation discovered earlier by Morgan and Mayall (1957) between the central concentration of light and the dominant spectral type contributing to the blue light from the bright inner regions of galaxies. Morgan's notes to his classification tables describe some of the peculiarities noted by him in the central regions of galaxies; he also noted systems having small brilliant central formations superposed on a considerably fainter background. He called these N systems, a terminology borrowed later for a more active state of the nucleus.

A systematic survey of the central regions of galaxies has been conducted at the Byurakan Observatory mainly with a 20-21 inch Schmidt telescope with an image scale of 114 arcsec mm^{-1}. A classification scheme has been devised to denote the degree of central condensation on an arbitrary scale of integers 1 through 5, in increasing order of central condensation. The galaxies of class 5 show a nucleus clearly discernible from the background and indistinguishable from the stellar images. Class 4 represents galaxies with semistarlike nuclei of measurable angular diameters. The presence of a nucleus is inferred from the high degree of central condensation in galaxies of class 3. Galaxies of class 2 probably contain a faint nucleus below the limit of detection while those of class 1 probably do not possess a nucleus.

Table 1.1 modified from Ambartsumian (1965) to include the class 2s added subsequently, describes the observed and the inferred aspects of each class. The latter class appears similar to class 2 at relatively lower resolution, but individual 'hot spots' (s = split nuclei) appear on the images at an increased resolution. The interpretation about the existence of a nucleus is based on various observations, especially our own to be reported in later chapters. While the Byurakan class 2s contains galaxies similar to the ones with 'hot spots' described by Morgan (1958, 1959), the galaxies of class 4 and 5 are similar to Morgan's N types. A list of 711 galaxies classified at the Byurakan Observatory has been published by its directorate (Byurakan, 1975).

Table 1.1

Byurakan Scheme of Classification of Central Regions of Galaxies

Nuclear Type	Pattern	Interpretation
1	No appreciable condensation at the centre	No nucleus present
2	Weak condensation at the centre	Probably a nucleus exists
3	Strong concent [illegible] the centre, but no star-like image	A nucleus definitely exists, but cannot be distinguished from the background
4	Starlike nuclear image at short exposures, but nebulous at long exposures	A nucleus is seen surrounded by the dense part of the bulge
5	Starlike nuclear image even when the exposure differ from the limiting	A bright nucleus which stands out on the background
2s	Weak condensation at low resolution, but split up into several bright condensations at moderate resolution	Nucleus is hidden among the bright emission line regions

Ambartsumian (1965) points out that some of the galaxies classified in the Byurakan scheme would exhibit higher degree of central condensation when the resolution is increased. A change in the classification is also prompted by employing a different region of the electromagnetic spectrum.

A qualitative description of the central regions of about 1150 galaxies has been given by de Vaucouleurs and de Vaucouleurs (1964; hereinafter RCBG). The descriptions include the relative brightness (extremely bright, very bright, bright, faint etc.), degree of compactness ('nucleus', core, barlike core, centre, etc.) and size (very small, small, large etc.) and also information on peculiarities in shape, presence of dark lanes and other complexities. A comparison of the brightness information with Byurakan class shows that the galaxies of Byurakan classes 3, 4 and 5 possess bright central compact regions (referred to as 'nuclei' in RCBG) against the classes 1 and 2. The central brightness increases along the sequence 3 to 5 and 2s.

All the schemes of classification mentioned above come quite close to the descriptions of the presence or the absence of the nucleus and the perinuclear formations and their relative brightness when they are present.

As would be apparent in subsequent chapters, they can guide us in choosing the galaxies where these substructures are the most conspicuous.

1.4 Enhanced Activity in the Nuclei of Galaxies

The discovery of the nuclear jet in M87 by H.D. Curtis in 1918 and Seyfert's (1943) discovery of high excitation emission lines of large Doppler widths in the nuclei of some galaxies drew the attention towards the existence of enhanced form of activity in the nuclei of galaxies. Similar as well as more enhanced forms of activity have been discovered in the recent years in a large number of galaxies. Notable surveys include the UV bright galaxies discovered by Markarian et al (1978 and references therein) at the Byurakan Observatory. A large fraction of Markarian galaxies exhibit characteristics similar to the ones described by Seyfert. Discovery of the radio galaxies, quasars, the OSQs (Optically Selected Quasars) and related objects, have also added enormously to the data on active nuclei.

Several lines of argument favour the interpretation that the Seyferts, radio galaxies and quasars present the same phenomena in increasing degrees. The intrinsic brightness of the nuclei increases and the energy distribution becomes more and more non-thermal in the above order. Large changes in brightness over time scales of months and also the interstellar scintillation results restrict the region of highest activity to very small absolute dimensions. The resulting high volume emissivity added to the other inferences like the rapid variability, large amount of relativistic particles under the influence of magnetic fields, and large mass motions make these objects most intriguing. Little is known about the central compact object which governs these processes. Black holes seem to be the current fancy, though models exist based on massive rotators (spinars) and more exotic objects.

There are two extreme possibilities regarding the formation of nuclei. The first one that suggests their formation by accretion during the evolution of a galaxy (Zwicky, 1967) has a large number of adherers. Ambartsumian (1958, 1960, 1961, 1971, 1976) who has drawn attention towards various probable and possible manifestations of nuclear activity is inclined to believe in the second possibility that galaxies are formed by ejection from active nuclei. Different evidences for the ejection of gas from the active nuclei, though suggestive of this, could alternately result from accretion and subsequent explosion (Shields and Wheeler, 1978).

If the active nuclei continue to lose mass at the rate suggested by the observed outflow of gas, the total mass lost by them in 10^8-10^9 years will be comparable to the mass of the nuclei themselves. The extreme cases of activity like the quasars and OSQs radiate an energy equivalent to the rest mass of the nuclei, over the same time scales. These facts guggest that the active nuclei cannot have life times longer than 10^8-10^9 years. Secondly, the fraction of galaxies with active nuclei is about a few per cent. If the nucleus of every galaxy passes through an active phase, this phase should last a few per cent of its age. The corresponding value of 10^8-10^9 years is the same as the estimated life of an active nucleus, and hence suggests that all galaxies pass through a phase of enhanced nuclear activity.

While the morphological study of galaxies has been dominated by the outer regions like the spiral arms, the active nuclei have attracted attention to the very compact systems at the centres of galaxies. The structures in the immediate surroundings of a nucleus have been studied in less detail. The investigations presented in this work deal with the formations around the nuclei of galaxies.

CHAPTER 2

GALAXIES WITH BRIGHT PERINUCLEAR FORMATIONS

It has become increasingly evident in recent years that most and perhaps all galactic nuclei exhibit some degree of activity. The differing degrees and apparent forms of activity are based most probably on very few parameters and constitute a single class of phenomena. The classification of the forms of activity is logically the first step towards understanding the nature of the activity.

The higher forms of activity occur less frequently in space. Hence the nearest galaxies with more active nuclei are, on an average, farther from us than the ones with less active nuclei. It is, therefore, necessary to know how nearby examples of lesser activity would appear at greater distances. Particularly useful will be the identification of features which convert the less active ones into the more active ones when enhanced (Burbidge, 1971). Hence a morphological study of central regions of galaxies is imperative.

2.1 An Operational Approach for the Morphological Study of the central Regions of Galaxies

Morgan et al (1971), in a morphological comparison of non-Seyfert and Seyfert galaxies, noted that the Seyferts are characterized by a 'nucleus-shoulder-arms' structure; that is, the luminosity profiles of Seyferts exhibit three distinct substructures - a semistarlike or starlike nucleus, a pronounced shoulder and an exponential disc. We identify the shoulders to be due to the perinuclear formations. Morgan et al (1971), in an operational approach to establish the relationship between normal spirals and Seyferts, defined an operator F which yields Seyferts when it acts upon normal spirals. The operation of F results in a brightening of the nucleus, enhancement of the perinuclear formation and a decrease in the brightness of spiral arms.

Since all the morphological changes between different types of galaxies are continuous, we postulate an operator $F^{\frac{1}{2}}$ which, when operated on normal galaxies, yields morphological characteristics intermediate between those of normal and of Seyfert galaxies. This means an intermediate degree of enhancement of nucleus and the perinuclear formations without a pronounced decrease in the brightness of the disc component. The most conspicuous characteristic of these galaxies would be a bright perinuclear formation with a nucleus embedded in it without the high contrast typical of the Seyfert galaxies. We will present finding lists of such galaxies in the next section.

2.2 Galaxies with Bright Perinuclear Formations

Morgan discovered multiple 'hot spots' in the central regions of several spiral galaxies and noted these in the foot notes of his Yerkes classification tables (Morgan 1958, 1959). Sersic and Pastoriza (1965) continued with this line of thought and extended the list of so called peculiar nuclei based on the photographs of southern galaxies obtained at Cordoba. They also recognized another class of formations, termed 'Amorphous Nuclei' which are 'spherical' formations in the central regions of galaxies 'surrounded by diffuse and asymmetric structure'. They included the dumb bell-like formations also as a variant of this class of objects. Sersic extended the survey further (Sersic and Pastoriza, 1967, Sersic, 1973) by visual inspection of plates in the Hubble plate collection at the Hale Observatories.

Sersic (1968) states the main criterion of his classification of 'peculiar nuclei' as a 'luminosity profile in which there is a change of slope and some structure due to the existence of high excitation gas clouds around the true nucleus of the galaxy'. Identifying the change of slope in the luminosity profile with the edge of the 'shoulder' described in the Seyfert galaxies by Morgan et al (1971), we conclude that Sersic's list comprises of galaxies with bright perinuclear formations. These are the best available candidates for $F^{\frac{1}{2}}$ spirals. Sersic's final list of 64 galaxies (Sersic, 1973) together with four additional galaxies from the list of Sersic and Pastoriza (1965) is presented in Table 2.1.

Keel and Weedman (1978) recently observed the central regions of 931 galaxies photographically on a uniform system at an image scale of 99 arcsec mm^{-1}. The list consists of (i) galaxies described in RCBG as containing a 'very bright nucleus' (VBN) or 'extremely bright nucleus' (eBN), or (ii) galaxies belonging to the Byurakan classes 4 or 5, with the common restriction that they are all north of declination -20°. The observed galaxies are classified into five classes based on the relative brightness of the spiral arms (from 1 - very bright to 5 - not seen). A rank is also assigned to the relative brightness of the central regions. Ten galaxies from their list are stated to resemble Seyfert galaxies morphologically. Peculiarities in the central regions of some galaxies are described in the foot notes to the tables while special attention is drawn to three galaxies in the text itself.

We list in Table 2.2 galaxies which are not included in Sersic's list, which most probably resemble the former in their central formations. The list is based on the descriptions of Morgan (1958, 1959) Keel and Weedman (1978) and isolated cases drawn from other sources.

While Tables 2.1 and 2.2 together are far from complete and hence not amenable for absolute statistics, they still form a fairly large sample for relative statistical considerations which we investigate in the next two sections.

2.3 Relation of Central Formations with the Outer Morphology

Sersic (1968) studied statistically twenty galaxies from his list which form a statistically complete sample to a limiting magnitude of 11.0. He concluded that the 'peculiar nuclei' (as he termed them) prefer barred (SB) and intermediate (SAB) families (11 and 9 galaxies respectively) against non-barred, SA (None). He also noted a lack of preference for any Hubble type.

Heckman (1978) analysed a sample based on the foot notes of Morgan (1958, 1959) and came to conclusions which differ from those of Sersic. Heckman's sample indicated that the parent galaxies of 'peculiar nuclei' do not favour barred or nonbarred families while they are peaked around early Hubble types (SO, SO/a). He attributed the difference with Sersic's results to 'subconscious biases' in the sample of the latter 'toward associating nuclear peculiarity with certain non-nuclear morphological types'.

Sersic has inspected more nonbarred galaxies than barred ones to a limiting magnitude of 11.0 (Sersic, 1968). Hence a subconscious bias of the type suggested by Heckman may not creep easily into Sersic's list. It is conceivable though, that the general term 'peculiarity' might have been used by different authors to denote different phenomena. Heckman's list includes a larger range of 'peculiarities' than the ones included by Sersic, and hence the conclusions of the former pertain to the complete range of events. Heckman's list includes the following central peculiarities in addition to bright perinuclear formations classified by Sersic:

(i) dust arcs and dust lanes (NGC 2855, 3593, 3626, 3628, 3957)

Table 2.1

Sersic's list of Galaxies with Bright Perinuclear Formations

S.No.	NGC	Yerkes	RMT	DDO	BYU	RCBG	SERSIC
(1)	(2)	(3)	(4)	(5)	(6)	(7)	(8)
1	210	gk	SAB(s)b	I	3	eBN	AN
2	255	g	SAB(rs)bc	II	2	svB elong N	HS
3	613	f	SB (rs)bc		2s	seBN	HS
4	922		SB (s)cdp	II-III		BN	HS
5	925	af	SAB(s)d	II-III	2	noBN?	HS
6	1087	a	SAB(rs)C	III	4	double N?	dB
7	1097	a	SB (s)b		2s	eBsN	HS
8	1140	k	Im			vBN	dB
9	1255		SAB(rs)bc	II		vsvBN	HS?
10	1300	g	SB (rs)bc	I	4	vseBN	AN
11	1326	k	(R)SB (r)0^{+}				-
12	1365	fg	SB (s)b		2s	eB complex N	HS
13	1415	gk	(R)SAB(s)0/a	III		vBN	HS
14	1433		SB (r)a			seBN	AN
15	1530		SB (rs)b			vsvBN	HS
16	1672		SH (s)b		2	vBN	AN
17	1808	f	(R)SAB(s)0/a		2	vB complex N	HS
18	2196	k	(R')SA (s)a	I-II		B diff N	AN?
19	2763	af	SB (r)cdp	IV		vBsh B 'bar	AN
20	2903	f	SAB(rs)bc	I-II	2s	vBN	HS

Table 2.1 - continued

(1)	(2)	(3)	(4)	(5)	(6)	(7)	(8)
21	2935	g	(R')SAB(s)b	I		eBN	AN?
22	2997	f	SAB(rs)c			vsvB complex N	HS
23	3177	g	SA (rs)b	II-III	4	vsvBN	HS
24	3206		SB (s)cd			sh B bar	-
25	3310	g	SAB(r)bcp	II	5	vBvsN	HS
26	3346	af	SB (rs)cd	II		vB sh central segment	HS
27	3351	g	SB (r)b	II	2s	eBN	HS
28	3359	a	SB (rs)c	II	1	vsN	HS
29	3504	g	(R)SAB(s)ab		4	eBN	-
30	3611	g	SA (s)ap		4	svBN	AN
31	3627	g	SAB(s)b	II	3	svBN	HS?
32	3682		SA (s?)O/a				-
33	3955		IO or pec	III	2	B complex bar	HS
34	3956	f	SA (s:)c	IV		svB bar or N	HS?
35	4051	f	SAB(rs)bc	II	5	vseBN	HS
36	4064	af	SB (s)a:p	III	3	innermost vB segment	HS
37	4124	g	SA (r)O+			vsvBN	AN?
38	4151	g	SAB(rs)ab		5	seBN	AN
39	4178	af	SB (rs)dm	II	2	sB narrow bar	HS
40	4212	f	SA (rs?)bc	III	4	BN	AN
41	4245	k	SB (r)	III	3	vsvBN	HS
42	4250		SAB(r)O+			vsvBN	AN
43	4258	g	SAB(s)bc		3		HS
44	4303	f	SAB(rs)bc	I	4	eBN	AN
45	4314	g	SB (rs)a		4	eBN	HS

Table 2.1 - continued

(1)	(2)	(3)	(4)	(5)	(6)	(7)	(8)
46	4321	fg	SAB(s)bc	I	2s	vBN	HS
47	4369	g	(R)SA (rs)a			vB complex centre	HS
48	4394	g	(R)SB (r)b	II	3	eBN	-
49	4419	gk	SB (s)a		2	B bar	AN?
50	4446						AN?
51	4457	k	(R)SAB(s)0/a		3	vBN	-
52	4501	g	SA (rs)b	I	4	vsBN	AN
53	4593	g	(R)SB (rs)b	II		vBN	-
54	5236	fg	SAB(s)c			eBN	AN
55	5248	f	SAB(rs)bc	I	2	eBN	HS
56	5383	fg	SB (rs)p	II		eB complex N	HS
57	5430	f	SB (s)b		4	svBN	-
58	5597	af	SAB(s)cd			vseBN	HS
59	5728	fg	SAB(r)a:	II		vBN	AN
60	5850	g	SB (r)b	I	2	vBN	AN
61	6217	af	(R)SB (rs)bc	I-II	5	svBN	-
62	6907	f	SB (s)bc	I-II		vsBN	AN
63	6951	f	SAB(rs)bc	I-II	3	eBN	HS
64	7410		SB (s)0+		3	eBN	HS
65	7424		SAB(rs)cd			sB elong diff N	AN
66	7552		(R')SB (s)ab		5	eBN	AN
67	7741		SB (s)cd	II	2	no BN	-
68	7769	f	(R')SA (rs)b		5	eBN	-

Table 2.1 - continued

Columns: (1) Serial Number, (2) NGC designation, (3) Yerkes type from Morgan (1958, 1959), (4) Revised Morphological Type from de Vaucouleurs (1963), (5) DDO type from van den Bergh (1960), (6) Byurakan type from Byurakan (1975), (7) Description of central region from RCBG, (8) Sersic type from Sersic (1973).

Table 2.2

Additional list of Galaxies with Bright Perinuclear Formations

S.No.	NGC	Yerkes	RMT	DDO	BYU	RCBG	Description (Ref.)
(1)	(2)	(3)	(4)	(5)	(6)	(7)	(8)
1	16	k	SAB0$^-$			vsN	Elongated nucleus (1)
2	128	k	S0p		3	vBpN	Notched nucleus (1)
3	1068	g	(R)SA(rs)b		5	vBN	Second brightest in (2)
4	2633	fg	SB(s)b		5	vsvBN	Hot Spots (1)
5	2782	g	SAB(rs)ap		4	eBN	Hot Spots (3)
6	3032	g	SAB(r)0°			svBN	Seyfert-like (2)
7	3115	k	S0-		3	vBN	20th brightest in (2)
8	3190	k	SA(s)ap	II-III	4	-	Seyfert-like (2)
9	3395	a	SAB(rs)cd:p		2	vsvBN	Large irregular nucleus(2)
10	3412	gk	SB(s)0°		3	vBN	14th brightest in (2)
11	3489	k	SAB(rs)0$^+$		3	vsvBN	11th brightest in (2)
12	3631	fg	SA(s)c	I	2	eBN	Hot Spots (1)
13	3681	g	SAB(r)bc		3	B diff N	Elongated nucleus (1)
14	3732	k	SAB(s)0/a:			vBvsN	Very bright nucleus (1)
15	3773	k	SA0:		4	vBN	Elliptical nucleus (2)
16	3998	k	SA(r?)0°		4	vBN	15th brightest in (2)
17	4026	k	S0		3	vsvBN	Inclined core (2)
18	4041	g	SA(rs:)bc	II		vB centre	Hot Spots (1)
19	4111	k	SA(r)0$^+$:		3	vsvBN	10th brightest in (2)
20	4194		SB0p			eBN	Irregular nucleus (2)

Table 2.2 - continued

(1)	(2)	(3)	(4)	(5)	(6)	(7)	(8)
21	4216	g	SAB(s:)b	II	4	seBN	Bright arms very close to nucleus (2)
22	4274	gk	(R)SB(r)ab	II-III	3	vBN	Double nucleus (2)
23	4385	g	SB(rs)0+:	II-III	4	vsvBN	Seyfert-like (2)
24	4460	gk	SB(s)0+?			B elong centre	Hot Spots (1)
25	4500		SB(s)a			eBN	Complex nucleus (2)
26	4559	fg	SAB(rs)cd	II-III	5	vs not vBN	Barlike nucleus (2)
27	4569	a	SAB(rs)ab		5	vseBN	Seyfert-like and 6th brightest in (2)
28	4570	k	SO		3	svBN	9th brightest (2)
29	4691	f	(R)SB(s)0/a		2s	vB complex bar	Hot spots (1)
30	4736	g	(R)SA(r)ab	II	3	eBN	Bright inner spiral structure; 4th brightest in (2)
31	4747	f	SB?(s)c:		2		Hot spots (1)
32	4800	k	SA(rs)b		4	vBN	Distinct core; Seyfert-like (2)
33	4861	a	SB(s)m:	IV-V		B core	Hot spots (1)
34	5005	gk	SAB(rs)bc	II	4	eBN	17th brightest in (2)
35	5055	g	SA(rs)bc	II	5	vsvB stellar N	Seyfert-like (2)

Table 2.2 - continued

(1)	(2)	(3)	(4)	(5)	(6)	(7)	(8)
36	5195	f	IOp		4		19th brightest in (2)
37	5253	fg	IBmp			vB core	Hot spots (1)
38	5408						Hot spots ? (4)
39	5493	k	SOp		5	vB diff N	16th brightest in (2)
40	5548	g	(R')SA(s)0/a		5	eBN	7th brightest in (2)
41	5633	g	(R)SA(rs)b		2	sBN	Hot spots (1)
42	5653	g	(R')SA(rs)b		2	vBN	Spotty, bright nucleus(1)
43	5678	f	SAB(rs)b	II	2	vsBN	Hot spots (1)
44	5713	a	SAB(rs)bcp		4	eBN	Brilliant, mottled inner portion (1)
45	5921	f	SB(r)bc	I-II	4	eBN	Seyfert-like (2)
46	6052	a	IBmp			vBN	Irregular nucleus (2)
47	6143	g	SAB(r)bc:			vsBN	Double nucleus (2)
48	7177	g	SAB(r)b	II	3	eBN	Core and part of arm bright (2)
49	7332	k	SOp		4	vBp central bulge	13th brightest in (2)
50	7469	g	(R')SAB(rs)a		5	eBN	3rd brightest in (2)
51	7714		SB(s)b:p			eBN	Seyfert-like and 8th brightest in (2)
52	7727		SAB(s)ap		4	vsB diff N	Complex or multiple nucleus (2)

Table 2.2 - continued

Columns:

(1) Serial number

(2) NGC designation

(3) Yerkes classification from Morgan (1958, 1959)

(4) Revised Morphological Type from de Vaucouleurs (1963)

(5) DDO Luminosity type from van den Bergh (1960)

(6) Byurakan Classification from Byurakan (1975)

(7) RCBG descriptions

(8) Descriptions of central regions from other references indicated in the brackets

References:

(1) Morgan (1958, 1959)

(2) Keel and Weedman (1978)

(3) Sakka et al (1973)

(4) Bohuski et al (1972)

(ii) rings and ring-like structures (NGC 473, 3081, 4128, 4233, 4324, 4435, 5750)

(iii) eccentric nuclei in a pair of interacting galaxies (NGC 4782-4783).

If these galaxies are excluded, the list resembles Sersic's list in the criteria of classification.

We have reanalysed Heckman's data excluding the above galaxies. We have also reanalysed Sersic's data (Figures 1 and 2 of Sersic, 1968) by converting them into the fractions of total number of galaxies investigated in each bin. The results are compared in Figures 2.1a and b after normalization. The conclusions that follow are:

(a) bright central formations favour the families AB and B as noted by Sersic (1968), but probably to a slightly lesser degree.

(b) bright central formations favour revised Hubble types Sa and Sb which are slightly later along the Hubble sequence than the ones indicated by Heckman (1978).

Despite the small numbers, the agreement between the two samples is clear.

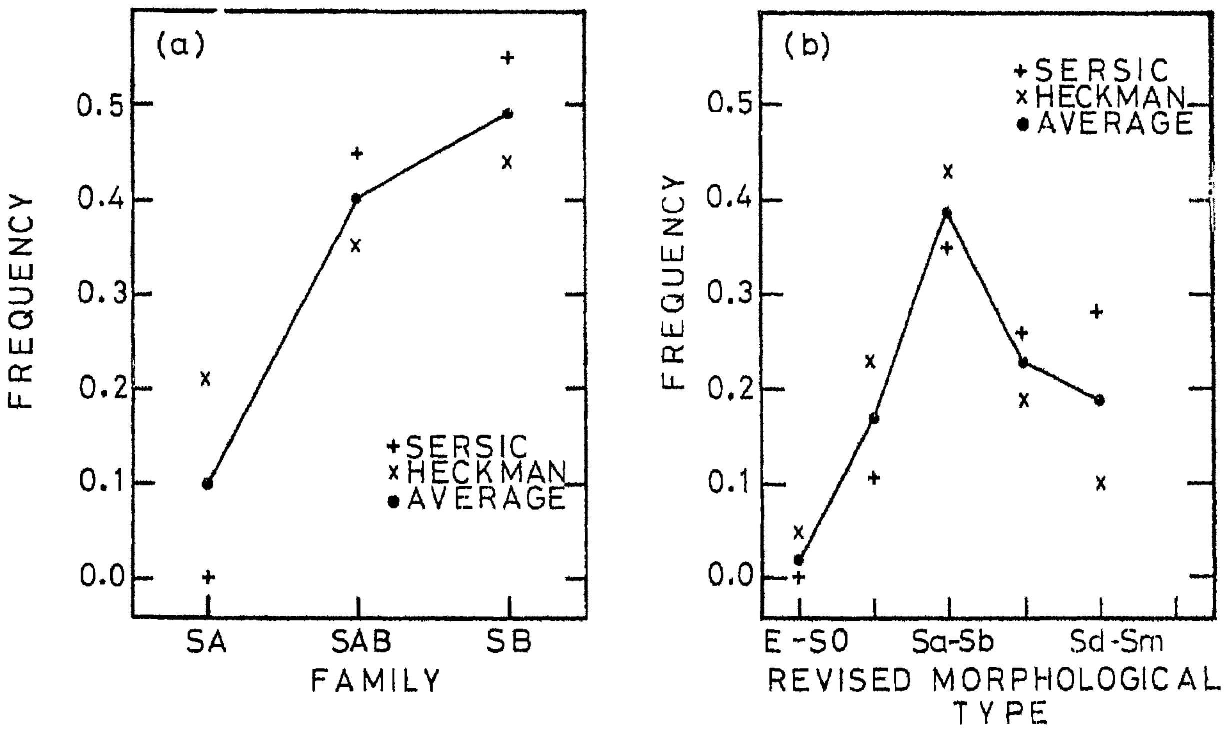

Fig.2.1 Frequency distributions of bright perinuclear formations with (a) Family and (b) Revised Morphological Type. +: Sersic's sample complete to $11^m.0$; and x: Heckman's sample excluding formations dissimilar with Sersic's formations.

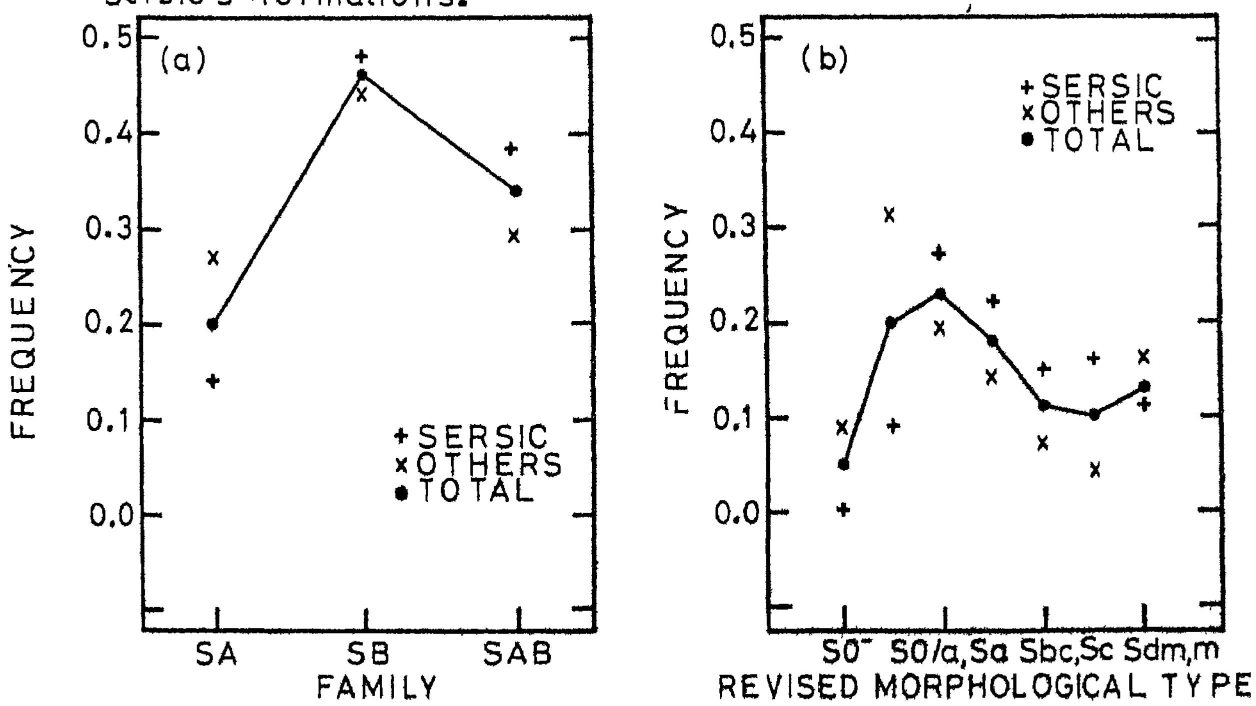

Fig.2.2 Same as above; +: galaxies from Sersic's finding list (Table 2.1); x: galaxies from our supplementary list (Table 2.2).

We continue the analysis on similar lines, with the total sample of Sersic (Table 2.1) and the additional list in Table 2.2. Figures 2.2a and 2.2b show the frequency distribution in different families and different Hubble types (T) respectively. The relevant data has been compiled from de Vaucouleurs (1963). An extension of the analysis into DDO luminosity types L (Van den Bergh, 1960) and de Vaucouleurs luminosity index ($\Lambda = (L+T)/10$) is shown pictorially in Figures 2.3a and 2.3b respectively.

The comparison of Figures 2.1a and b with the Figures 2.2a and b indicates a slight relative increase in the families A, and in types SO and SO/a, in the latter sample. This may be an indication of the presence of subclasses in the perinuclear formations with a mixing, in differing proportions, of the different samples considered. This is a selection effect introduced in an incomplete sample. A subclass is possible at the lower luminosity end too as evidenced from Figures 2.3a and b ($L \sim 6$ and $\Lambda \sim 0.8$). The classification of perinuclear formations are considered in detail in Chapter IV.

2.4 Perinuclear Formations and the Classification of Central Regions

The Yerkes system of classification of central

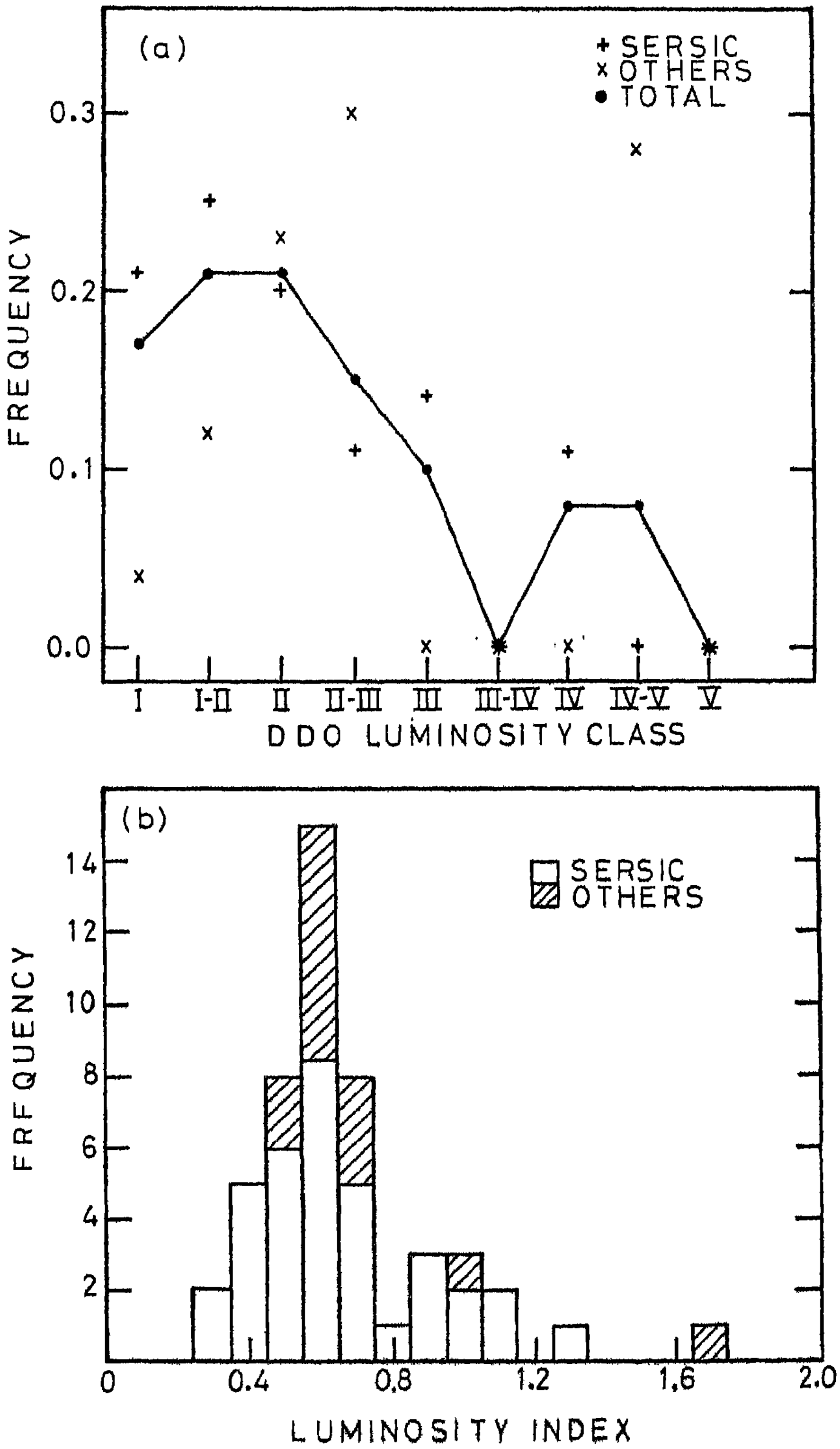

Fig.2.3 Frequency distribution of bright perinuclear formations with (a) DDO luminosity class and (b) deVaucouleurs' luminosity index.

condensation, Byurakan scheme of 'nuclear' classification and RCBG descriptions provide useful qualitative indices which are probably mutually related. One may form a uniform classification scheme based on RCBG descriptions with indices eBN ("extremely bright nucleus"), vBN ("very bright nucleus"), BN ('bright nucleus'), N ('nucleus')

and NO ('faint nucleus' and 'nucleus' without brightness information) and O ('no bright nucleus'). The last class 'O' may include a large number of galaxies where the absence of 'nucleus' is not explicitly mentioned, but the discriptions only deal with short or small central bar or a bright inner segment.

Figures 2.4a, b and c show the distribution of bright central formations with the Byurakan classes and RCBG descriptions as well as against Yerkes types. The class O in the second case includes only those galaxies for which the absence of RCBG 'nucleus' is explicitly mentioned. The figures indicate that the galaxies with bright central formations are peaked around Yerkes type g, and more strongly so at the Byurakan classes 5 and 2s, and RCBG classes vBN and eBN.

A subclass possibly exists at Yerkes class af, Byurakan 1 and 2 and RCBG N and O. A glance through

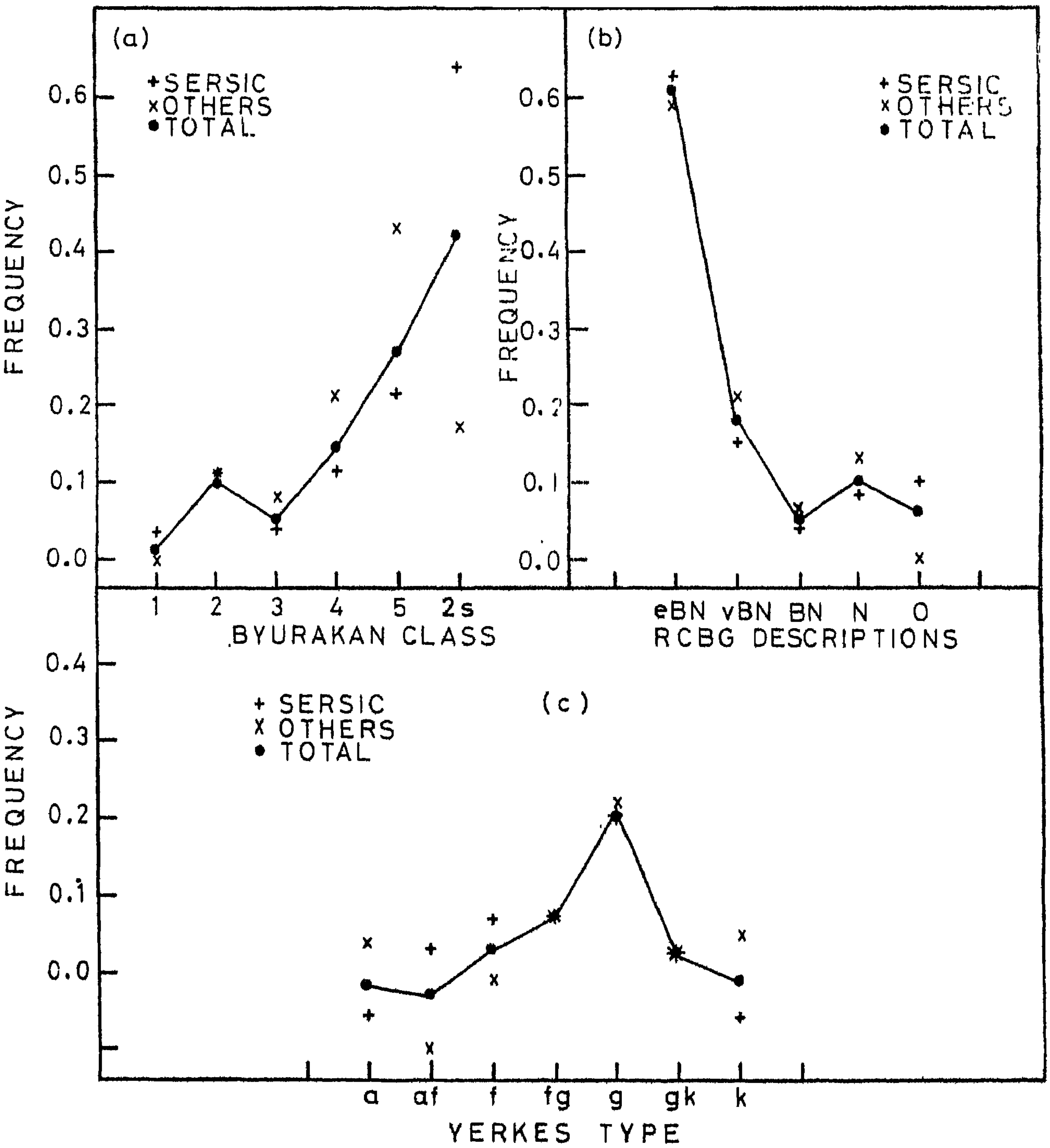

Fig.2.4 Frequency distributions of bright perinuclear formations with (a) Byurakan class, (b) RCBG descriptions, and (c) Yerkes types.

Tables 2.1 and 2.2 shows that the galaxies forming these secondary peaks in different figures are identical and are also of later luminosity class and higher luminosity index. This subgroup will be identified and described in detail in Chapter IV.

2.5 Observational Desideratum on the Perinuclear Formations

Having recognized the substructures in the central regions of galaxies it is imperative to study their dimensions, content, form and dynamics. A few important requirements from optical observations have been noted below.

a) Morphology of perinuclear formations and its relationship with the outer structure is the easiest datum obtainable through photography. It can provide clues to the formation of this subsystem.

b) A knowledge of the luminosity distribution in the perinuclear formations and the spatial scales assists in studying the structure and stability of such systems.

c) Spectroscopic data on stellar and nonstellar content of the nucleus and the perinuclear formations reveal the physical processes at play as well as provide an idea of present and past star formation rates in these regions.

d) The spectroscopic observations also yield information on the noncircular and circular motions. While the latter help in estimating the mass of the central formations, the existence of the former may indicate distortions in the density distribution, or mass outflow.

The structures of relevance are of the order of several seconds of arc for the brighter Shapley-Ames galaxies. Conventional photoelectric photometry cannot easily achieve a resolution of a second of arc with an equivalent accuracy of centering. One needs a two dimensional storage medium like a photographic plate or the modern solid state detector arrays while deriving surface photometric parameters. Photoelectric calibration of such data is desirable to establish the zero point of the observations.

The best possible image scale is essential for obtaining both the surface photometric and the spectroscopic data on the perinuclear formations, and one needs to work at the limit of atmospheric seeing. Observations from a space telescope would certainly improve our knowledge on these formations.

A sizeable number of central formations need to be observed to establish the class of events, to recognize subclasses, to establish the common features and to study the dispersions about the average properties. An effort encompassing all these features would necessarily be a very ambitious one. Hence, we limit our programme to the following:

i) High resolution relative photographic surface photometry in integrated light for a sizeable number of central regions of galaxies for studying the classes, structure and dimensions of formations.

ii) High resolution relative photographic surface photometry in wide bands in the blue and in the infrared for a few galaxies for deriving the colours of different subsystems.

iii) Emission line spectroscopy of some galaxies to detect the presence of and the extent of emission lines as an indicator for the existence of gas ionized by young stars.

iv) Wide slit spectroscopy of a few galaxies to obtain monochromatic pictures in the emission lines and to study their spatial distribution.

These observations would hopefully form a basis and provide a motivation for more detailed and far more accurate observations of a few representative galaxies in different classes of central formations.

CHAPTER 3

THE OBSERVATIONS

The higher surface brightness of the central regions of galaxies renders them relatively easy objects to observe. However, the spatial resolution required in studying the structures in the central parts is not achieved due to the limit set by the atmospheric 'seeing' effect. Fortunately the perinuclear formations (size 1-4 kpc) can be studied with a fair degree of accuracy for the nearer ones among the Shapley-Ames galaxies.

We have used the Kavalur 1-m Ritchey-Chretian system for this investigation. All the observations were recorded photographically to utilize the multiplex effect of the photographic emulsion, as well as to reach the atmospheric limit on the resolution.

3.1 Photographic Surface Photometry

The photographic observations were obtained at the F/13 cassegrain focus of the 1-m reflector. employing a Varo 8605 image tube. This is a single stage electrostatic focusing image tube with a fibre optic input and output of 40mm diameter. The tube is operated in a cathode grounded configuration which reduces the tube background considerably. A fibre optic extension of 1cm is provided at the output for effective shielding.

The S-20 photocathode of the image tube has good response in the photographic infrared upto 8700Å. The fibre optic input window cuts off the ultraviolet light of wavelengths lower than 4000Å. The P-20 phospher screen emits predominantly in the green. Kodak IIaD plates were used to register the image both for this reason as well as to match the resolution of the image tube (64 lp mm^{-1}). The plates were exposed in contact with the output face of the fibre optic extension.

The image scale of 15 arcsec mm^{-1} at the F/13 cassegrain focus of the Kavalur reflector implies that with a detector resolution of 64 lp mm^{-1}, a little over 4 resolution elements cover a second of arc or 18 elements for a square second of arc. This number ensures a good signal above the grain noise.

The radial decrease and the azimuthal variations in the efficiency of the electrostatic image tubes, as also the 'chickenmesh effect' of the fibre optics were not serious since the images of interest were small (1-2 mm). A few galaxies were observed in two spectral bands.

A BG 12 filter of 1 mm thickness was used to isolate the blue region between 4000Å and 4500Å. A Wratten 89B filter was used for the region 7000 - 8700Å. The nuclei appeared more prominent in the infrared and the hot spots and other types of formations more distinct in the blue. A large number of galaxies was observed in "integrated" light ($\lambda\lambda$ 4000-8700) to obtain a 'composite picture' where all the different components are clearly visible. The photographic data is listed in Table 3.1.

3.2 Photographic Isodensitometry

An image stored on a photographic emulsion needs to be converted to a linear scale of intensity. The process of isodensitometry provides the contours of constant density. A photographic method is simpler and less expensive in comparison with those obtained by current isodensity tracing microphotometers. It is adequate too in most of the cases including the present one where the variation of sky and other background is not significant over the image.

Early photographic isodensitometry was based either on the isohelic method employing a positive-negative combination, or on the Sabattier effect. Recently a

Table 3.1

Galaxies photographed in the Integrated Light

NGC	NGC	NGC	NGC
16	1433	3346	4258
210*	1530	3351	4369
255	1672	3504	5236
613*	1808*	3611	5248
922	2196	3627	5597
925	2763	3955	5728
1087*	2782	3956	5850
1097*	2903*	4064	6907
1140	2935	4124	6951
1300	2997	4151	7177*
1326	3177	4212	7410
1365*	3206	4245	7552
1415	3310	4250	7741

* also observed in blue and infrared bands

professional contour film is made available by the Agfa-Gevaert Company. This Agfacontour film can provide an equidensity contour by a single exposure.

The single layer emulsion consists of 95% AgCl and 5% AgBr with a few Ag_2S seeds. The development is done in a special bromide-free developer. The silver chloride is reduced to silver by chemical development in the highly exposed regions, and by physical development in the region of lower exposure. The more sensitive silver bromide is reduced to silver in the regions of intermediate exposure. The resultant bromide ions prevent further development of silver chloride in this region and thus a less darkened contour is obtained.

A schematic characteristic curve of Agfa-contour is presented in Figure 3.1. The silver chloride is largely sensitive to blue while the silver bromide not much sensitive to colour, the use of a yellow filter moves the negative part (part due to the physical development) towards higher exposure. Thus narrow ranges of density can be contoured by introducing yellow filters of high density.

A contour of first order can be used
second order contours where the original contours are

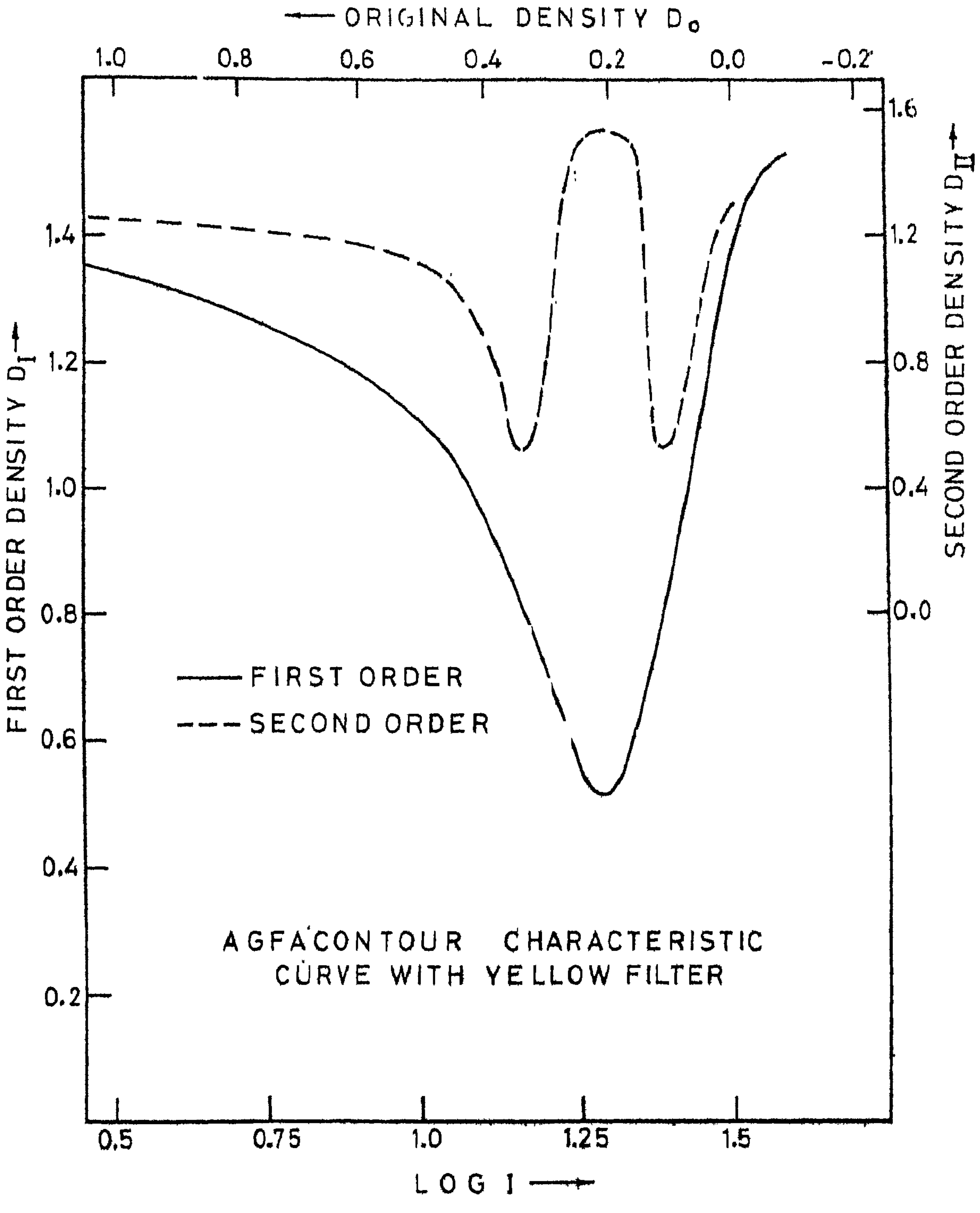

ORIGINAL DENSITY D_o
1.0
0.8
0.6
0.4
0.2
0.0
-0.2
FIRST ORDER DENSITY D_I
SECOND ORDER DENSITY D_{II}
1.4
1.2
1.0
0.8
0.6
0.4
0.2
1.6
0.0
FIRST ORDER
SECOND ORDER
AGFACONTOUR CHARACTERISTIC
CURVE WITH YELLOW FILTER
0.5
0.75
1.25
1.5
LOG I

Fig.3.1

split into two. The process can be repeated further, but may result in a degradation of photometric quality at every such step.

We have employed 3 mm of OG1 in conjunction with a commercial yellow filter. A density width of 0.15 in the first order and 0.02 in the second were achieved. The third order contours were used only in the regions of lowest intensity variation outside the perinuclear formations. We have restricted ourselves to a density range between 0.5D to 1.5D and used original photographs of different exposures to span a larger range in intensity.

We have exposed the photographs onto Agfacontour film through an enlarger. A working magnification of 4X was employed for facilitating the superposition of contours. This magnification also allows the original resolution of the photograph to be retained since the resolution of the Agfacontour film is lower (40 lp mm^{-1}). The superposition of different pairs of contours was achieved by centering the corresponding contours of field stars. The centroid of the contours of stars can be superposed more accurately in this way than in the conventional method of superposing the uncontoured images of the stars directly.

As an illustration of the method, we present in Figure 3.2 the isodensity contours of NGC 1097. The

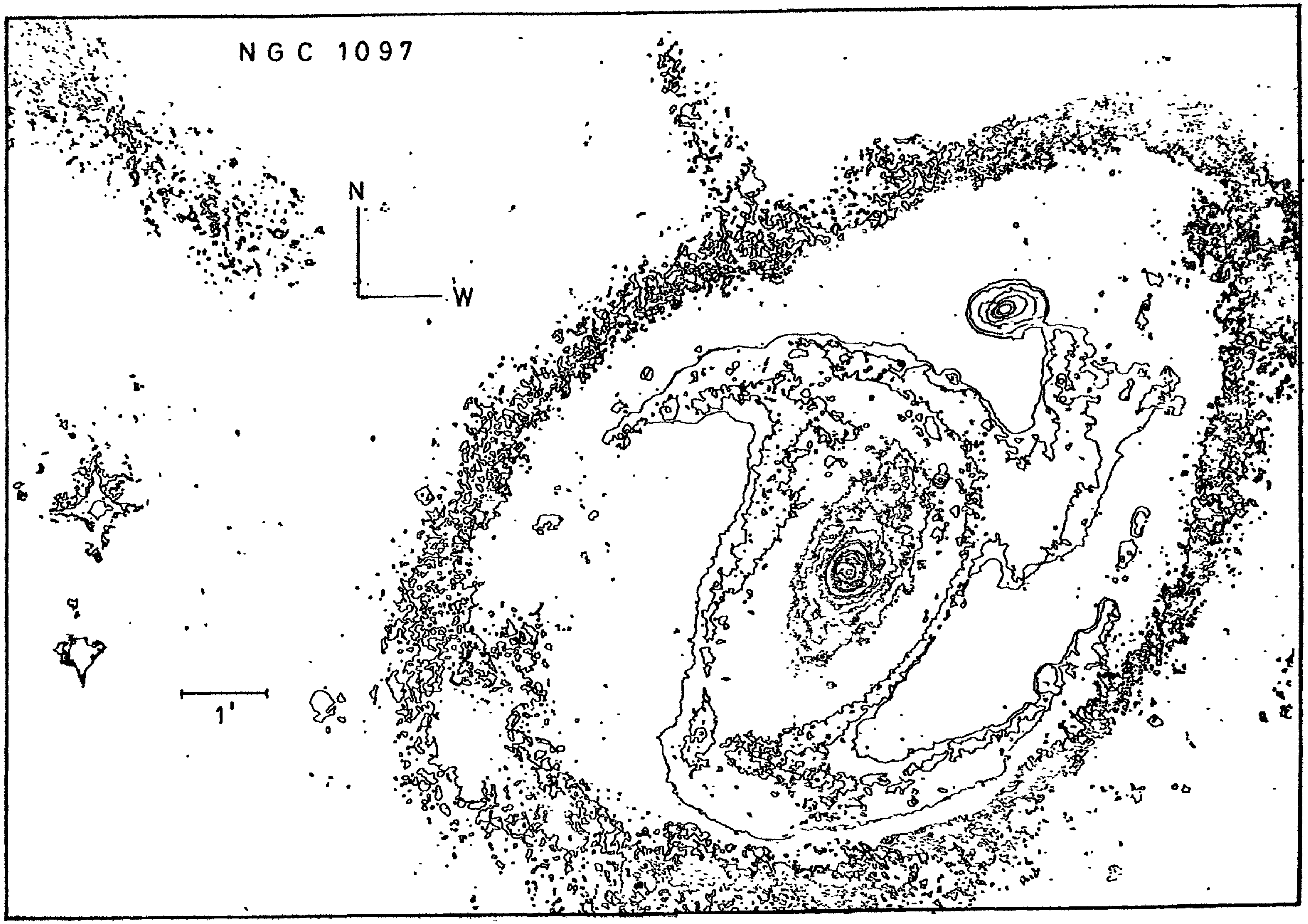
NGC 1097
N
W
1'

inner regions are based on our photographs while the outer regions are based on three published prints (Sandage, 1961 p.46; Wolstencroft and Zealey, 1975 plates I and II). The sky noise has been suppressed physically with Kodak Opaque. Two of the four jets discovered by Wolstencroft and Zealey (1975) and Lorre (1978) (see also Arp, 1976) are clearly visible.

3.3 Calibration of Isodensity Contours

The isodensity contours can be calibrated by obtaining a microphotometric scan of the original image such that the scan cuts across all the densities presented in the composite contours picture. The densities at the position of each contour can be measured and reduced to relative intensity by the usual methods employed in photographic photometry.

We have used a Carl Zeiss microphotometer with a chart recorder, equipped with a rotatable platform for the plate. It is necessary to position the central region of maximal density accurately on the path of the scan. We used two field stars to set the path of the scan accurately as follows. Denoting the centroids of the two stars by A and B, and the density peak at the centre of the galaxy by C, the distances AB, BC and AC were accurately measured on the contour picture using an Abbe comparator. The included angle at A was then calculated. While setting the plate at the beginning of a scan, the star A was initially centred to an accuracy of a few μm, the line AB was aligned with the direction of scan and the platform was turned through the angle A about the star A to bring the line AC in the direction of scan. With an optimum distance of a few millimetres between A and C and with the least count $0^\circ.1$ of the platform, it was possible to reach an accuracy of 10μm in the alignment of the scan path. A scanning aperture of 33μm x 33μm was used which corresponds to a square of sides 0.5 arcsec at the image scale of 15 arcsec mm^{-1}.

The characteristic curves for the photographic plates were obtained using the exposures obtained at an auxiliary spectrograph employing a calibrated rotating sector in front of a wide slit. The image tube response was assumed linear.

The photometric accuracy was estimated by comparing the reduced scans of different exposures of the same galaxy. The probable error is $0^m.05$ which is partly due to the inaccuracies in the orientation of the scan path. A comparison of two scans of the same plate, with the orientation arranged independently each time, gave a typical error of 0.025 for the latter.

3.4 The Presentation of Surface Photometric Data

The results of the surface photometry in the integrated light have been presented graphically in Chapter V in the following ways:

a) Isophotal contours or the isodensity contours calibrated in terms of relative intensities.

b) Equivalent luminosity profiles or the luminosity profiles as a function of an equivalent radius defined as $(A/\pi)^{\frac{1}{2}}$ where A is the area of an isophote of given intensity level.

Some galaxies were observed in the wide blue and infrared bands (cf. section 3.1). The luminosity profiles for these galaxies have been presented in Chapter VI both in blue and in infrared. The profiles have been obtained from the microphotometric scans along a line close to the major axis of the outer isophotes whenever possible. An accurate positioning on the major axis was not possible since the presence of a field star is necessary on the path of the scan for an accurate centering of the central peak in intensity. An estimated accuracy of 10 μm or better is achieved in centering the nucleus on the scan path (cf. section 3.3).

3.5 Spectroscopic Observations

Slit spectra of the central regions of 22 galaxies were observed in the region $\lambda\lambda$4500-7000. The slit was oriented east-west in general. The details of observation are presented in Table 3.2.

The spectrograph designed by Dr. M.K.V. Bappu is equipped with a mirror slit which facilitates accurate centering of faint objects. A mirror collimator of 70 cm focal length and a camera of 17.5 cm focal length give a reduction of 4 between the slit and the plate, in normal situations. The Varo 8605 image tube described in section 1 is placed at the focus of the camera and the spectrograms are obtained with the II-aD plates in contact at the output of the image tube.

A grating with 80 grooves mm^{-1} blazed at 8700Å was used to obtain some spectrograms in the first order red at a dispersion of 607Å mm^{-1}. Another grating with 300 grooves mm^{-1} blazed at 6400Å gave a dispersion of 166Å mm^{-1} in the same region. The latter grating was used for sometime at negative angles (blaze direction towards the camera) which gave a dispersion of 146Å mm^{-1}. As Hollars and Reitsema (1975) have shown, the mounting at positive angles results in less light loss at the

Table 3.2

Details of Slit Spectrograms

NGC	Dispersion (Å mm^{-1})	Emission Lines detected
210	166	None
922	607, 146	H_α , [NII]
1140	166	H_α , H_β , [OIII], faint [NII], [SII]
1326	607, 166	H_α , [NII] faint [SII]
1808	607	H_α + [NII], [SII]
2196	607, 166	None
2763	607, 166	None
2903	146	H_α , [NII], faint [SII]
2935	607, 166	None
2997	607, 166	H_α , [NII], faint [SII]
3177	607	H_α + [NII], faint [SII]
3310	607	H_α + [NII], [SII] , faint H_β , [OIII]
3346	607	faint H_α + NII Suspected
3611	607	H_α + [NII], faint [SII]
3627	607	None
3955	607	faint H_α + [NII]
3956	607	faint H_α + [NII]
4064	607	H_α + [NII]
5430	607	faint H_α + [NII] , [SII]
5597	607	H_α + [NII], [SII]
5728	607, 166	H_α , [NII], [OIII], faint H_β , [SII]
5850	607	None

gratings while giving slightly lower dispersion. This method was adopted during rest of the observing programme.

The radial velocities were measured for the observed galaxies whenever emission lines were detected. Our values (Prabhu, 1978) agree well with the values published earlier, whenever available. They also agree well with the values of Sandage (1978) who has used spectra with similar dispersion (see Table 3.3). The discordant value for NGC 5430 is most likely due to the faintness of the emission lines measured (H_α by us, and H_β by Sandage). Further spectra were not obtained after Sandage's (1978) results were published since they included most of the galaxies from our list for which no spectroscopic information was published previously.

The spectrograms were scanned to obtain the profiles of emission lines when present. The emission lines detected in the spectra of the observed galaxies have been listed in Table 3.2.

3.6 Spectroscopy with a wide slit

A spectrograph can be used to obtain monochromatic images of high purity. The principle was first utilized

Table 3.3

Comparison of Radial Velocities of some of the Programme Galaxies

NGC	V_o (TP) km s^{-1}	Error (TP) km s^{-1}	V_o km s^{-1}	Error km s^{-1}	Reference.
922	3056	34	3010	15	(1)
2903	512	24	449		(2)
2997	886	27	800	44	(1)
5236	274	20	395		(3)
5430	4560	170	3277	83	(1)
5597	2938	130	2573	39	(1)
5728	2897	20	2879	16	(1)

TP: Prabhu (1978) ; (1) Sandage (1978)
(2) Simkin (1975)
(3) Pastoriza (1975)

in solar prominence spectroscopy when a wide slit permits viewing the spatial aspects of a prominence. The spectroscope used for such a purpose needs ofcourse high dispersive power. When it is required to obtain monochromatic images of objects of small angular dimensions in the light of bright emission lines, it is sufficient to widen the slit of a spectrograph to let the integrated image pass through. The widening is consistent with the dispersion used. This technique is especially valuable when one wants to intercompare the surface intensity distribution in the light of different emission lines. Bappu et al (1974; see also Bappu, 1978) have obtained the monochromatic images of the nucleus of comet Kohoutek in the lines D_1 and D_2 of sodium, by such a technique, while Elliot and Meaburn (1973) have studied the core of Orion nebula in the lines of [OII] $\lambda\lambda$ 3726, 3729 in the same manner.

We have observed NGC 2903, 5236 and 5728 with similar techniques.

The velocity field in galaxies may distort the image even over the small extent of perinuclear formations. Hence, it is necessary to optimize the dispersion employed. We have chosen a dispersion of 160Å mm^{-1} for the observation of NGC 2903 and 5728. The velocity resolution at this dispersion ($20\,\mu m = 150$ Km s^{-1}) is low enough to keep the distortion to a minimum.

The distortion of the image due to the velocity field, on the other hand, can be used for an estimation of the velocity field itself. We illustrate this by the monochromatic images of NGC 5236 at a higher dispersion of 30Å mm^{-1} (Chapter VII).

Another source of distortion, which is common for all grating spectrographs, is Bowen's anamorphic reduction. This reduction R from the slit to the image plane is given by

$$R = \frac{\cos\beta}{\cos\alpha} \quad \frac{F_{coll}}{F_{cam}} \qquad .. (3.1)$$

in the direction of dispersion where α and β are the angle of incidence and of diffraction at the grating, F_{coll} the focal length of collimator and F_{cam} the focal length of the camera. The reduction along the length of the slit is simply

$$R = \frac{F_{coll}}{F_{cam}} \qquad .. (3.2)$$

Thus a contraction is introduced in the direction of dispersion by a factor of $\cos\beta/\cos\alpha$. The spectrograph used by us has a fixed angle of 60° between the collimated beam and the diffracted beam. One may then calculate the ratio $\cos\beta/\cos\alpha$ employing the grating formula and the condition $(\alpha+\beta) = 60°$. The corresponding value at the 166Å mm^{-1} dispersion (grating with 300 grooves mm^{-1}) amounts to 1.12 while at the 30Å mm^{-1} dispersion (grating with 1800 grooves mm^{-1}) it is 3.35, a much higher value.

The largest possible slit width is fixed by the condition that the images of H_α and [NII] λ 6584 should be resolved. This corresponds to 600 μm or 9 arcsec in the case of 166Å mm^{-1} dispersion (reduction: 4.5) and to 9 mm or 135 arcsec in the case of 30Å mm^{-1} dispersion (reduction: 13.4). While we have employed the limiting value at 166Å mm^{-1} dispersion we used only a 2 mm slit at the 30Å mm^{-1}, to let in only the central hot spots of NGC 5236, thus enhancing the contrast between the continuum and the emission lines, and not losing spatial resolution.

CHAPTER 4

A MORPHOLOGICAL CLASSIFICATION OF PERINUCLEAR FORMATIONS

A morphological classification should precede any further study of perinuclear formations, since it helps to recognize the properties that are physically and dynamically significant. We propose a morphological classification scheme of perinuclear formations in the following, based only on the geometrical aspects. We will correlate it with the spectroscopic information on the stellar and gaseous content. We will also look for the correlations of different classes of objects with the morphology of outer regions as well as with the descriptions of central regions at lower resolution. Finally we will compare the structure in the central region of our galaxy with the perinuclear formations reported here and classify the former.

4.1 A Classification scheme of the Perinuclear Formations

The seeing limited photographs of the central regions of 50 galaxies listed in Table 3.1 show three major types of formations:

a) Elliptical formations of smooth intensity distribution (Class ϵ), often showing a bright nucleus superposed on these. The nucleus is generally redder than the perinuclear formation. Typical examples are NGC 210, NGC 1300 and NGC 2196.

b) 'Hot spots' arranged in certain degree of spiral symmetry about a relatively redder central spot (Class σ). There is an underlying redder population of smooth intensity distribution which delineates this spiral pattern better. Typical examples are NGC 1097, NGC 1365 and NGC 2903.

c) Irregular formations (Class ι) forming a short barlike pattern of non-uniform surface brightness. The surface brightness of this type of formations is generally much lower than that of type σ or type ϵ formations. Typical examples are NGC 255, NGC 925 and NGC 7741.

The transitions from one type of perinuclear formations to another is rather smooth and it is easy to recognize the types of intermediate nature $\epsilon\sigma$ and $\sigma\iota$ The type $\epsilon\sigma$ shows some rudimentary spiral pattern (e.g. NGC 1326). The transition from σ to ι appears rather abrupt though some galaxies labelled σ by us (e.g. NGC 1808) show a slight tendency towards the group $\sigma\iota$. The galaxies included by us in Class $\sigma\iota$

generally have too few 'hot spots' like the 'dumbbell like' formations (Sersic, 1973) in NGC 1087 and NGC 1140.

Finally, a few galaxies could not be classified according to the above scheme. These galaxies listed as '$\varkappa$' in Table 4.1 have compact perinuclear formations which appear similar to the type N described by Morgan (1958) in that the formations are brilliant and small; our examples could be slightly more compact on an average. Some of these (e.g. NGC 7769) could be probably distant examples of types ϵ or σ, that have inadequate angular resolution, while some could be nuclei without bright perinuclear formation. Formations seen in NGC 1087 and NGC 1140 (Nucleus + one hot spot ?) could possibly be transitions between the classes σ and $\varkappa$, though placed in $\sigma 1$ by us.

Table 4.1 summarizes our classification of observed galaxies while contrast prints of all the observed galaxies are presented in Figure 4.1 through 4.6.

4.2 Stellar and Gaseous content of different Classes of Perinuclear Formations

The central hot spots of galaxies have been extensively observed since the early work by the Burbidges

Table 4.1

Galaxies with Different Types of Perinuclear Formations

ϵ	$\epsilon\sigma$	σ	$\sigma\iota$	ι	κ
210	1326	613	922	255	1530
1300	1415	1097	1087	925	3504
1433	1672	1365	1140	3206	3611
2196	2763	1808	4369	3346	4151
2935	4258	2903		3955	4212
3627	5248	2997		3956	4250
4124	5597	3177		4064	7769
4245	6907	3310		7741	
5850	7552	3351			
6951					
7410		5236			
		5728			

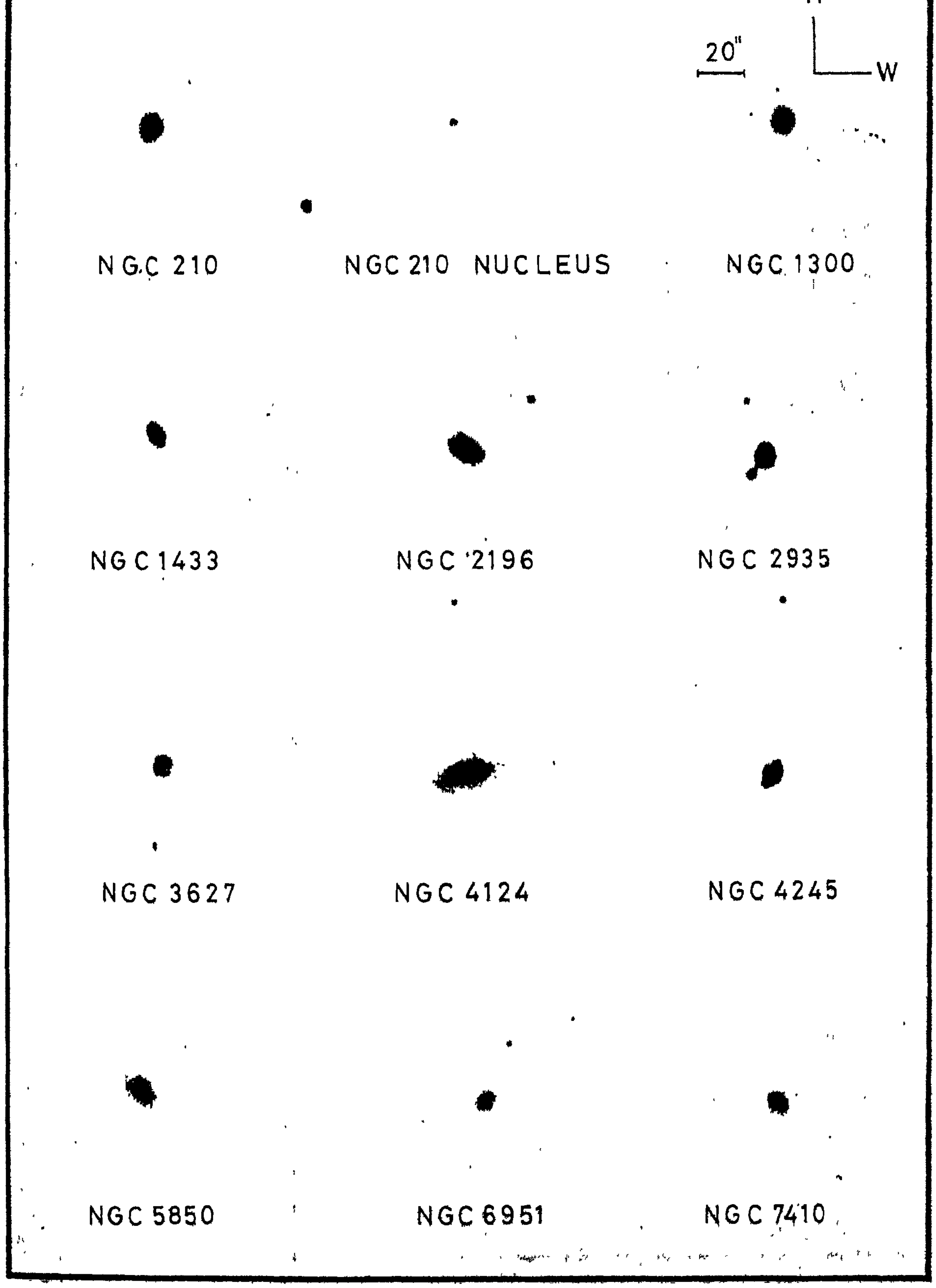

Fig. 4.1 Perinuclear Formations of class ϵ

Fig. 4.2 Perinuclear Formations of class $\epsilon 6$

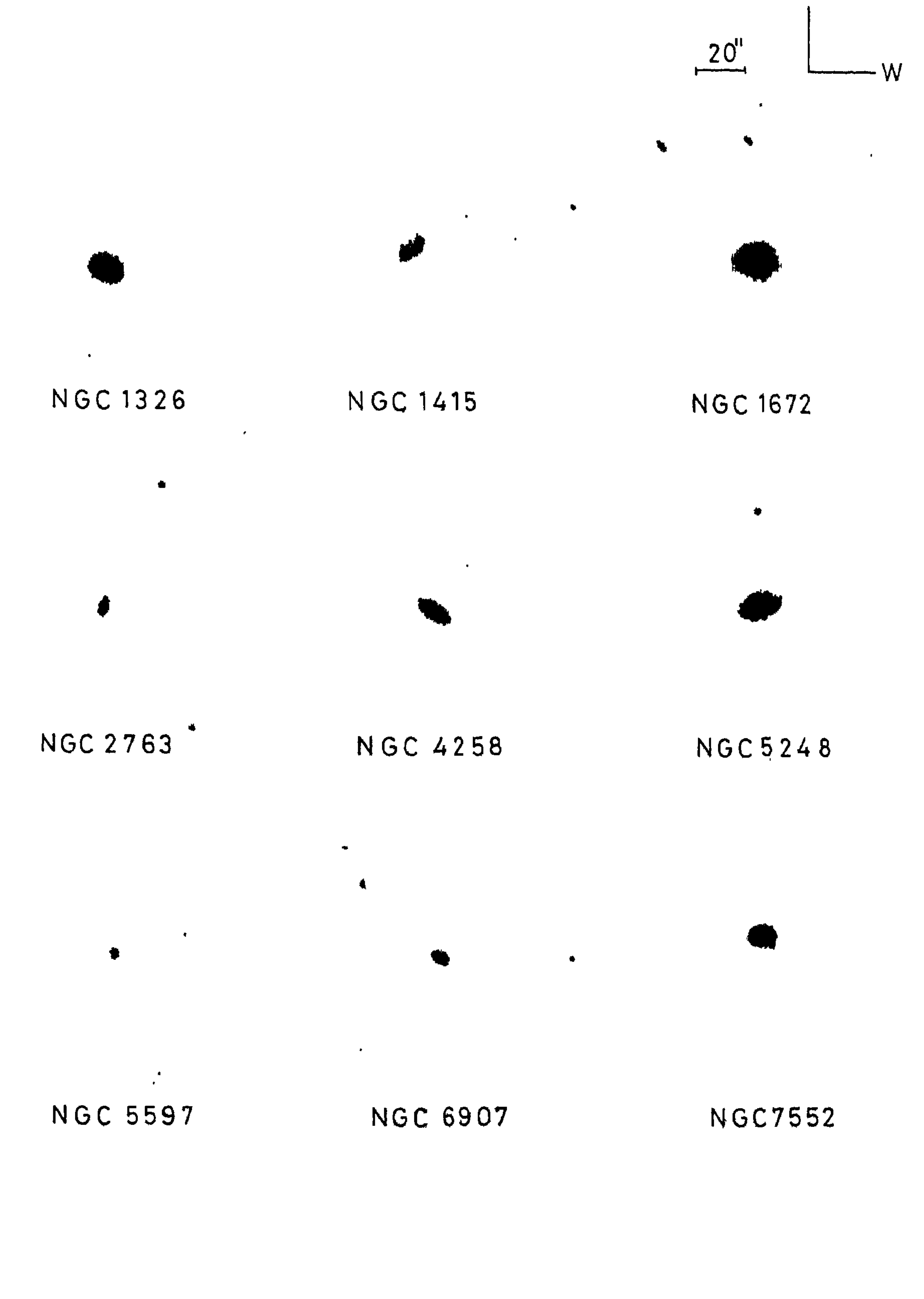

Fig. 4.3 Perinuclear Formations of class 6

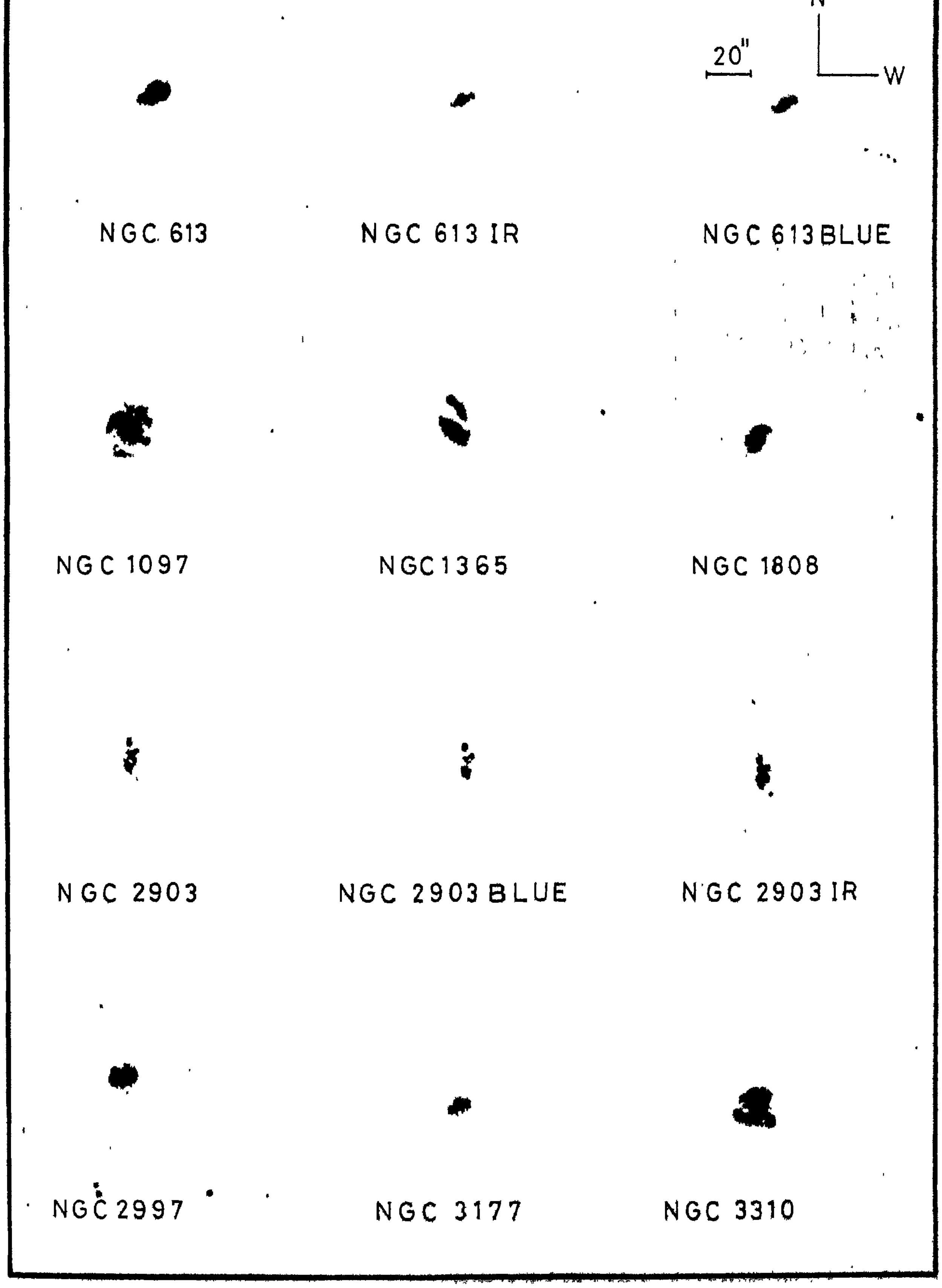

Fig. 4.3 continued

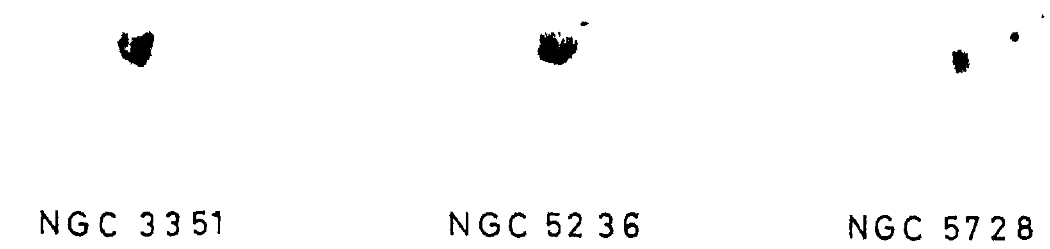

Fig. 4.4 Perinuclear Formations of class 6i

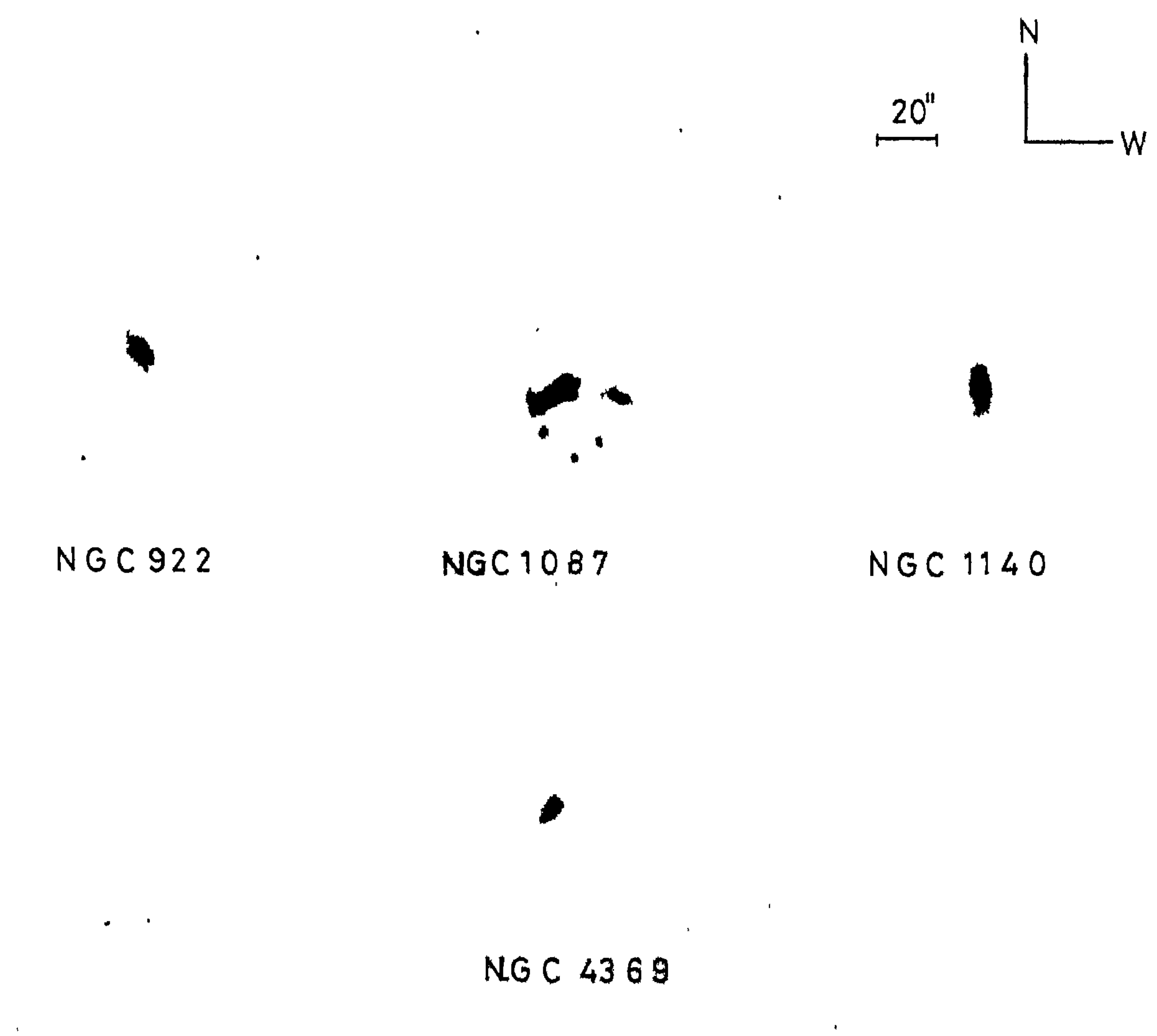

Fig. 4.5 Perinuclear Formations of class i

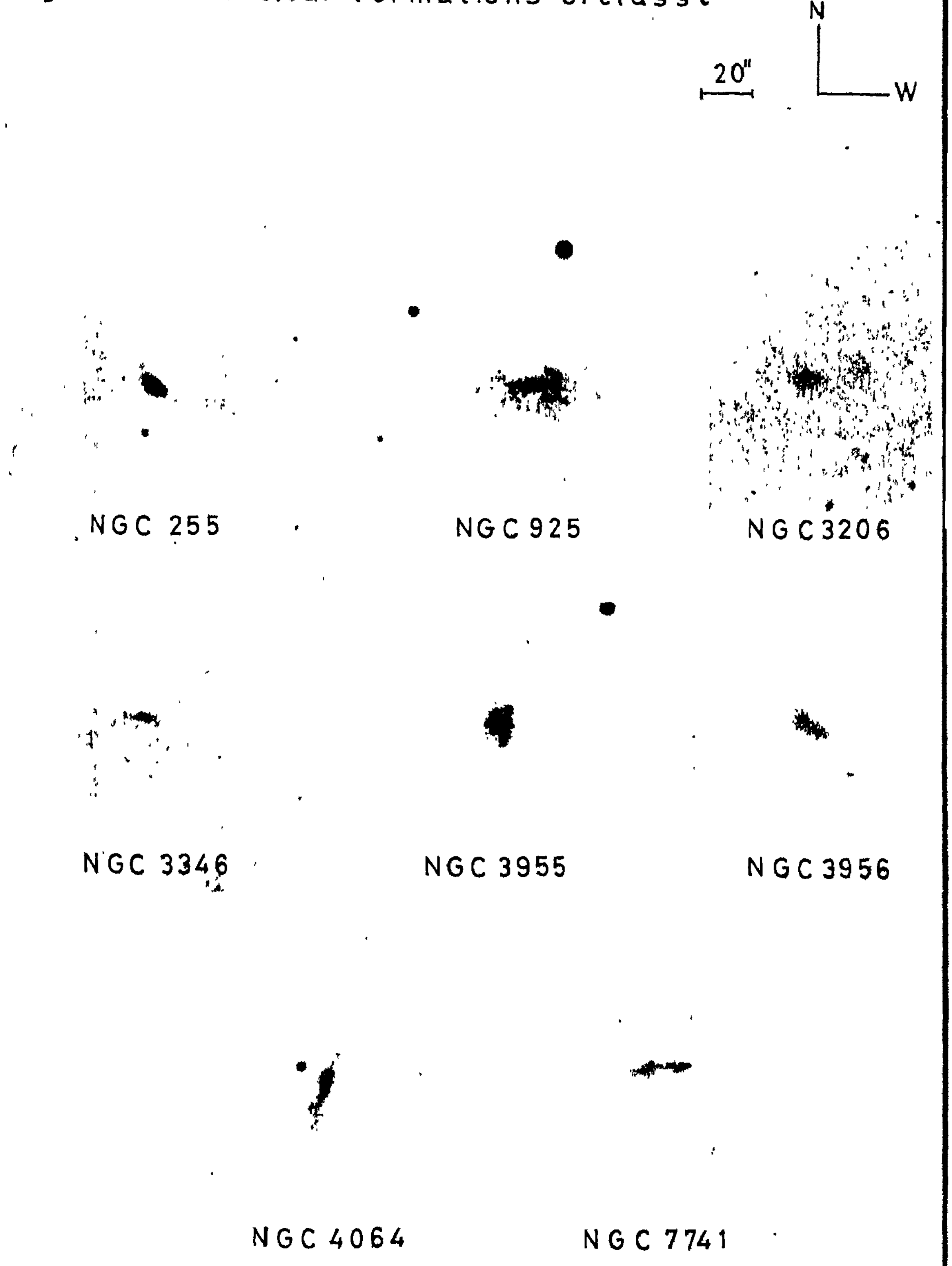

Fig.4.6 Perinuclear Formations of class K

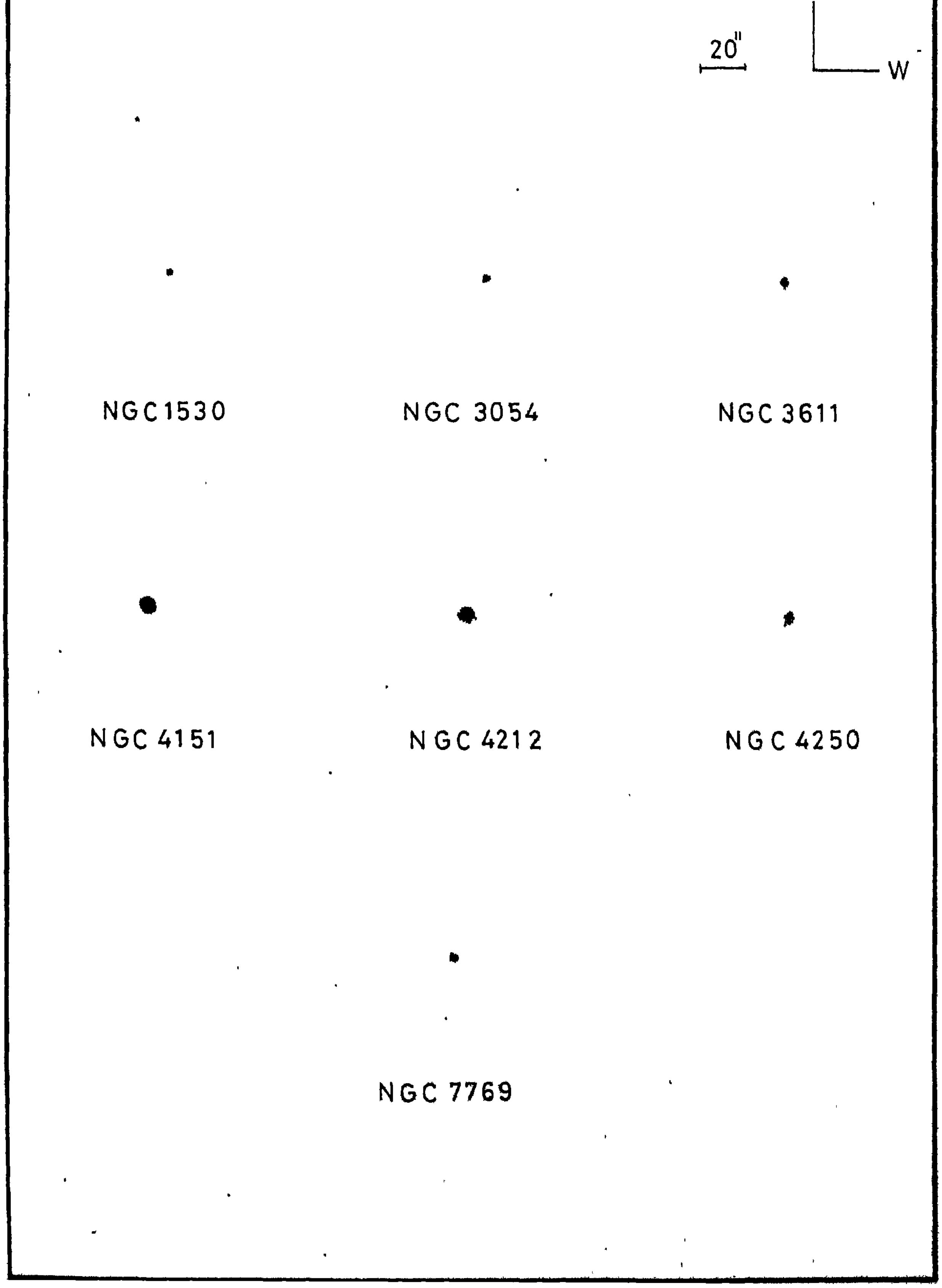

and their associates (cf. Osmer et al. 1974 and references therein). Hot spots are observed to be similar to other extragalactic HII regions, except that they are more reddened as indicated by the large H_α/H_β ratio and strong absorption line of NaI D.

The Class σ comprises of the brighter of the formations of hot spots while Class ι consists of the fainter formations. The interpretation of published spectra of typical members of these classes is consistent with the idea that the formations σ and ι have undergone recent bursts of star formation resulting in bright ionized regions around young O and B type stars.

The formations of Class ϵ, on the other hand, generally present only absorption lines in their spectra, apart from the emission of [OII] λ 3727. This fact is borne out by our observations listed in Table 3.2 and also by the observations of Sandage (1978) for NGC 2196, 2935 and 4124 and of de Vaucouleurs and de Vaucouleurs (1961) for NGC 1433. The Class ϵ formation of NGC 6951 is the only known exception to this observation (Burbidge, 1962).

The Class $\epsilon\sigma$ appears similar to class σ in its spectroscopic properties. It may be noted, however, that one member of this class, NGC 2763, does not show any emission line (Table 3.2; Sandage, 1978).

The differences between ϵ formations and the Classes $\epsilon\sigma$ and σ are apparent in their colours too. Adopting one-tenth of the face-on diameter (RCBG) as the approximate size of the perinuclear formations, we find that ϵ formations are redder in both $(U-B)_0$ and $(B-V)_0$ colours corrected for the absorption in our galaxy (Figure 4.7).

4.3 Correlations with the Types of Parent Galaxies

We have noted in Section 3.3 that a subgroup associated with Sc and Scd galaxies with lower luminosity exists among the perinuclear formations. We will presently examine the mean types of the parent galaxies of different classes of formations in order to identify this class with one of the morphological classes described in Section 4.1. These investigations will also assist in the discovery of possible correlations between the morphology of perinuclear formations and the outer morphology of galaxies.

We plot in Figure 4.8a the average morphological types of the parent galaxies for the different perinuclear classes. A correlation is evident; the mean type of the

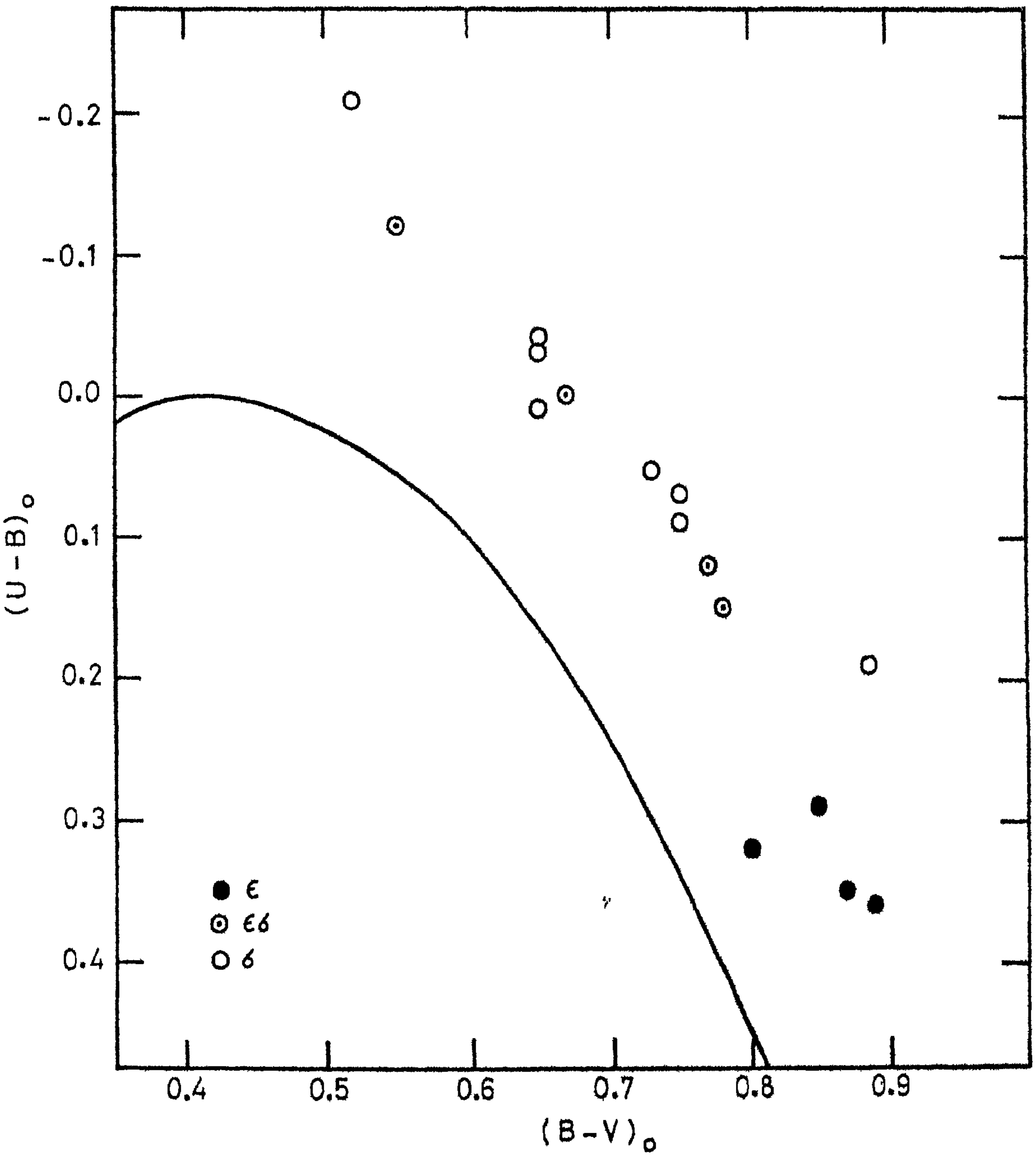

Fig.4.7 TWO COLOUR DIAGRAM FOR PERINUCLEAR FORMATIONS

parent galaxy varies smoothly from type Sab at ϵ formations to the Sc at ι formations. Correlations are also apparent with the DDO luminosity types (Figure 4.8b), Yerkes types (Figure 4.8c) and de Vaucouleur's luminosity index (Figure 4.8d). Mean lines are drawn in the figure taking note of the fact that Class $\sigma\iota$ contains too few galaxies for estimating reliable average type, and that NGC 2763 deviates greatly from the average of its Class $\epsilon\sigma$; Class κ is excluded since it does not follow the sequence $\epsilon - \iota$. All of these correlations may not be independent, since correlations of the morphological types with DDO types as well as Yerkes types have been noted already (cf. de Vaucouleurs, 1977; Morgan et al. 1971).

Finally, we plot mean Byurakan types of different perinuclear formations in Figure 4.8e. We have treated the class 2s as similar to Class 2. The mean types are indicated also when we follow the sequence of Byurakan classes 1-3-4-2-5-2s suggested by Tovmassian and Terzian (1973). Though weak correlations as shown are apparent one needs to be cautious since the low resolution employed for the Byurakan classification renders the latter as only indicative. Our results presented in Chapter V show that the nucleus appears less and less

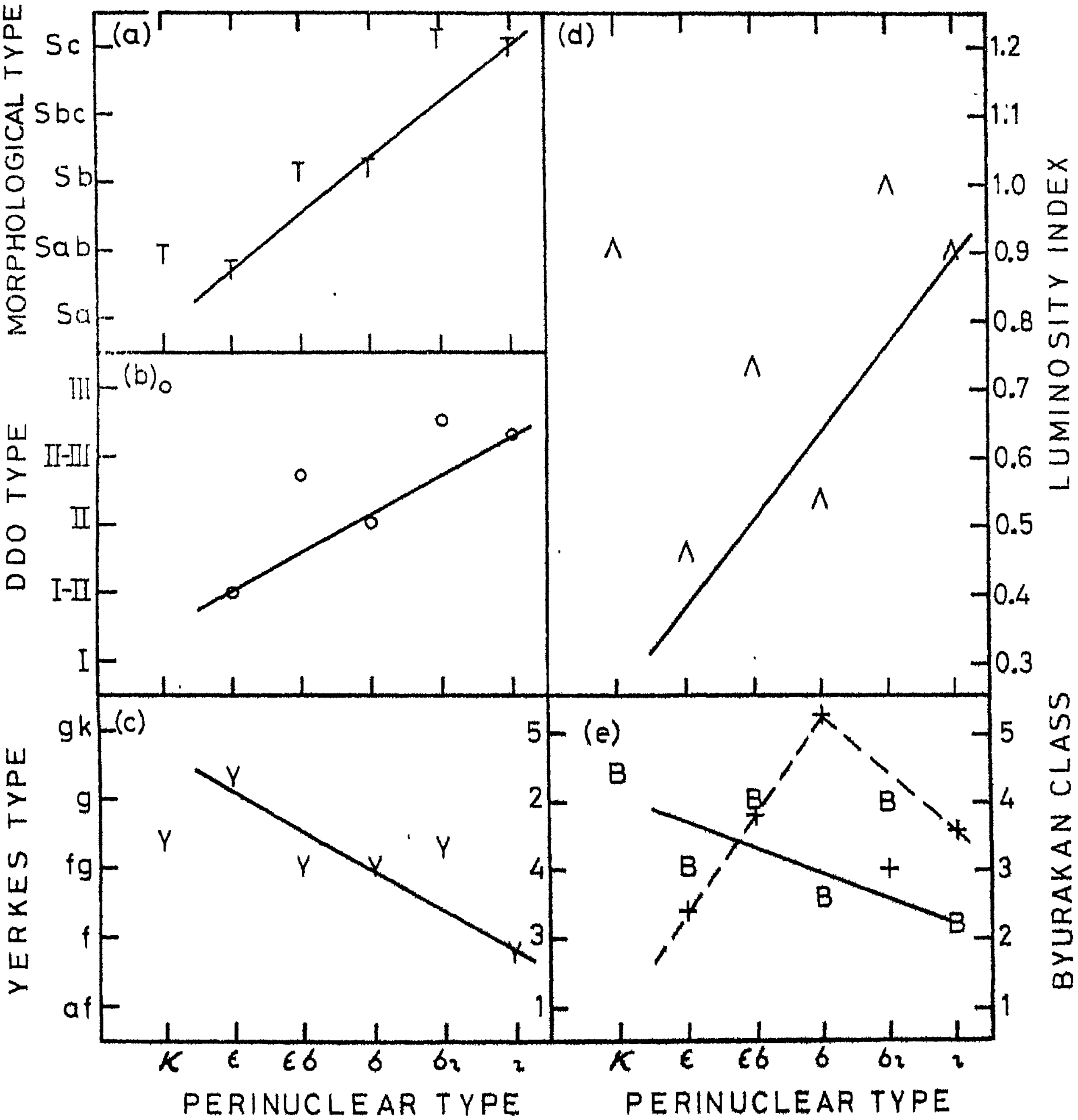

Fig.4.8 Mean Morphological types (a), DDO types (b), Yerkes types (c), Luminosity Indices (d), and Byurakan types (e) for different classes of perinuclear formations. Crosses and the dashed line in (e) correspond to ordinates at left.

dominant as we move from Classes ε to ℓ ; the central condensation within the perinuclear formations also decreases in the same order.

4.4 Morphology of the Galactic Centre

The centre of our galaxy is a few thousand times closer to us than the galaxies investigated here. The structure around the galactic centre can consequently be studied at a high spatial resolution. Though our position in the plane of the disc forbids the observations in the optical range, investigations have been carried out at the infrared and the longer wavelengths (cf. Oort, 1977 for a review). The continuum radiation at a few microns wavelength is dominated by the stellar component, at 10–100 μm by the hot dust, at a few centimeters by the thermal radiation from ionized hydrogen, and at decimeter wavelengths by non-thermal radiation. The 21-cm observations yield the neutral hydrogen component while the molecular lines of hydroxyl, formaldehyde, carbon monoxide and others yield information on the molecular cloud complexes. The recombination lines, especially that of NeII line at 12.8 μm and H109α at 5010 MHz, have been used to map the nuclear HII complex.

The thermal radiation from the stellar component, hot dust and HII regions as well as the molecular lines and the recombination lines could be used to construct a composite picture of the galactic centre in the optical region. While the 2.2μm observations of Becklin and Neugebauer (1968) cover only a radius of 50pc from the centre, the thermal radiation at centimeter wavelengths has been observed over a larger spatial range (Downes and Maxwell, 1966). The latter observations reveal several HII regions, the brightest one centered at the 2.2μm peak and the brightest source at all the wavelengths -- Sagittarius A. While this peak resembles the nuclei observed in other galaxies, the remaining HII regions appear similar to the hot spots, seen around the nuclear hot spot.

We proceed to compare the 3.75cm map of the galactic centre with our isophotes of the central region of NGC 2903, one of the nearest Class σ formation in our list. The galactocentric radial velocity of the dynamical centre of NGC 2903 is 375 kms^{-1} (Simkin, 1975). Assuming a Hubble constant of 50 kms^{-1} Mpc^{-1}, we obtain a distance estimate of 7.7 Mpc. At this distance one second of arc corresponds to 37.5 pc. The resolution employed by Downes and Maxwell (1966) is 4'.2 or roughly

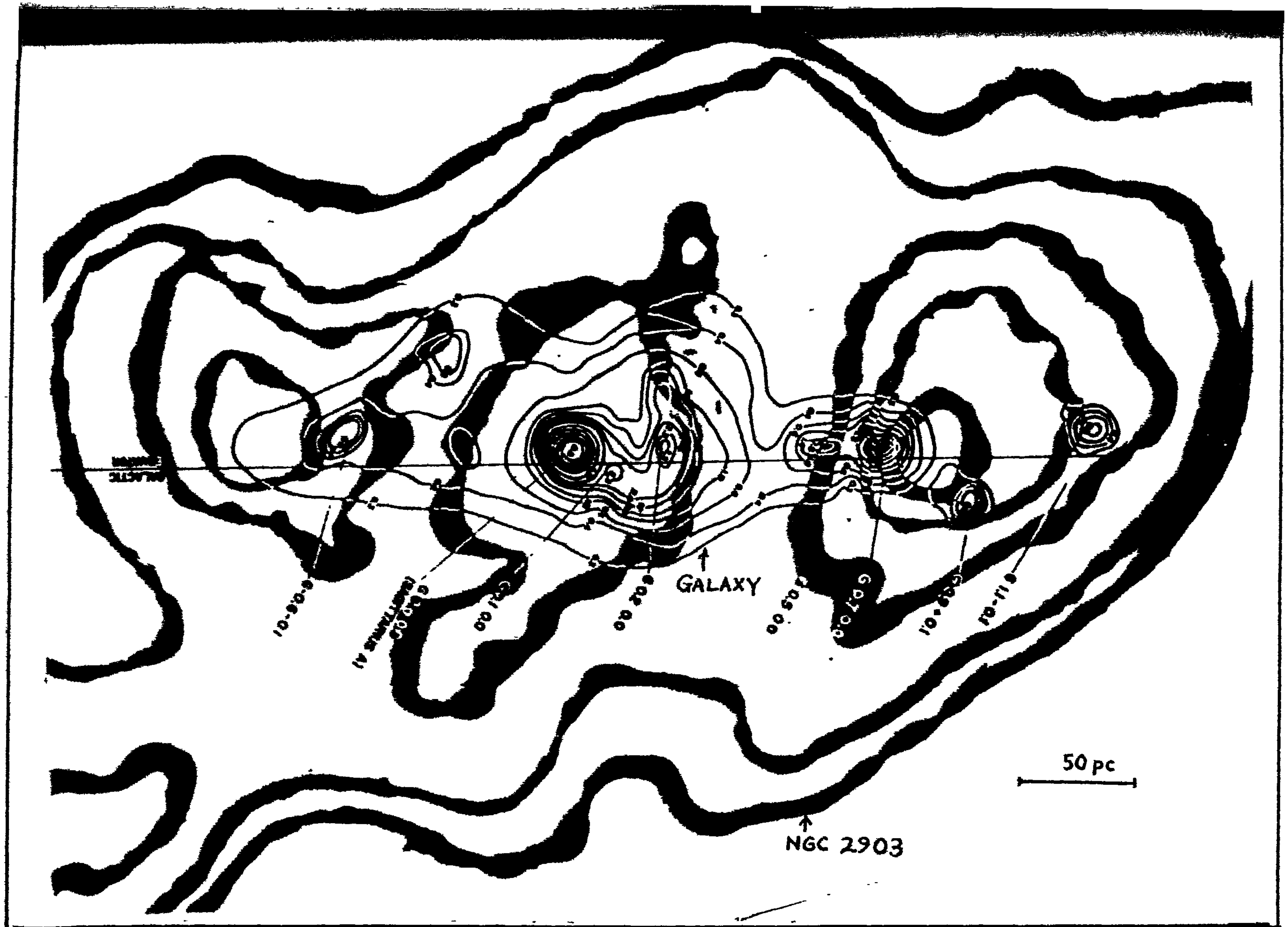

FIG.4.9 CENTRAL REGION OF OUR GALAXY COMPARED WITH THAT OF NGC 2903.

10 pc at an estimated distance of 8.7 kpc of the galactic centre (Oort and Plaut, 1975). Thus there is no great disparity in the resolutions of these two pictures of the galactic centre and the centre of NGC 2903.

We reproduce in Figure 4.9 the 3.75cm map of Downes and Maxwell (1966) as well as the isophotes of NGC 2903. The spatial scale of the map of galactic centre is arranged to match the scale of the map of NGC 2903. The resemblance is striking.

The nucleus of NGC 2903 which is not noticeable on the blue pictures (cf. Figure 3 of Oka et al. 1974) is prominent in our isophotes. This nucleus is very red and appears on our photograph because of the S-20 response of the Varo 8605 to wavelengths upto 8700Å.

--

CHAPTER 5

PHOTOGRAPHIC SURFACE PHOTOMETRY OF PERINUCLEAR FORMATIONS

The distribution of surface brightness is a very good indicator of the surface distribution of mass density when the contributions from gas and different types of stars stay constant relative to each other, within the area being investigated. Hence, the surface photometric parameters have been widely used for obtaining structural models of systems of stars and galaxies (King, 1966; Freeman, 1970).

The luminosity profiles of galaxies are also used for isolating different subsystems of spiral galaxies. The major subsystems like the bulge and the exponential disc can be identified very easily in the luminosity profiles. Likewise, the perinuclear formations are also apparent in the luminosity profiles and can be recognized by a point of inflexion in them. The surface photometric data also includes the shapes and orientations of the equal intensity contours which are useful, in the particular case of perinuclear formations, to check for the presence of triaxial, prolate spheroidal or ovoidal distortions.

5.1 Presentation of Data

We present in Figure 5.1 through 5.27, the calibrated equal intensity contours of perinuclear formations of some of the galaxies from Table 3.1. The intensities relative to the central peak are tabulated in Tables 5.1 through 5.27 for all the galaxies. The isophotes are numbered in an increasing numerical order from the centre outwards.

The luminosity distribution is also presented graphically as equivalent luminosity profiles in figure 5.28 onwards. These profiles show the variation in the relative intensity as a function of the equivalent radius defined as $r^* = (A/\pi)^{\frac{1}{2}}$, where A is the area of a given isophotal contour. The equivalent radius defines a mean radius and is useful also when the surface intensity distribution does not exhibit a circular or elliptical symmetry. The equivalent luminosity is obtained by integrating the intensities over an area. The equivalent luminosity profile thus represents the area with surface brightness higher than a given value. Keeping this aspect in mind, we have summed all the areas enclosed by different unconnected contours of a

FIG.5.1 NGC 210

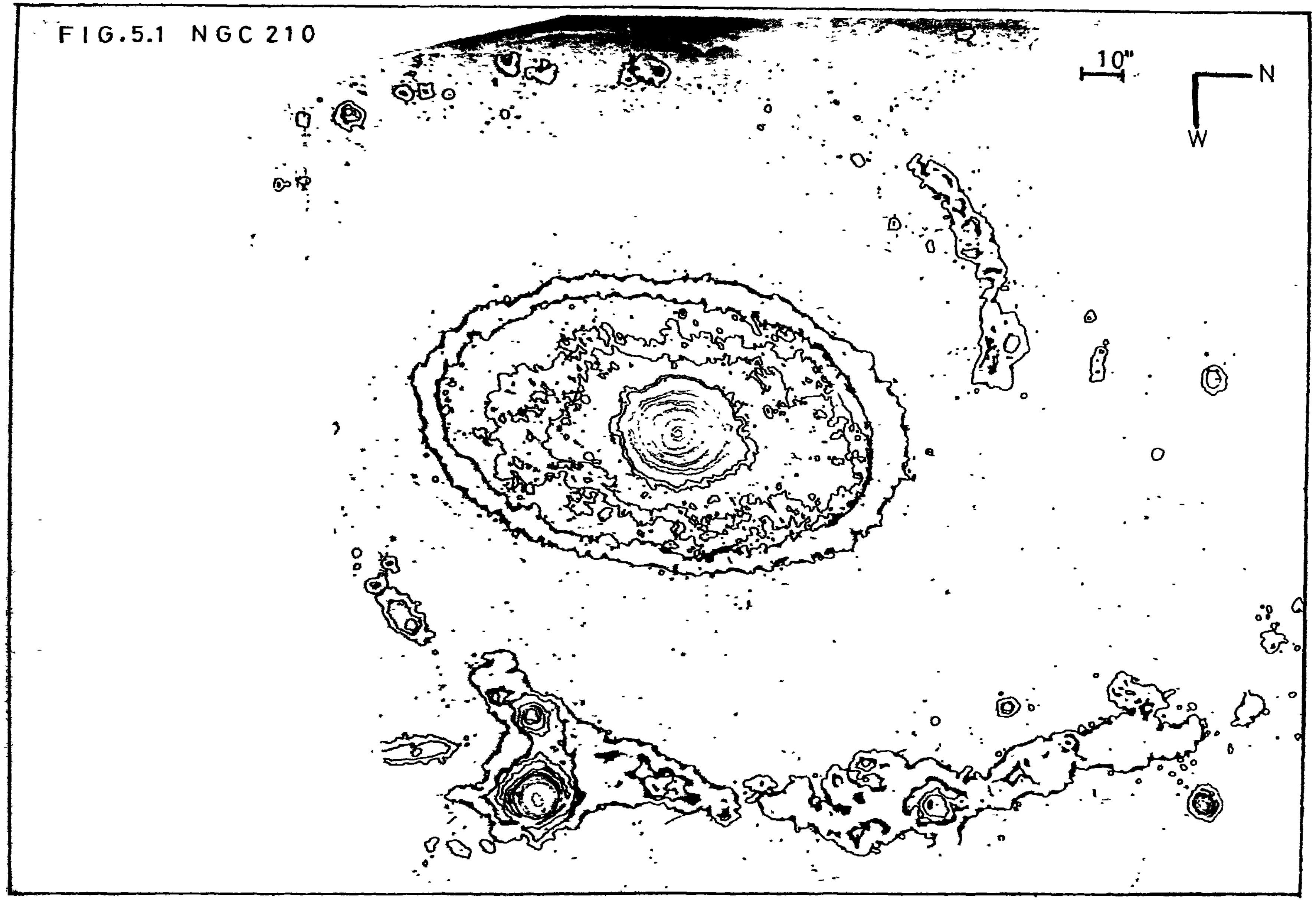

given intensity while constructing equivalent luminosity profiles of formations with hot spots. However, the contrast between the hot spots and the background is lower in our pictures in integrated light ($\lambda\lambda$ 4000-8700) than in the blue or H_α pictures, generally published. Hence, such unconnected regions are few and account for less than ten per cent of the total area.

The following sections include notes on and descriptions of the individual objects.

5.2 NGC 210

This galaxy has a bright elliptical perinuclear formation typical of Class ϵ . A starlike nucleus is visible both in the blue and in the infrared; an example of Byurakan Class 3 that exhibits a nucleus at higher resolution. The nucleus is slightly displaced ($\sim$1 arcsec) from the centroid of the perinuclear formation. The latter presents a slightly oval shape.

The isophotes are presented in Figure 5.1 and the corresponding intensities listed in Table 5.1. The outer isophotes (lens and the spiral arms) are obtained from the print published by Sandage (1961) and hence could not be calibrated for intensity. The equivalent luminosity profile is shown in Figure 5.28.

FIG.5.2 NGC 255

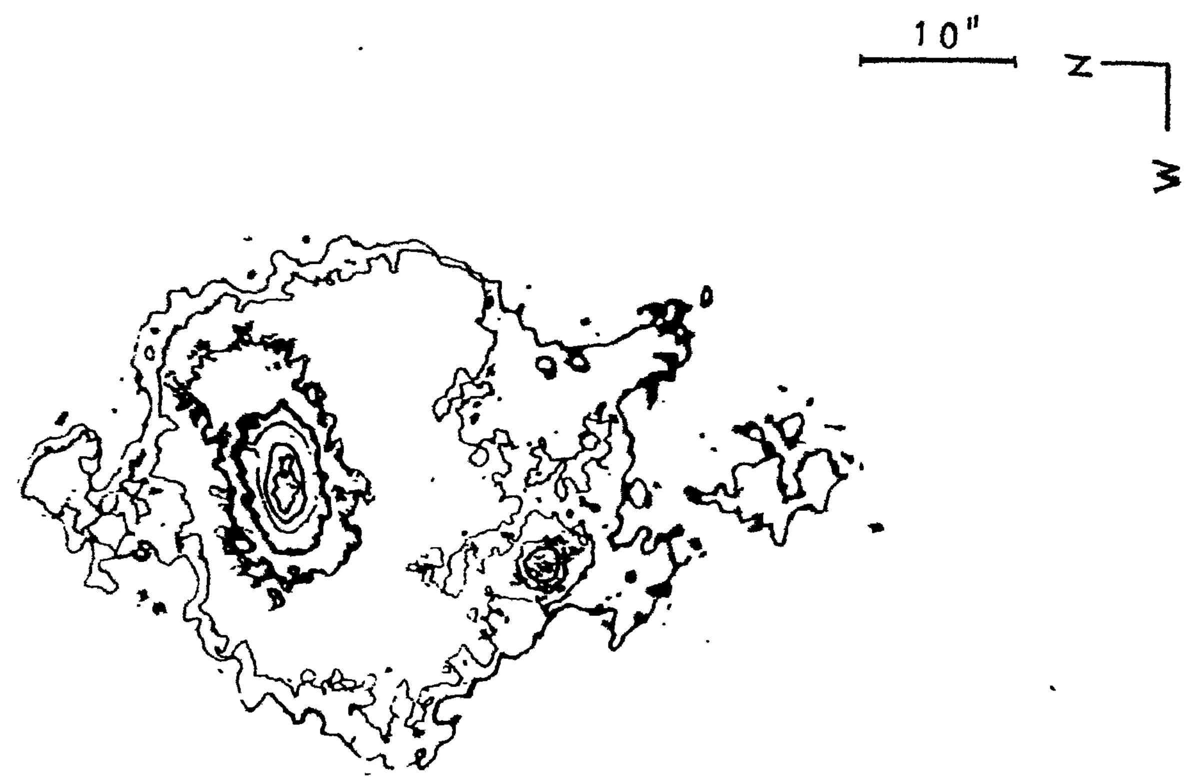

The contours within the perinuclear formation are nearly elliptical. The position angle of the major axes of these ellipses decreases from 40° at the semi-major axis a = 5 arcsec to 350° at a = 25 arcsec to rise again to 0° which is the same as the position angle of the lens. The ellipticity, e increases from e = 0 for the nucleus to e = 0.9 at a = 60 arcsec, decreasing thereafter to e = 0.8 at a = 90 arcsec, a value close to e = 0.75 suggested by the axial ratio 0.66 of RCBG.

5.3 NGC 255

This galaxy has a perinuclear formation typical of Class 1 in shape, though its surface brightness is above the average of its class. The formation is bar-like and is displaced by about 4 arcsec to the east of the centre of the outer contours (Figure 5.2). There is an indication that the position angle of the bar and also the axial ratio vary from centre outwards as in the manner observed in NGC 210 (Section 5.2). Several condensations outside of the perinuclear formation appear to possess directional symmetry with respect to the latter. A starlike condensations, or a field star appears at 20 arcsec from the centre of the formation at a position angle of 259°.

FIG. 5.3 NGC 613

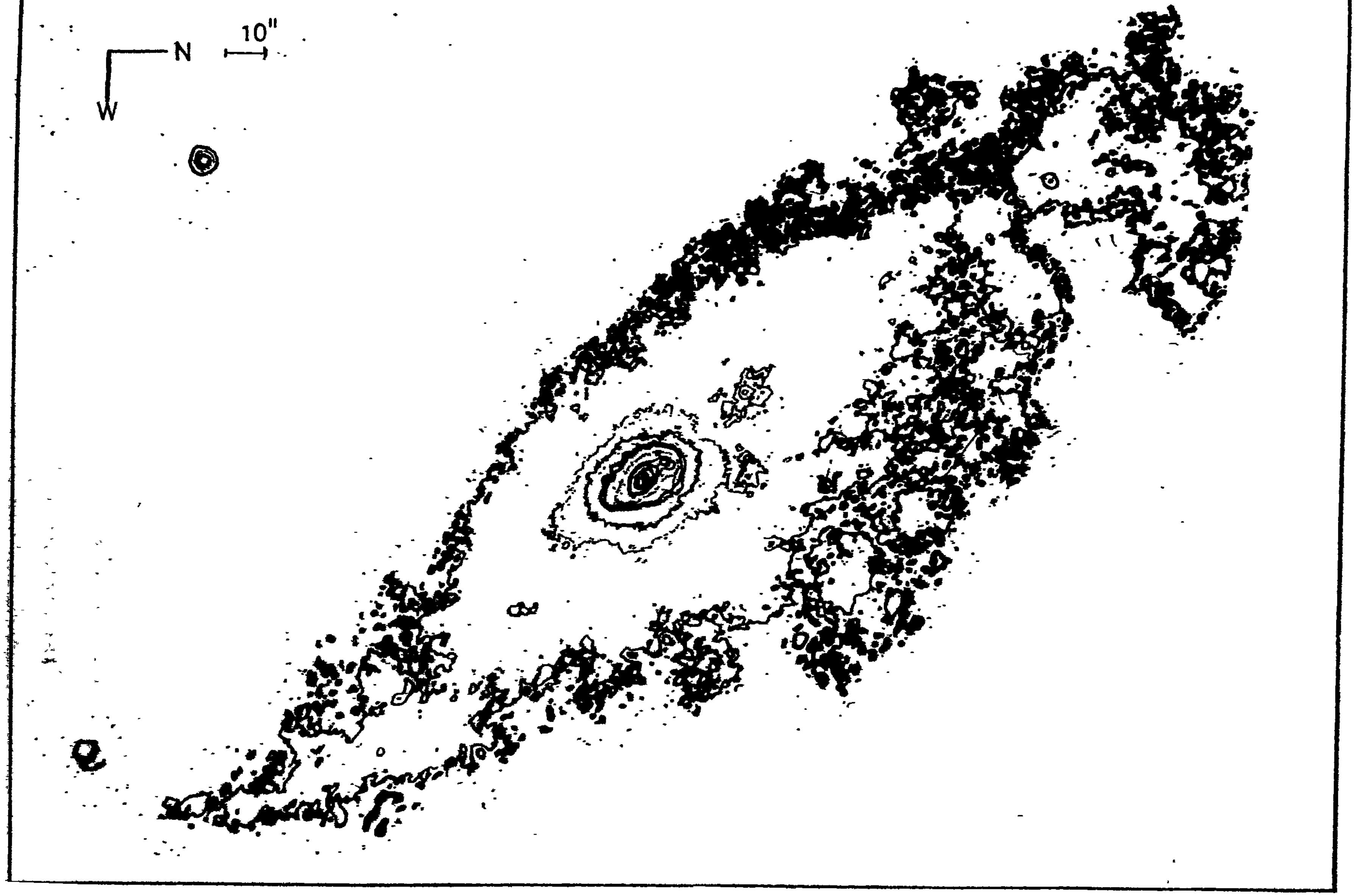

The equal intensity contours are shown in Figure 5.2, the intensity values in Table 5.2 and the equivalent luminosity profile in Figure 5.32.

5.4 NGC 613

We have grouped this galaxy with class σ though the central hot spots are not as distinct as in the typical examples. The contours are presented in Figure 5.3. The spiral pattern of the perinuclear formation appears rudimentary, but mimics the outer spiral structure of the galaxy. The outer contours of the formation are elliptical with an oval distortion. The position angle of the major axis and also the axial ratio appear to vary. The nucleus is identifiable, and is brighter in the infrared (cf. Figure 4.3). The equivalent intensity profile is shown in Figure 5.30 and listed in Table 5.3.

5.5 NGC 922

A formation typical of class σl. The contours are presented in Figure 5.4, intensities listed in Table 5.4 and the equivalent luminosity profile shown in Figure 5.31. The irregular extension of the outer contours to the south-west has the effect of reducing the slope of the outer region of the equivalent luminosity profile.

FIG.5.4 NGC922

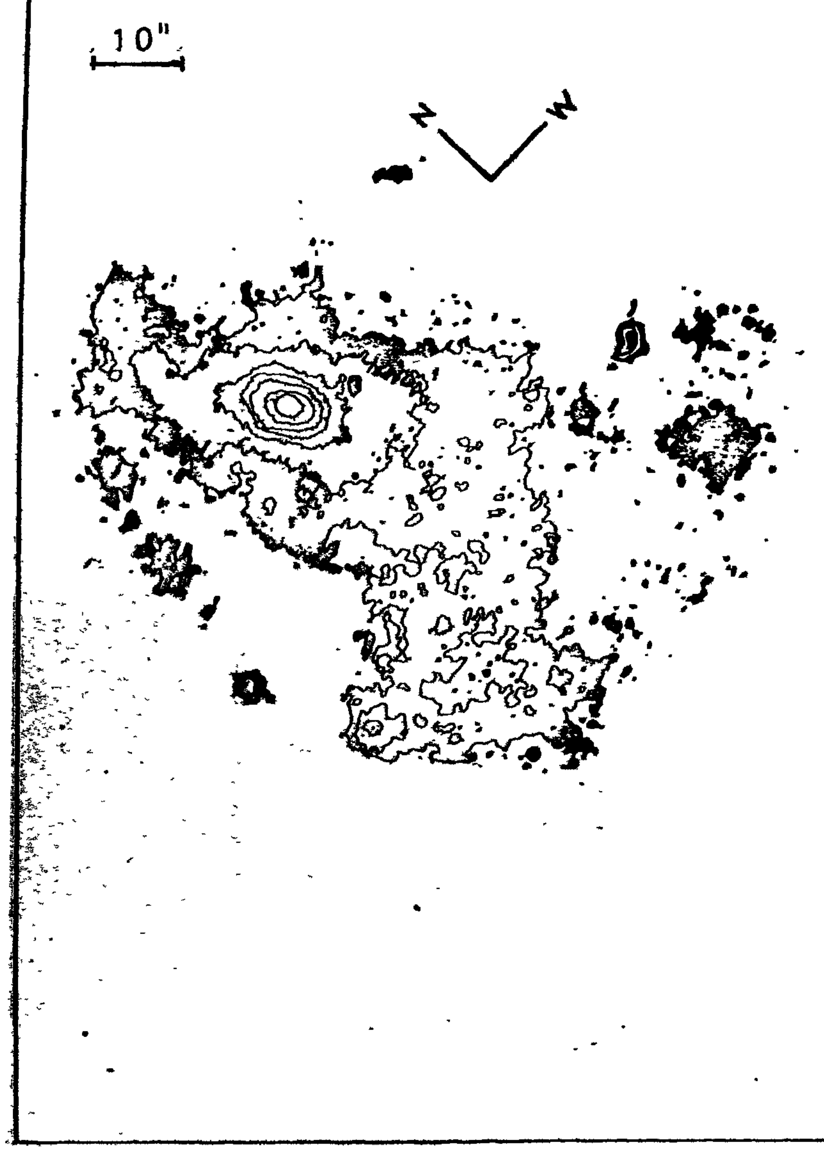

FIG.5.5 NGC 1087

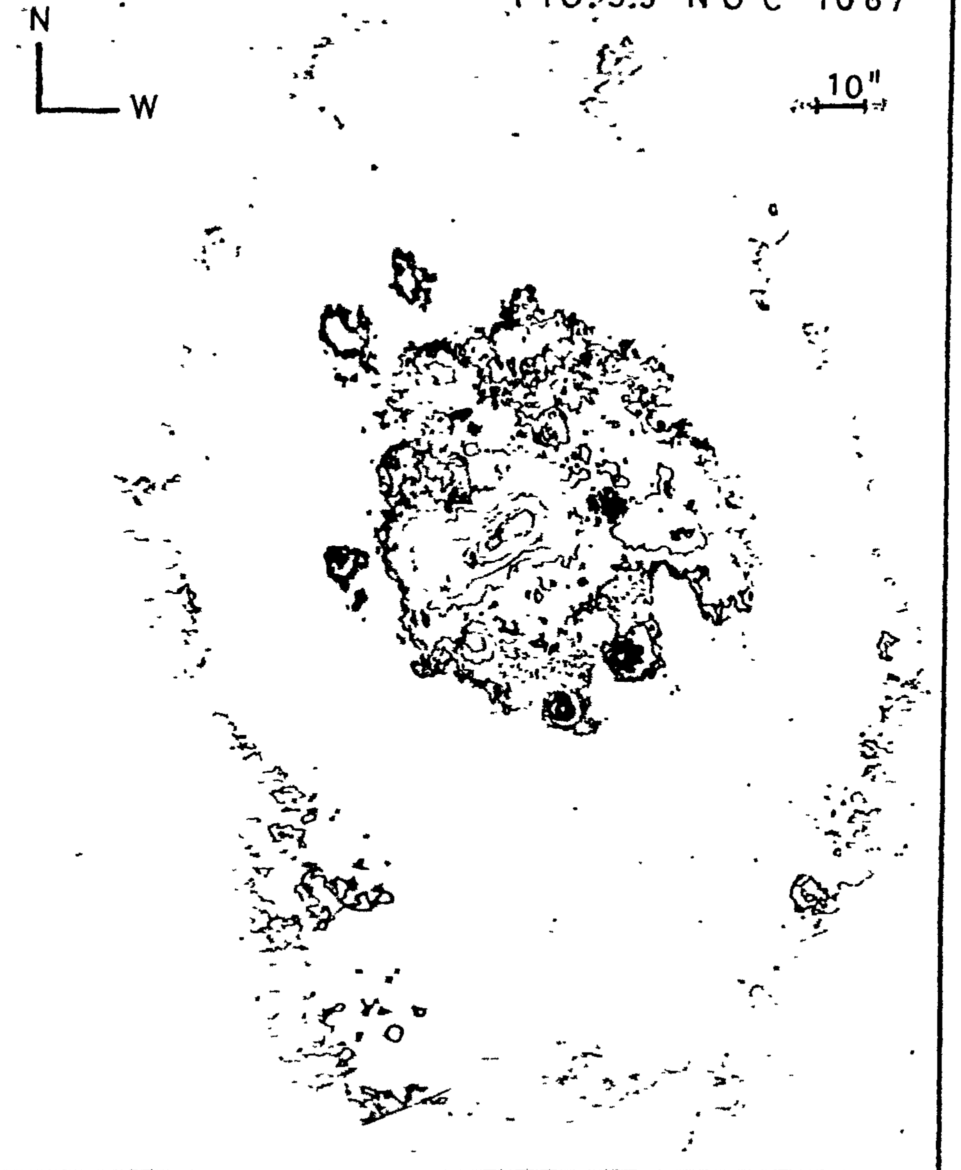

5.6 NGC 1087

This galaxy has a formation similar to that of NGC 255 (class ι), but is classed $\sigma\iota$ by us due to higher central condensation. The central peak, which probably contains an unresolved nucleus, is situated midway between the centre of the outer contours and the centre of the perinuclear formation itself. These are about 5 arcsec apart at a position angle of 130°. Several condensations in the main body of the galaxy have a directional symmetry about the intensity peak as in the case of NGC 255.

The contours are presented in Figure 5.5 and the intensities are listed in Figure 5.5. The equivalent luminosity profile is shown in Figure 5.31.

5.7 NGC 1097

This is a typical example of class σ with bright hot spots arranged in a spiral pattern about a bright nucleus. The spiral pattern mimics the outer spiral arms of the galaxy except that the latter emerge from the end is of a central bar. The outer contours of the formation are oval.

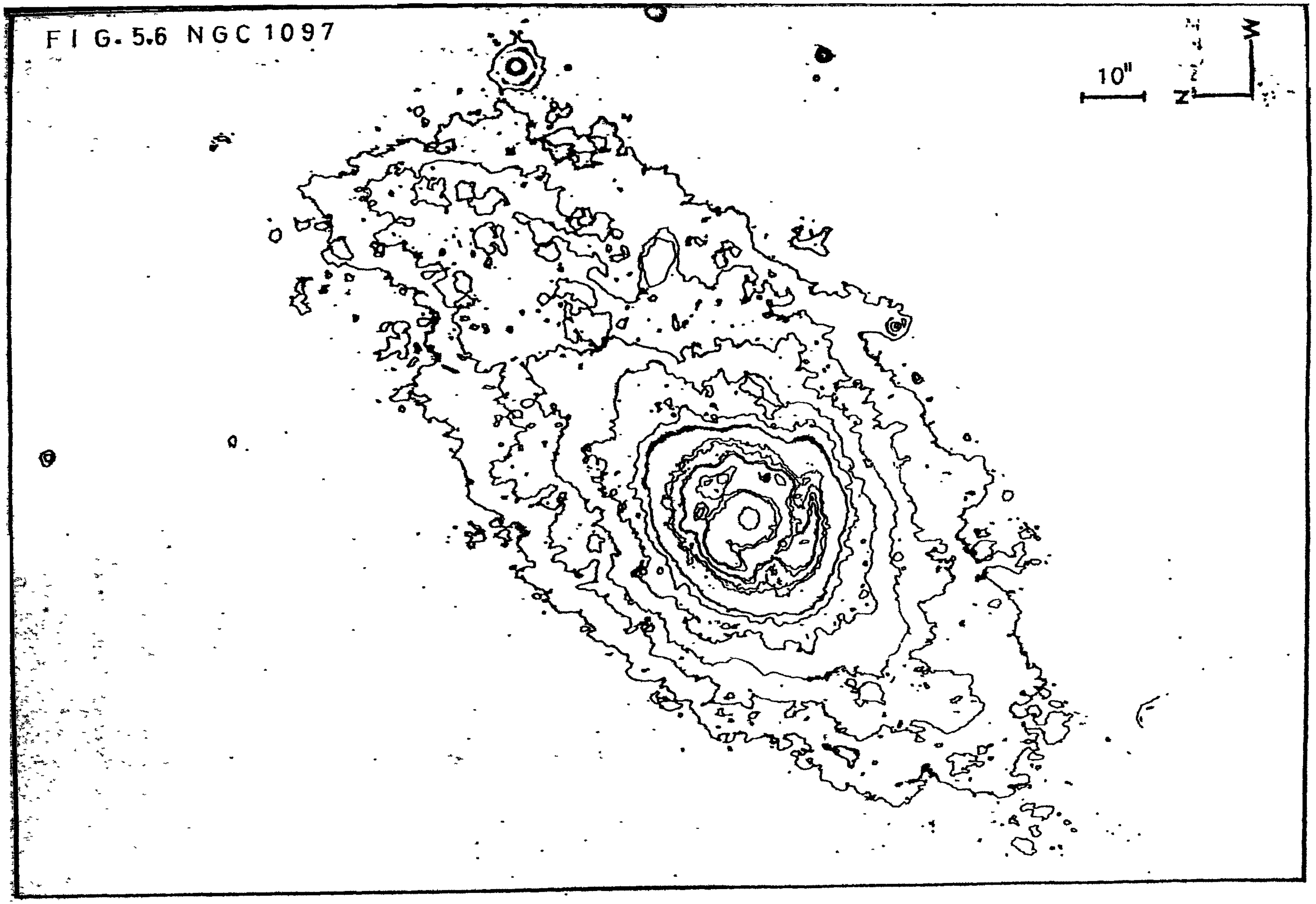

FIG. 5.6 NGC 1097

The contours are presented in Figure 5.6. The centre of the formation is 13 arcsec to the South-East of the centre of the bar. This may in part be due to the interaction with NGC 1097A which is 3'.5 to the North-West along the same position angle. Disturbances of this nature are evident on photographs of this galaxy (cf. Wolstencroft and Zealey, 1975).

The intensity values corresponding to different contours are listed in Table 5.6 and the equivalent profile is shown in Figure 5.30.

5.8 NGC 1140

Described by Sersic (1973) as dumb bell-like, the central region of this galaxy has two bright condensations symmetrically placed with respect to the centre of the outer contours of the perinuclear formation. The separation between the peaks in intensity is only 1.6 arcsec. The outer contours show a slight spiral distortion. Our classification as $\sigma\iota$ is rather uncertain and the formation appears more like a transition between ϵ and $\mathcal{K}$ with two nuclei instead of only one.

The contours appear in Figure 5.7, the intensity values in Table 5.7 and the equivalent luminosity profile in Figure 5.31.

FIG.5.7 NGC 1140

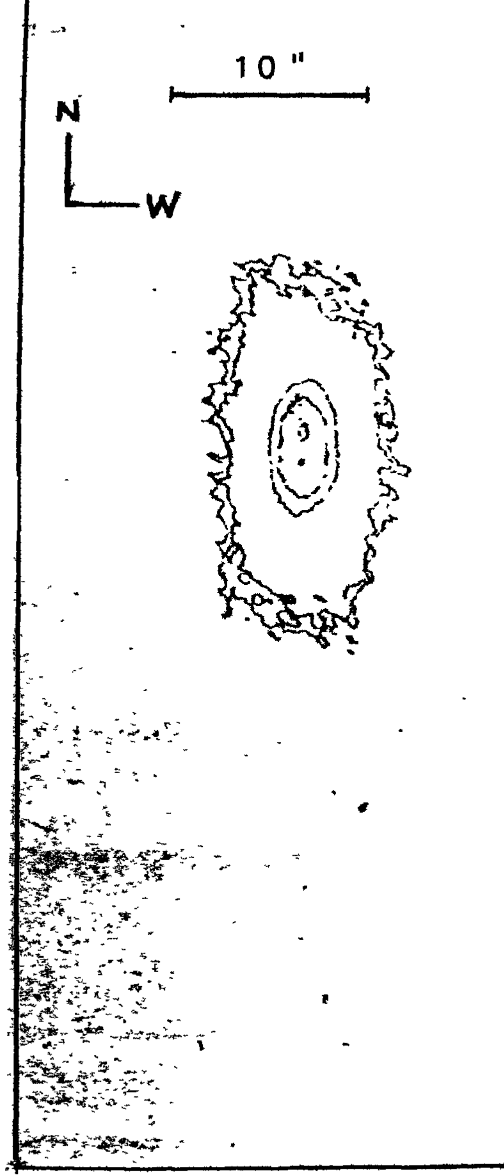

FIG.5.8 NGC 1300

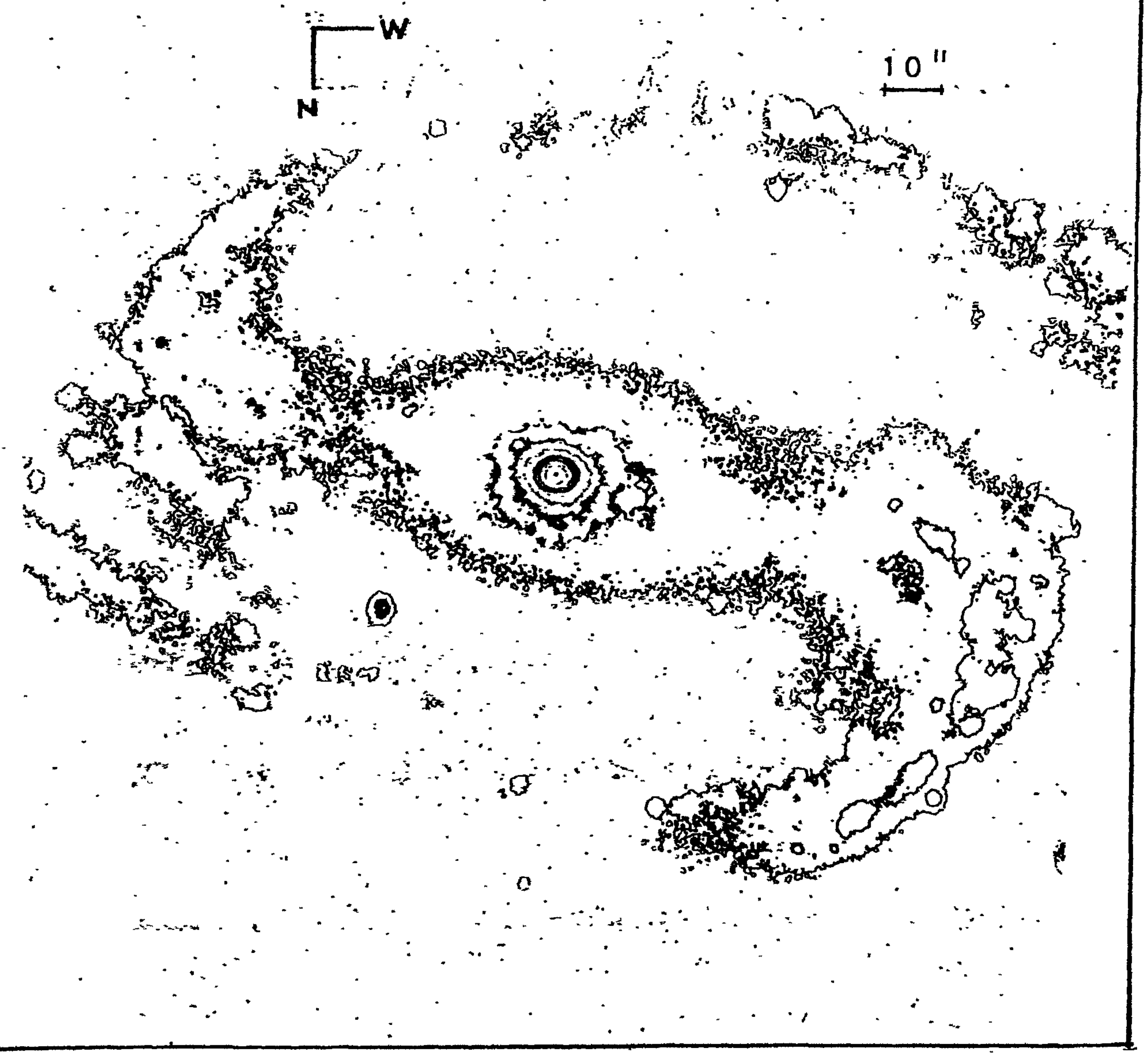

5.9 NGC 1300

The class ϵ perinuclear formation of this galaxy is similar to that of NGC 210 except that the nucleus is less bright in the former and the outer edge of the formation slightly diffuse. The position angle of the major axis and the ellipticities vary in a manner similar to that of NGC 210.

The contours presented in Figure 5.8 include the contours of the bar and the outer spiral arms obtained from the print published by Sandage (1961). We have not calibrated them for intensity. The intensities of all the other contours are listed in Table 5.8, while the equivalent luminosity profile is drawn in Figure 5.28.

5.10 NGC 1326

This galaxy has a perinuclear formation similar to those of NGC 210 and NGC 1300, but the edge of the formation is more diffuse than either of them, and the central condensation somewhat less. These facts make it appear like a transition between ϵ and σ and hence classed so by us.

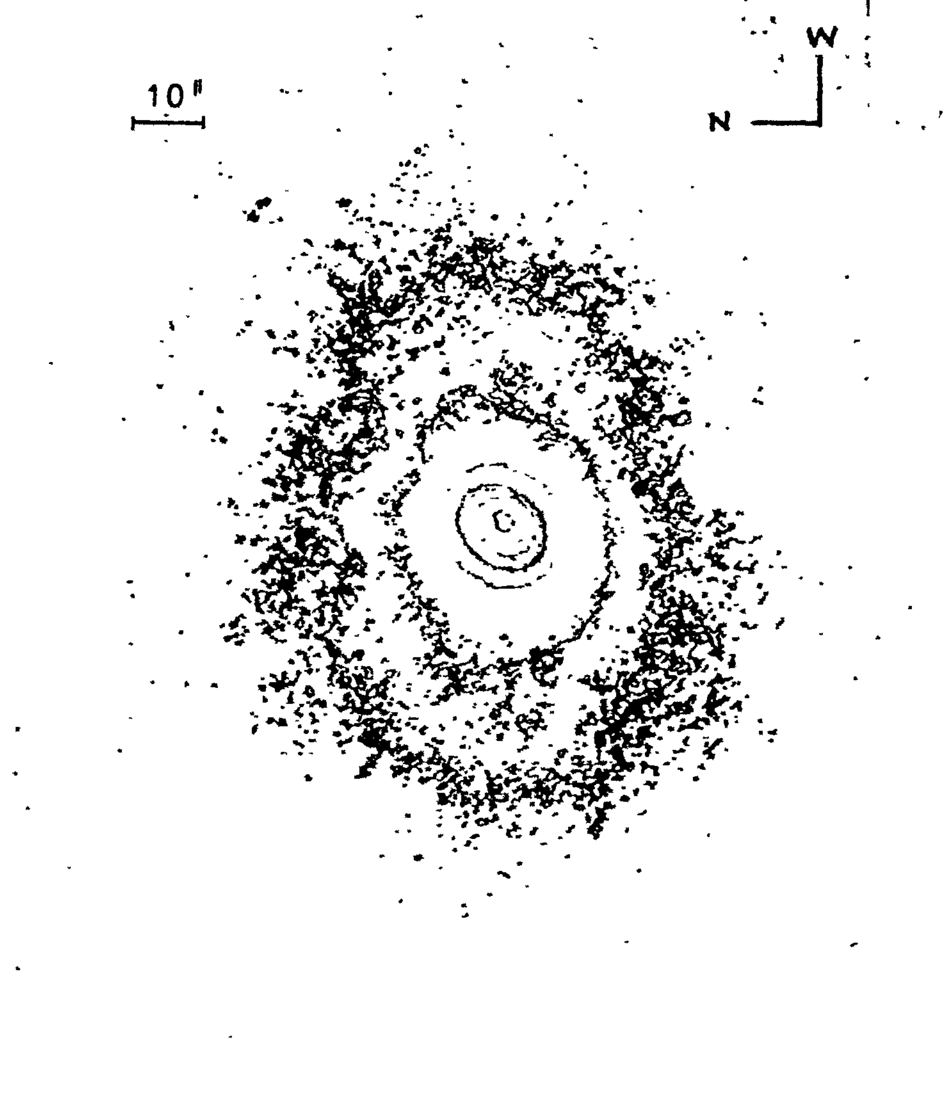

FIG. 5.9 NGC 1326

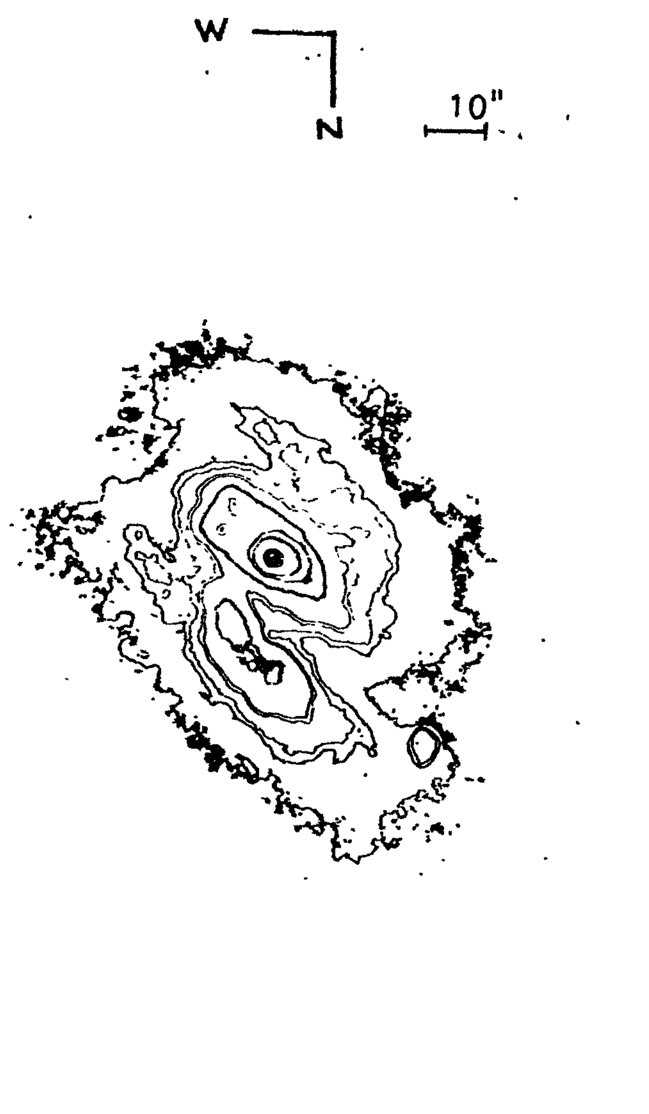

FIG.5.10 NGC1365

The contours are presented in Figure 5.9 and the intensity values listed in Table 5.9. There is a discontinuous change in the position angle of the major axis within the formation and in the outer contours. The formation is most likely a triaxial one as it resembles in this fact the 'bulge' of M31 ($\sim$2 kpc) for which stark (1977) has fitted triaxial models.

The equivalent luminosity profile is drawn in Figure 5.29.

5.11 NGC 1365

This is another typical example of a class σ perinuclear formation. The nucleus is, however, much brighter - the brightest among the σ formations investigated. It is extremely red (cf. Chapter 6). It may be noted that soft x-rays are detected from this galaxy (Ward et al. 1978), the two facts could be correlated.

The contours are presented in Figure 5.10 and the intensity values are listed in Table 5.10. The spiral pattern of the formation resembles the outer spiral arms of the galaxy. The equivalent luminosity profile is plotted in Figure 5.30.

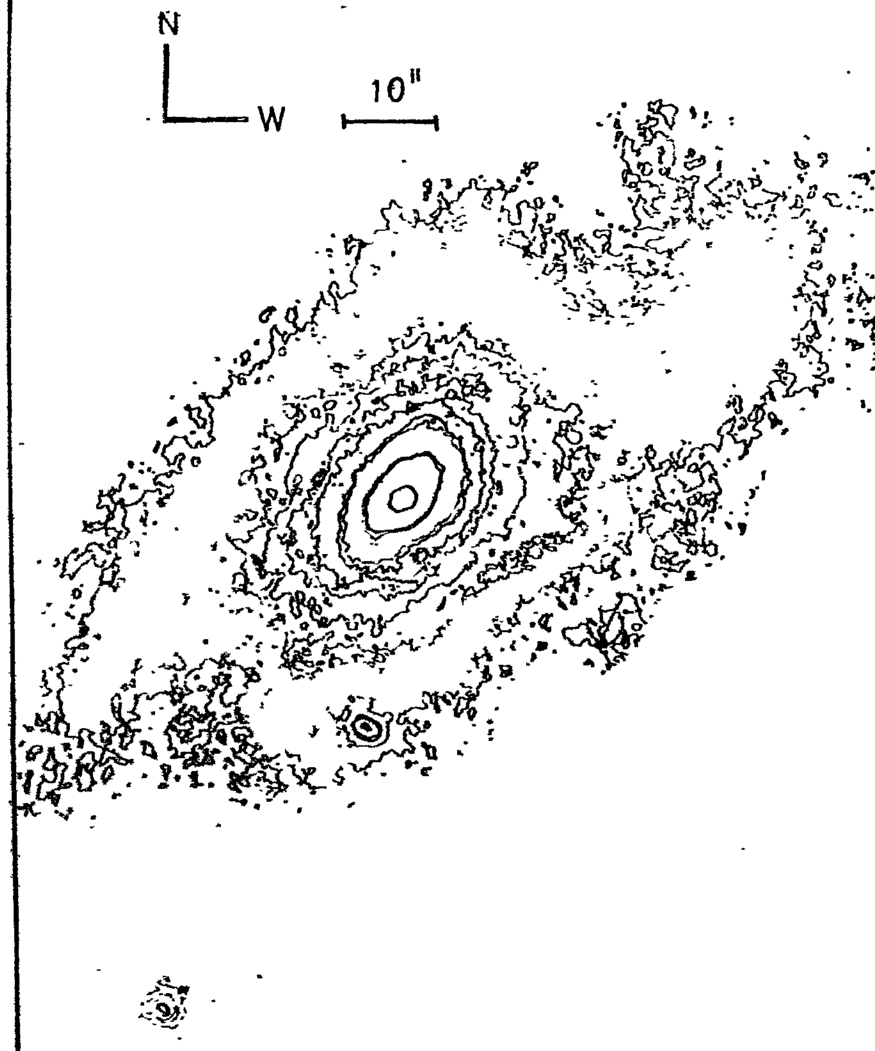

FIG.5.11 NGC 1415

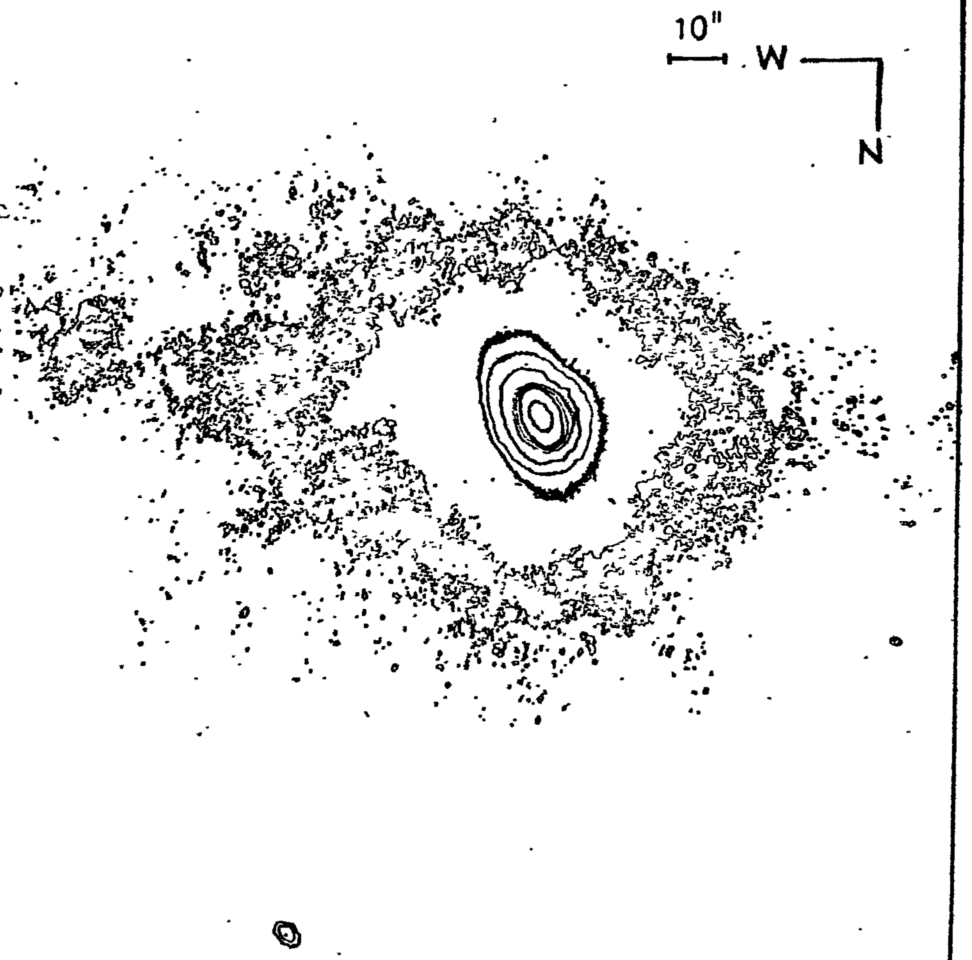

FIG.5.12 NGC 1433

5.12 NGC 1415

This is another example of $\epsilon\sigma$ type formation. The contours are presented in Figure 5.11 and the equivalent luminosity profile in Table 5.11 and Figure 5.29.

5.13 NGC 1433

This galaxy has a class ϵ formation with a slight distortion of the outer elliptical isophotes in the east. The major axis of the formation makes an angle of about 60° with the major axis of the main body of the galaxy. Contours are presented in Figure 5.12, and the equivalent profiles in Table 5.12 and Figure 5.28.

5.14 NGC 1530

A weak σ formation has a compact κ type for the central region. The spiral pattern of the inner regions opens out in the same direction as the outer spiral arms, but is wound tighter. The contours appear in Figure 5.13, and the equivalent profile in Figure 5.30 and in Table 5.13.

FIG.5.13 NGC1530

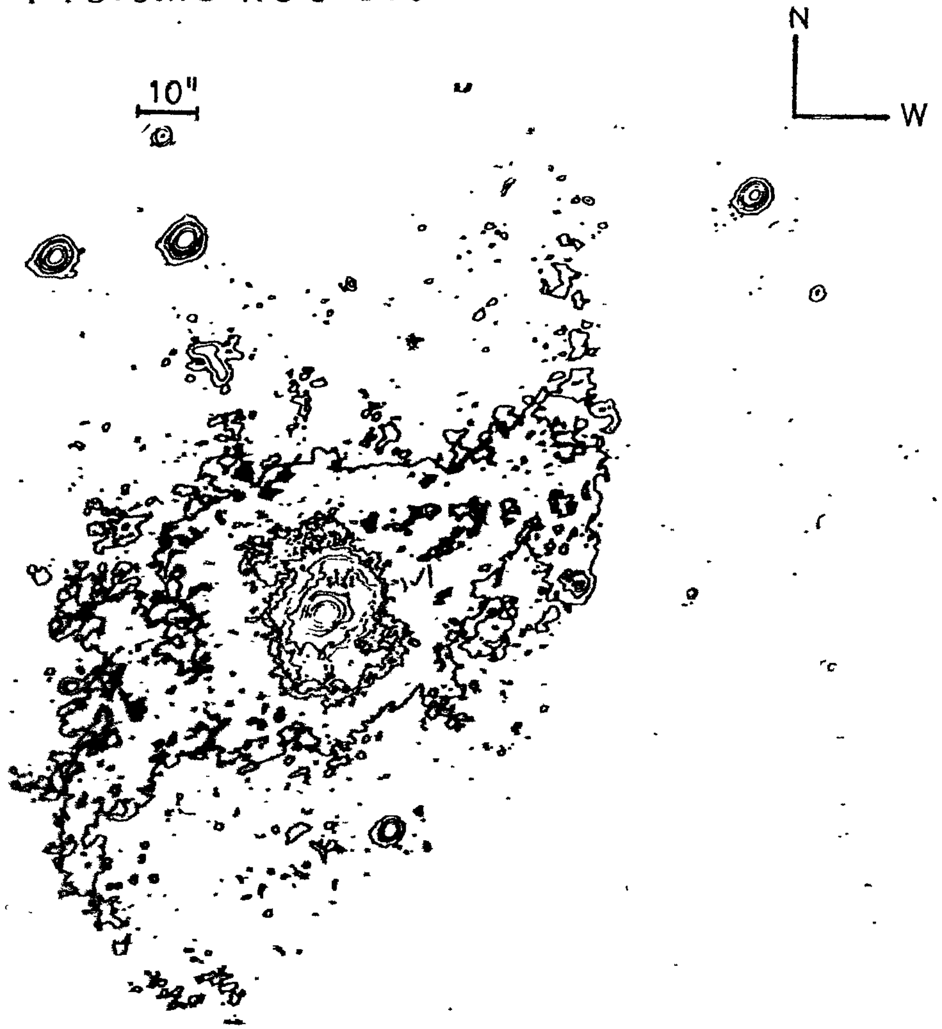

FIG.5.14 NGC 1672

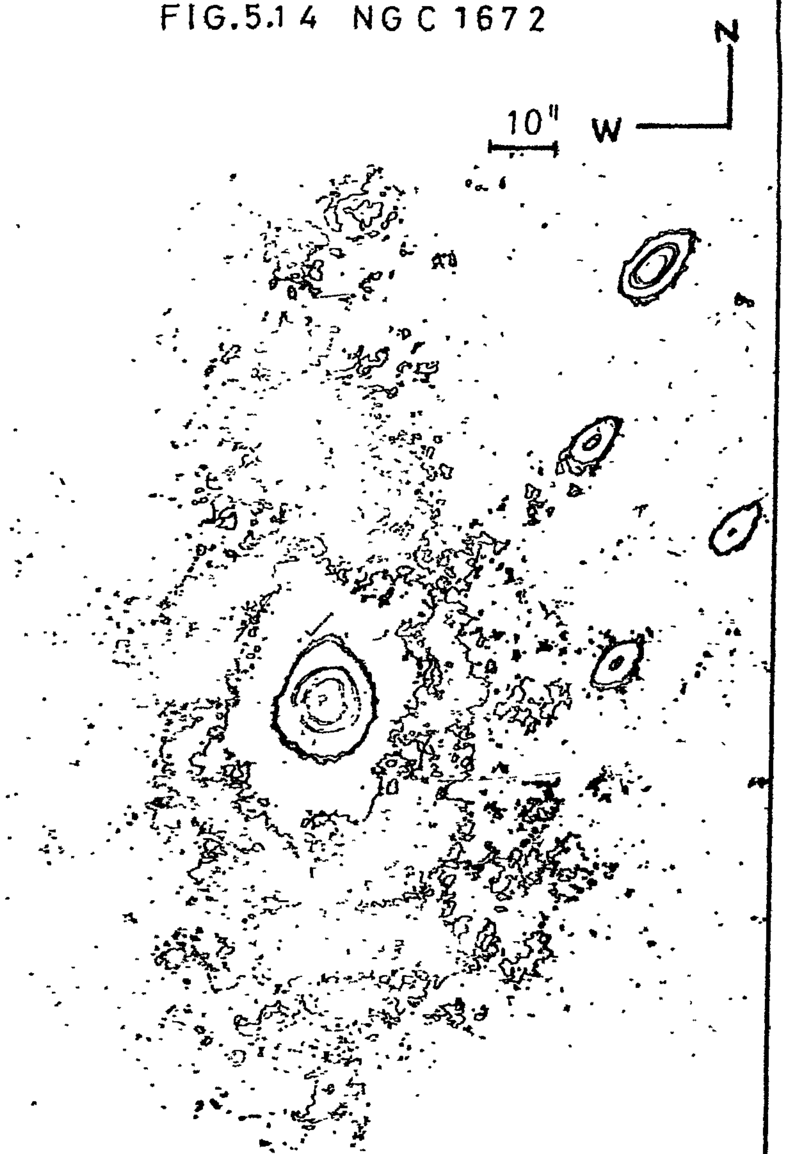

FIG. 5.15 NGC 1808

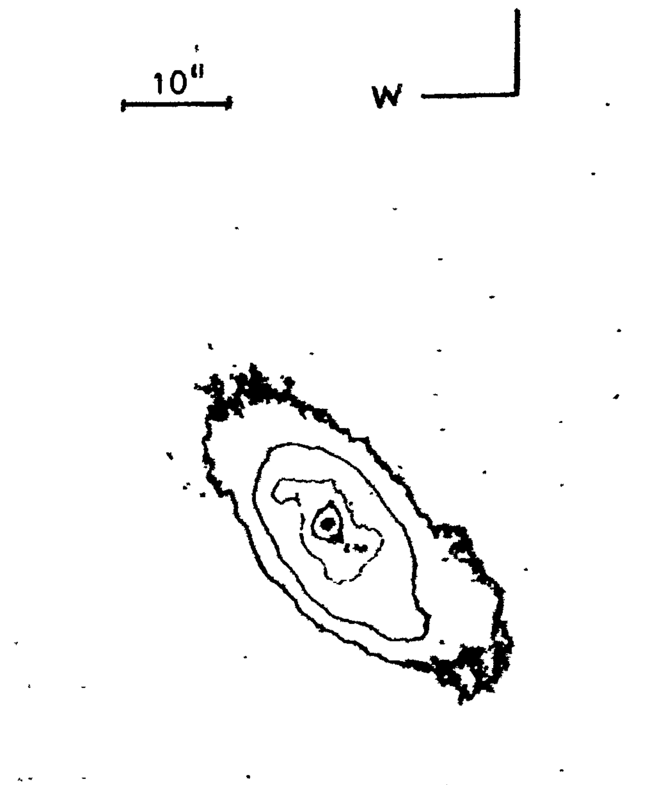

FIG. 5.16 NGC 2196

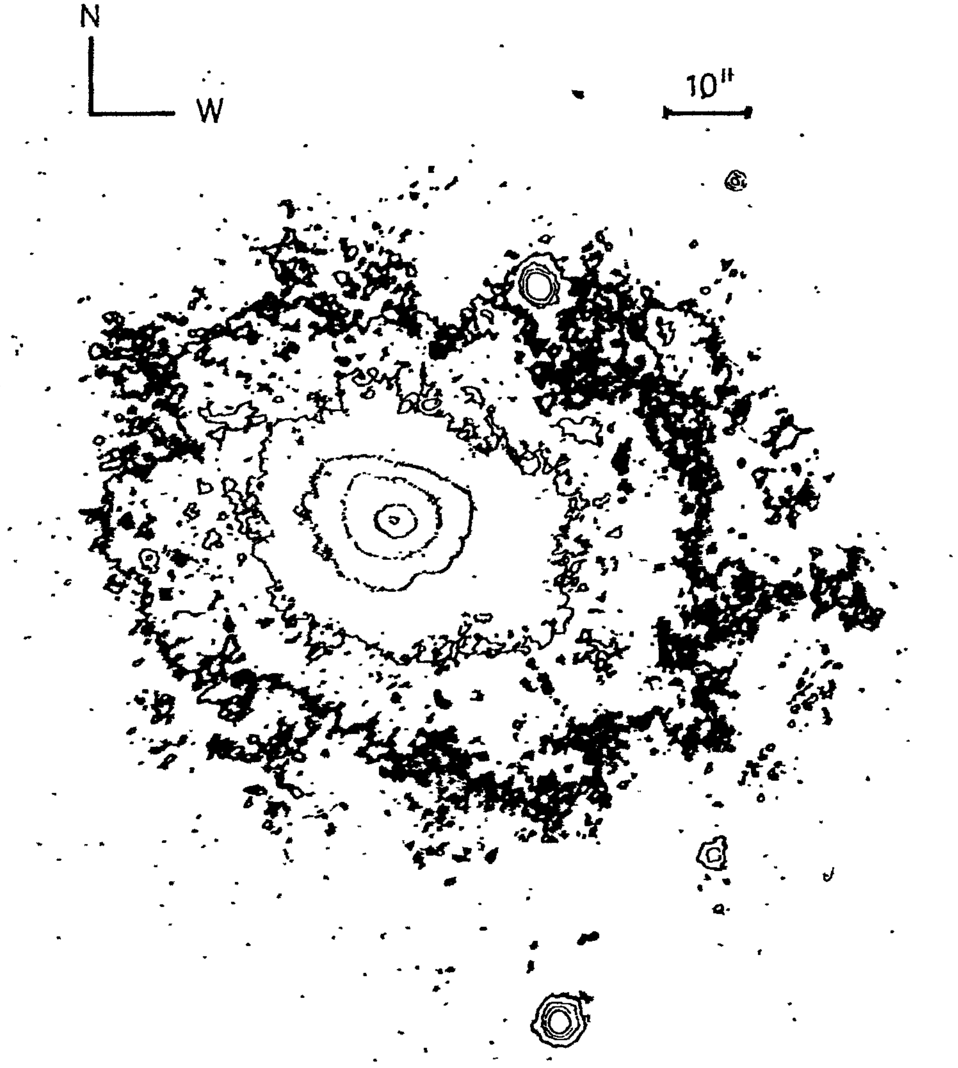

5.15 NGC 1672

This galaxy is grouped with $\epsilon\sigma$ formations because of some indications of rudimentary spiral structure.in the outermost regions of the perinuclear part of the galaxy. The inner isophotes exhibit pronounced oval distortion with a variation of position angle. The contours are presented in Figure 5.14 while the equivalent luminosity profile appears in Figure 5.29 and Table 5.14.

5.16 NGC 1808

This has a perinuclear formation somewhat similar to that of NGC 613, but it is more elongated. The nucleus is brighter relative to NGC 613. A rudimentary spiral structure is seen in the inner most region in the same direction as the outer spiral structure. Even the edge of the formation exhibits slight spiral distortion. The contours are presented in Figure 5.15 and the equivalent profile in Table 5.15 and Figure 5.30.

5.17 NGC 2196

This galaxy has an ϵ formation which tends a little towards σ . The outer isophotes of the formation resemble the outermost isophote of the perinuclear formation of NGC 613. The oval distortion is apparent.

FIG. 5.17 NGC 2903

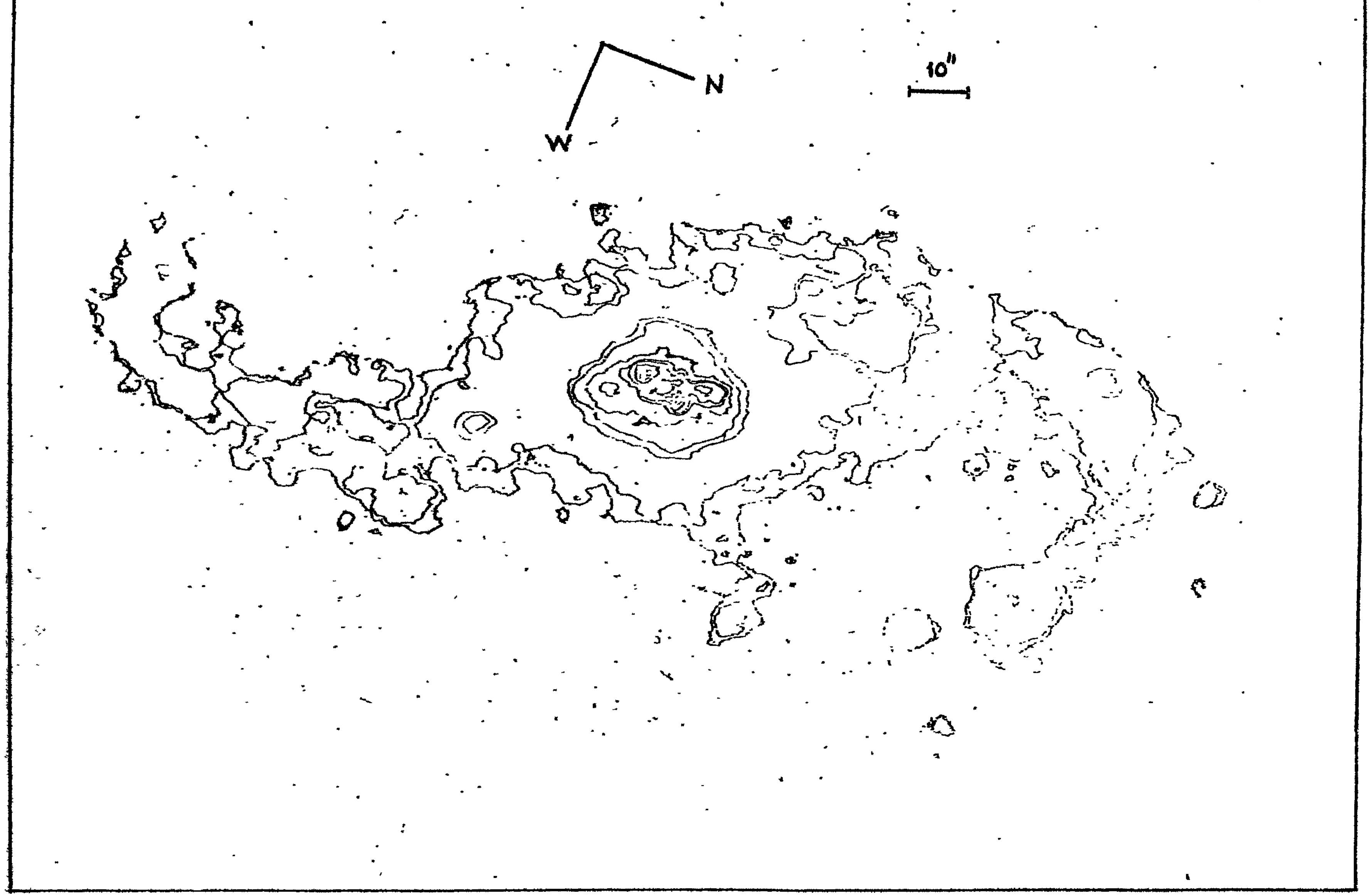

Contours appear in Figure 5.16 and profile in Table 5.16 and Figure 5.28.

5.18 NGC 2903

The σ type formation of this galaxy has already been compared with that of our galaxy, (Section 4.4). The hot spots are very bright and distinct. The central hot spot is very red and very much fainter than the other hot spots seen on blue photographs (Oka et al 1974 also cf. Chapter VI). The spiral pattern might be present with high inclination, but it is difficult to discern this due to the domination by a few bright hot spots. The symmetry of the hot spots with respect to the central red nucleus is evident. The outermost contours of the formation are distorted in a fashion intermediate between oval and spiral distortion (Figure 5.17). If the identification of this distortion is taken to be a spiral pattern, its direction is opposite to that of the outer spiral arms.

The equivalent luminosity profile is presented in Figure 5.30 and Table 5.17.

5.19 NGC 2935

The ϵ type formation of this galaxy shows a slight spiral distortion. The major axis of the

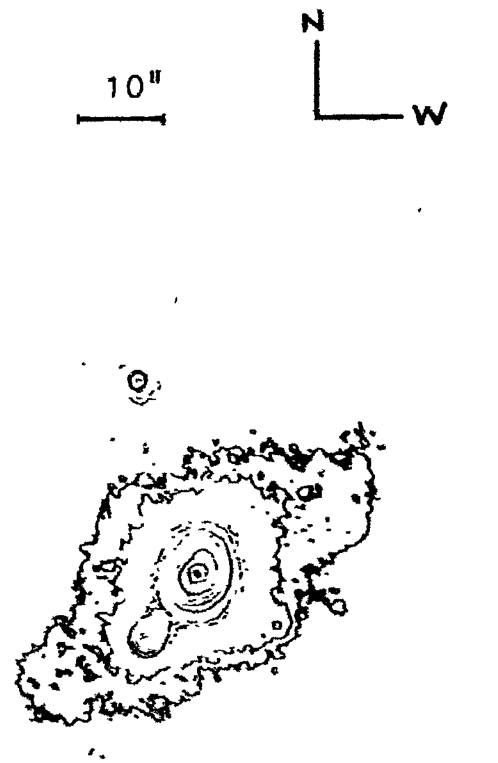

FIG.5.18 NGC 2935

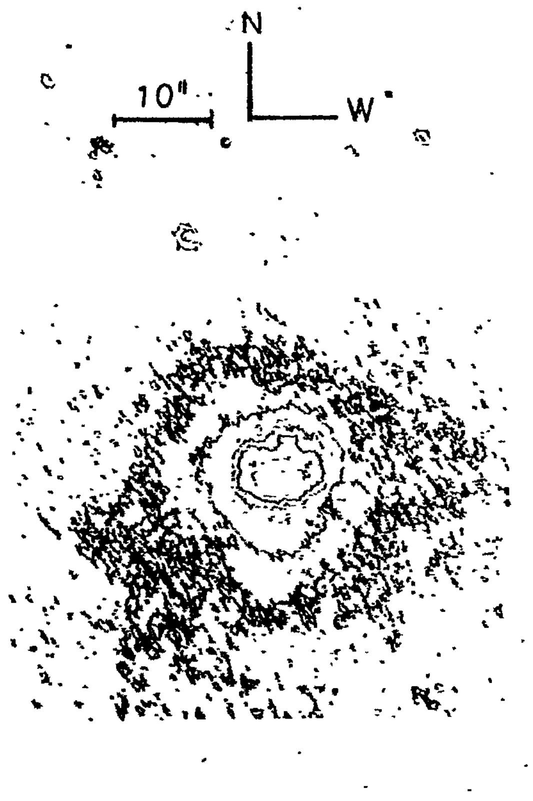

FIG.5.19 NGC 2997

FIG.5.20 NGC 3177

formation is at an angle of approximately 30° with the major axis of the main body (Figure 5.18). A field star is superposed near the edge of the formation and has been excluded from the equivalent luminosity profile (Figure 5.28, Table 5.18).

5.20 NGC 2997

The perinuclear formation of this galaxy is marginally in the σ class with a tendency towards ε . The outer isophote of the formation exhibits oval distortion. The nucleus is asymmetrically placed with respect to the centre of the intermediate contours (Figure 5.19). The equivalent luminosity profile appears in Figure 5.30 and Table 5.19.

5.21 NGC 3177

The central region of this galaxy shows spiral distortion typical of a σ type perinuclear formation. However, distinct hot spots are not visible. The contours are presented in Figure 5.20. The equivalent luminosity profile is shown in Figure 5.30 and the intensity values are listed in Table 5.20.

5.22 NGC 3310

A typical σ type formation. Hot spots and spiral distortion are apparent in the contours presented

FIG.5.21 NGC 3310

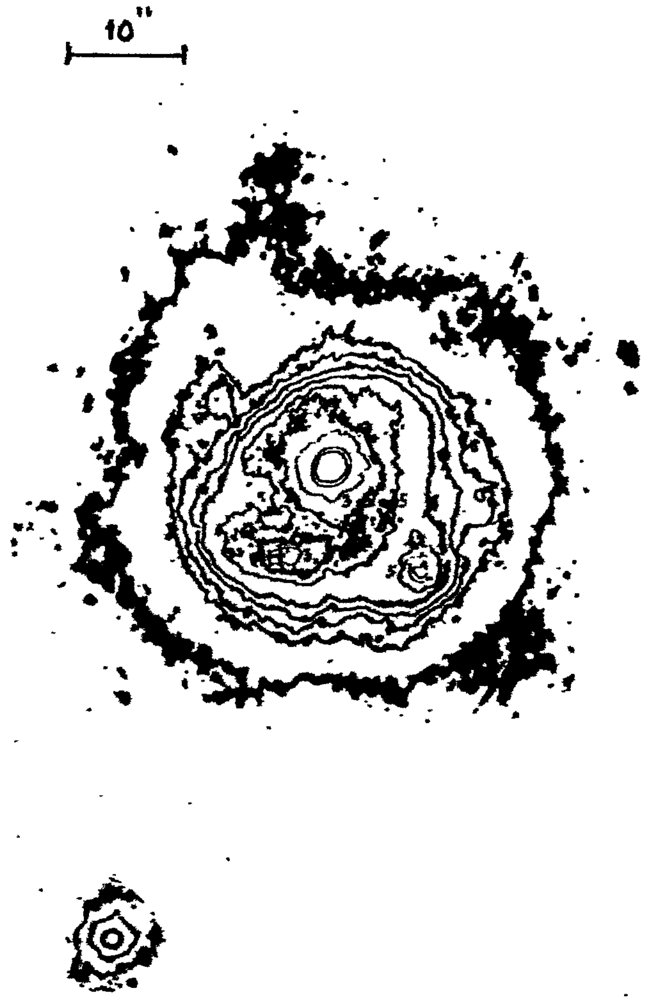

FIG.5.22 NGC 3351

FIG.5.23 NGC 3627

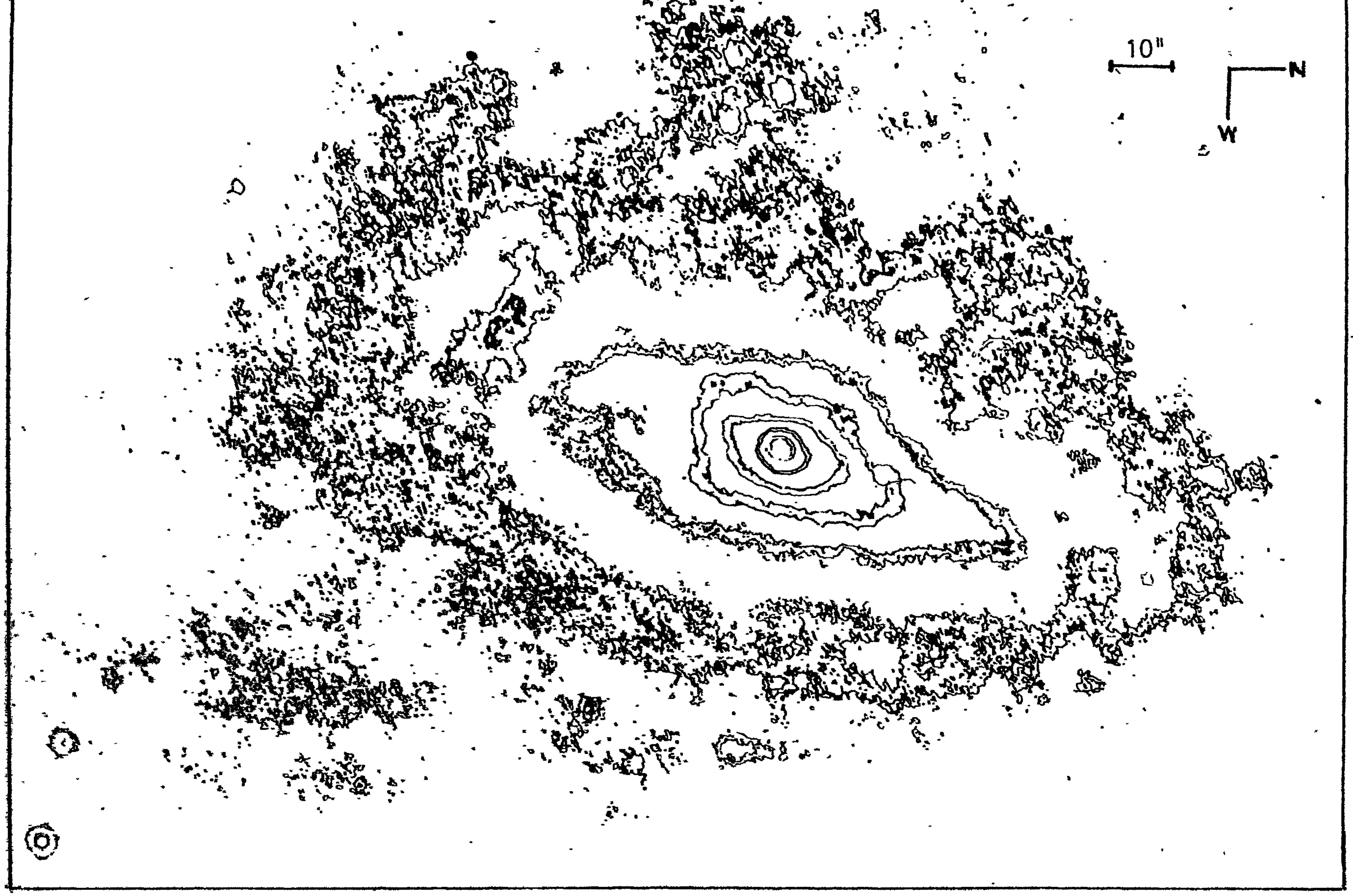

in Figure 5.21. The equivalent luminosity profile is presented in Figure 5.30 and Table 5.21.

5.23 NGC 3351

Another example of σ type perinuclear formation. Spiral distortion is, however, not very clear. Distinct hot spots are seen symmetrically placed with respect to the nucleus (Figure 5.22). The equivalent luminosity profile appears in Figure 5.30 and is listed in Table 5.22.

5.24 NGC 3627

Grouped with class ϵ , the perinuclear formation of this galaxy is not a typical example of the class. The contours presented in Figure 5.23 show that though the central region has nearly elliptical isophotes, the outer regions of the formation exhibit spiral distortion. Considering the fact that the perinuclear formation of this galaxy is the brightest among those investigated by us, one might expect such spiral distortions to be present in all classes of perinuclear formations. Some of these may, however, be too faint to be easily noticed in members of the group.

FIG. 5.24 NGC 3955

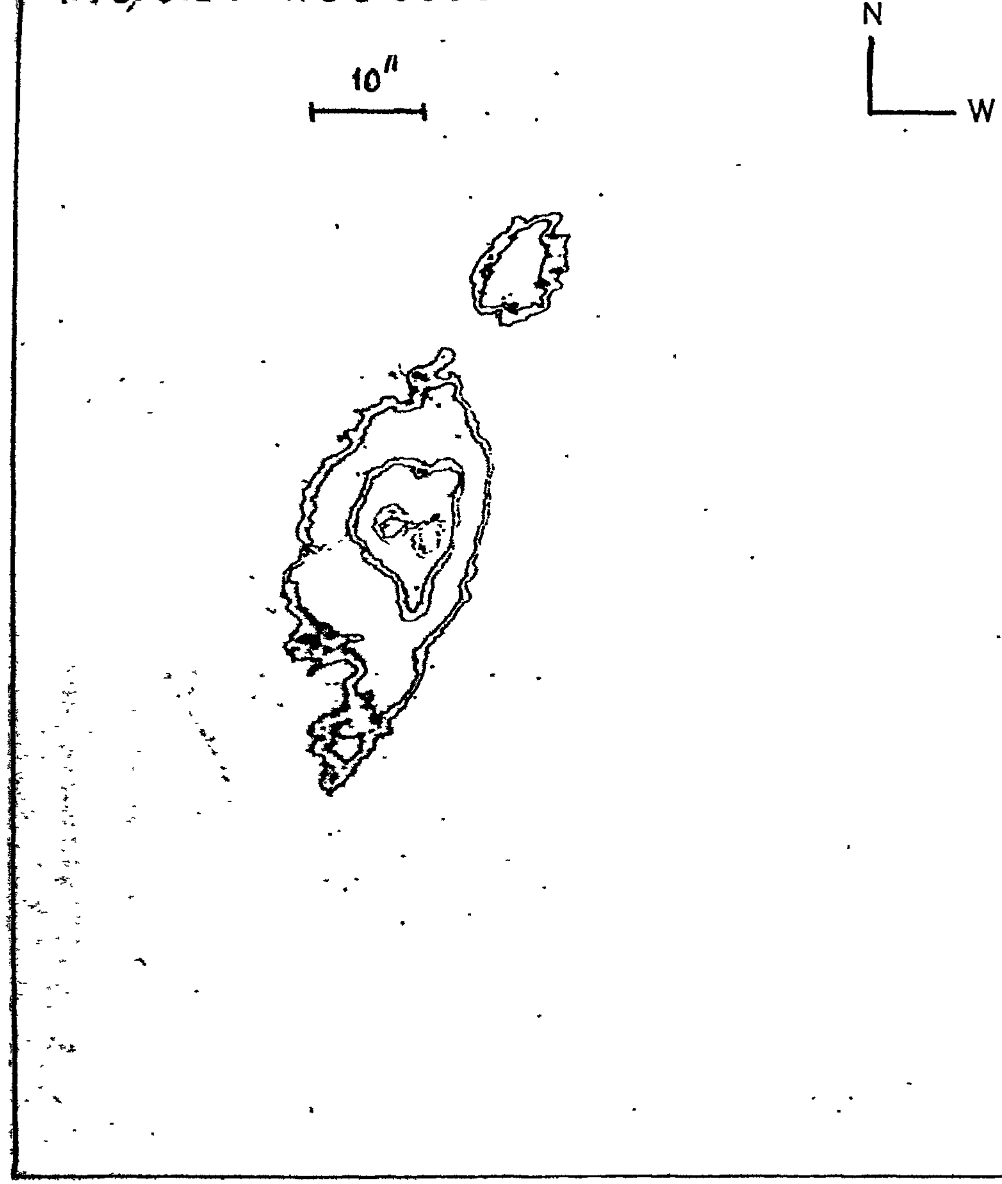

FIG. 5.25 NGC 4064

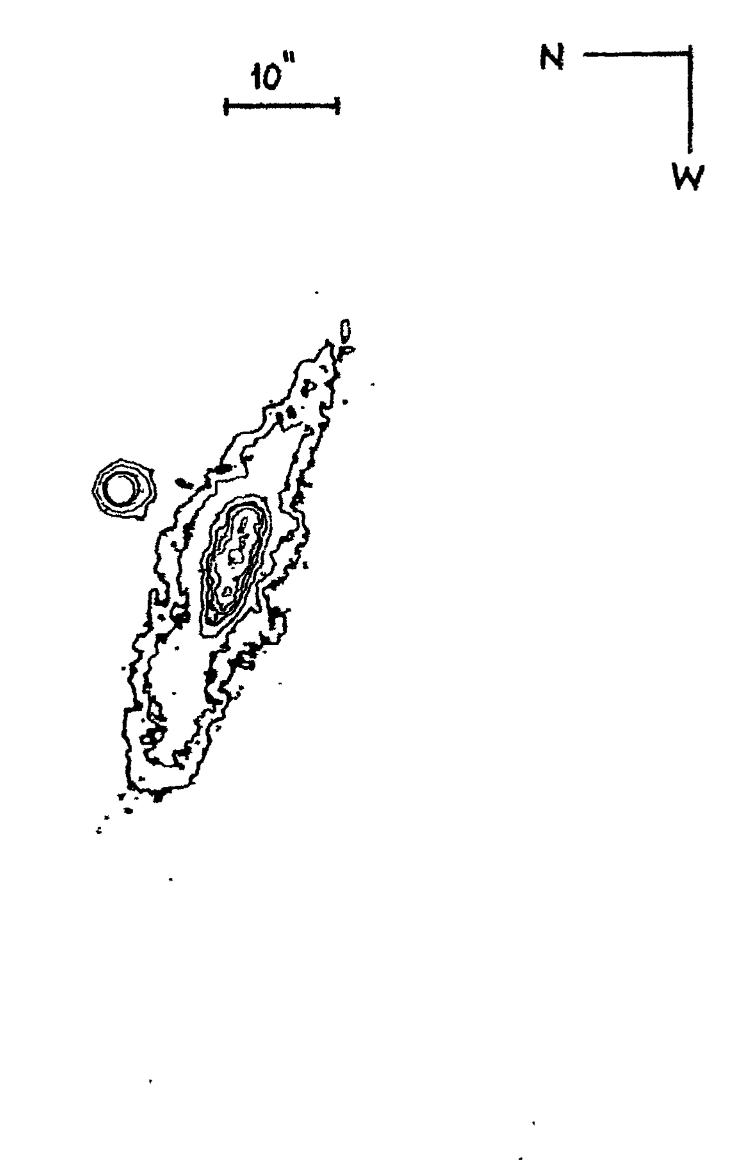

The equivalent luminosity profile is presented in Figure 5.28 and Table 5.23.

5.25 NGC 3955

The perinuclear formation of this galaxy is typical of formations of class τ . Hot spots are apparent in the contours presented in Figure 5.24. A slight spiral distortion is also present. The equivalent luminosity profile is presented in Figure 5.32 and listed in Table 5.24.

5.26 NGC 4064

This is another example of τ type formations. The contours presented in Figure 5.25 appear barlike. A few hot spots are seen in the central regions. The equivalent luminosity profile appears in Figure 5.32 and in Table 5.25.

5.27 NGC 5236

The perinuclear formation of this galaxy is a system with bright hot spots and is grouped with class σ by us. The oval distortions can be seen on the contours presented in Figure 5.26. No spiral features are evident. NGC 5236 is a relatively nearby galaxy (distance of 5.5 Mpc from the velocity 275 km/s

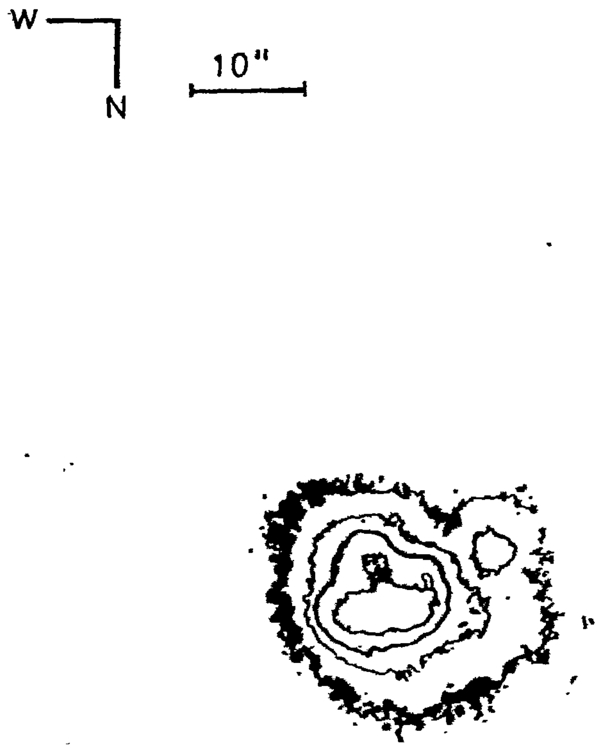

FIG. 5.26 NGC 5236

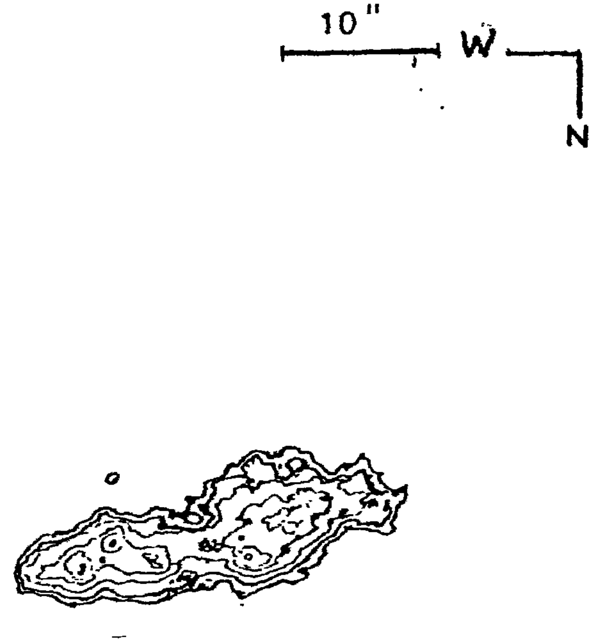

FIG. 5.27 NGC 7741

of Table 3.3 and H_o = 50 kms^{-1} kpc^{-1}). One may thus be looking at only the inner-most regions of the formation. Most probably we would have grouped the perinuclear formation of this galaxy with class $\mathcal{K}$, if the galaxy were placed ten times farther, an average distance of the galaxies investigated by us. The equivalent luminosity profile presented in Figure 5.30 and in Table 5.26 favour this point of view.

5.28 NGC 7741

This is another example of $\mathcal{L}$ type formations. Several faint hot spots are visible in the barlike formation of low surface brightness (Figure 5.27). The equivalent luminosity profile appears in Figure 5.32 and in Table 5.27.

Table 5.1

Equivalent Luminosity Profile of NGC 210

Isophote	Equivalent Radius r* (arcsec)	Log I
1	0.61	0.747
2	1.25	0.569
3	2.74	0.140
4	3.03	0.121
5	4.33	-0.208
6	4.87	-0.247
7	6.21	-0.367
8	6.65	-0.526
9	7.41	-0.593
10	8.62	-0.628
11	10.79	-0.682
12	11.75	-0.685
13	20.36	-0.738
14	25.65	-0.757

Table 5.2

Equivalent Luminosity Profile of NGC 255

Isophote	Equivalent Radius r* (arcsec)	Log I
1	1.17	0.976
2	2.01	0.880
3	2.95	0.692
4	4.22	0.538
5	6.96	0.308
6	14.77	0.052
7	19.41	-0.009

Table 5.3

Equivalent Luminosity Profile of NGC 613

Isophote	Equivalent Radius r* (arcsec)	Log I
1	0.33	0.985
2	0.73	0.895
3	1.41	0.833
4	2.13	0.807
5	2.71	0.698
6	3.89	0.559
7	5.16	0.547
8	5.79	0.480
9	7.96	0.305
10	11.71	0.100

Table 5.4

Equivalent Luminosity Profile of NGC 922

Isophote	Equivalent Radius r^* (arcsec)	Log I
1	2.46	0.815
2	3.58	0.635
3	4.28	0.465
4	5.96	0.395
5	11.90	0.320
6	24.11	0.260

Table 5.5

Equivalent Luminosity Profile of NGC 1087

Isophote	Equivalent Radius r* (arcsec)	Log I
1	1.11	0.943
2	1.62	0.828
3	1.95	0.785
4	2.77	0.642
5	3.88	0.550
6	5.61	0.422
7	8.63	0.405
8	-	-
9	21.84	0.365

Table 5.6

Equivalent Luminosity Profile of NGC 1097

Isophote	Equivalent Radius r* (arcsec)	Log I
1	1.71	0.715
2	5.65	0.425
3	6.82	0.298
4	10.27	0.137
5	10.98	0.090
6	12.53	0.059
7	13.55	-0.003
8	17.07	-0.115
9	18.87	-0.135
10	23.55	-0.205
11	29.54	-0.280
12	39.92	-0.300
13	51.94	-0.396

Table 5.7

Equivalent Luminosity Profile of NGC 1140

Isophote	Equivalent Radius r* (arcsec)	Log I
1	0.34	0.959
2	1.97	0.725
3	2.69	0.544
4	6.43	0.135
5	7.36	0.107

Table 5.8

Equivalent Luminosity Profile of NGC 1300

Isophote	Equivalent Radius r* (arcsec)	Log I
1	0.0	1.000
2	2.83	0.701
3	4.36	0.597
4	5.61	0.482
5	8.44	0.373
6	12.01	0.193
7	19.17	0.111

Table 5.9

Equivalent Luminosity Profile of NGC 1326

Isophote	Equivalent Radius r* (arcsec)	Log I
1	1.23	0.893
2	3.10	0.724
3	4.50	0.555
4	5.68	0.380
5	8.05	0.190
6	15.83	0.002
7	29.17	-0.148

Table 5.10

Equivalent Luminosity Profile of NGC 1365

Isophote	Equivalent Radius r* (arcsec)	Log I
1	1.00	0.851
2	2.11	0.641
3	2.75	0.544
4	5.69	0.376
5	8.46	0.214
6	9.12	0.193
7	11.38	0.124
8	13.24	0.083
9	19.97	0.017

Table 5.11

Equivalent Luminosity Profile of NGC 1415

Isophote	Equivalent Radius r* (arcsec)	Log I
1	1.81	0.670
2	2.62	0.583
3	2.82	0.560
4	3.15	0.368
5	3.50	0.345
6	6.45	0.242
7	7.38	0.192
8	9.22	0.152
9	11.46	0.142
10	21.76	0.042

Table 5.12

Equivalent Luminosity Profile of NGC 1433

Isophote	Equivalent Radius r* (arcsec)	Log I
1	2.31	0.820
2	2.61	0.798
3	4.50	0.635
4	4.68	0.620
5	5.46	0.575
6	6.03	0.561
7	8.12	0.499
8	8.37	0.438
9	10.74	0.310
10	13.07	0.213
11	30.48	0.119
12	43.80	0.069

Table 5.13

Equivalent Luminosity Profile of NGC 1530

Isophote	Equivalent Radius r* (arcsec)	Log I
1	1.49	0.889
2	2.13	0.810
3	3.04	0.693
4	4.03	0.643
5	7.36	0.583
6	8.26	0.563
7	10.15	0.513
8	13.37	0.491
9	34.76	0.403

Table 5.14

Equivalent Luminosity Profile of NGC 1672

Isophote	Equivalent Radius r* (arcsec)	Log I
1	0.40	0.965
2	3.01	0.947
3	3.62	0.776
4	4.84	0.628
5	5.73	0.556
6	8.33	0.487
7	8.84	0.297
8	19.38	0.132
9	36.78	0.122

Table 5.15

Equivalent Luminosity Profile of NGC 1808

Isophote	Equivalent radius r* (arcsec)	Log I
1	0.51	0.958
2	1.70	0.783
3	4.73	0.630
4	6.60	0.263
5	10.96	0.153

Table 5.16

Equivalent Luminosity Profile of NGC 2196

Isophote	Equivalent Radius r* (arcsec)	Log I
1	0.47	0.922
2	2.11	0.597
3	5.54	0.504
4	9.07	0.367
5	18.80	0.056
6	34.58	0.006

Table 5.17

Equivalent Luminosity Profile of NGC 2903

Isophote	Equivalent Radius r* (arcsec)	Log I
1	0.40	0.950
2	1.45	0.833
3	2.92	0.728
4	5.05	0.652
5	6.23	0.600
6	8.89	0.450
7	12.25	0.385
8	13.58	0.380

Table 5.18

Equivalent Luminosity Profile of NGC 2935

Isophote	Equivalent Radius r* (arcsec)	Log I
1	0.32	0.980
2	0.78	0.870
3	2.42	0.702
4	3.07	0.602
5	3.35	0.503
6	4.51	0.419
7	5.24	0.297
8	5.83	0.262
9	11.05	0.092
10	16.25	0.065

Table 5.19

Equivalent Luminosity Profile of NGC 2997

Isophote	Equivalent Radius r* (arcsec)	Log I
1	0.69	0.897
2	1.47	0.759
3	2.68	0.614
4	4.37	0.567
5	5.29	0.457
6	6.22	0.422
7	8.77	0.292
8	15.67	0.177

Table 5.20

Equivalent Luminosity Profile of NGC 3177

Isophote	Equivalent Radius r* (arcsec)	Log I
1	0.45	0.838
2	1.55	0.588
3	2.54	0.513
4	8.09	0.383

Table 5.21

Equivalent Luminosity Profile of NGC 3310

Isophotes	Equivalent Radius r* (arcsec)	Log I
1	1.62	0.676
2	1.77	0.522
3	2.57	0.322
4	4.60	0.215
5	8.69	0.188
6	9.48	0.082
7	10.01	0.066
8	11.19	0.007
9	12.67	-0.013
10	17.77	-0.039

Table 5.22

Equivalent Luminosity Profile of NGC 3351

Isophote	Equivalent Radius r* (arcsec)	Log I
1	0.46	0.956
2	1.29	0.906
3	1.80	0.832
4	2.51	0.778
5	3.76	0.565
6	4.15	0.488
7	5.01	0.408
8	6.02	0.328
9	7.65	0.278
10	10.95	0.178

Table 5.23

Equivalent Luminosity Profile of NGC 3627

Isophote	Equivalent Radius r* (arcsec)	Log I
1	1.61	0.825
2	1.94	0.762
3	3.43	0.584
4	3.64	0.569
5	6.54	0.377
6	7.71	0.353
7	11.14	0.227
8	13.06	0.175
9	20.14	0.142
10	22.56	0.102
11	43.51	-0.043
12	58.36	-0.063

Table 5.24

Equivalent Luminosity Profile of NGC 3955

Isophote	Equivalent Radius r* (arcsec)	Log I
1	1.51	0.973
2	2.24	0.925
3	4.98	0.858
4	5.78	0.790
5	10.92	0.680
6	12.66	0.665

Table 5.25

Equivalent Luminosity Profile of NGC 4064

Isophote	Equivalent Radius r* (arcsec)	Log I
1	0.86	0.985
2	2.62	0.910
3	3.33	0.889
4	3.50	0.855
5	4.13	0.805
6	8.19	0.732
7	10.99	0.690

Table 5.26

Equivalent Luminosity Profile of NGC 5236

Isophote	Equivalent Radius r*(arcsec)	Log I
1	3.38	0.625
2	5.40	0.370
3	7.36	0.090
4	11.31	-0.135

Table 5.27

Equivalent Luminosity Profile of NGC 7741

Isophote	Equivalent Radius r^* (arcsec)	Log I
1	0.42	0.965
2	1.76	0.948
3	3.40	0.900
4	5.11	0.872
5	6.61	0.860
6	7.04	0.835

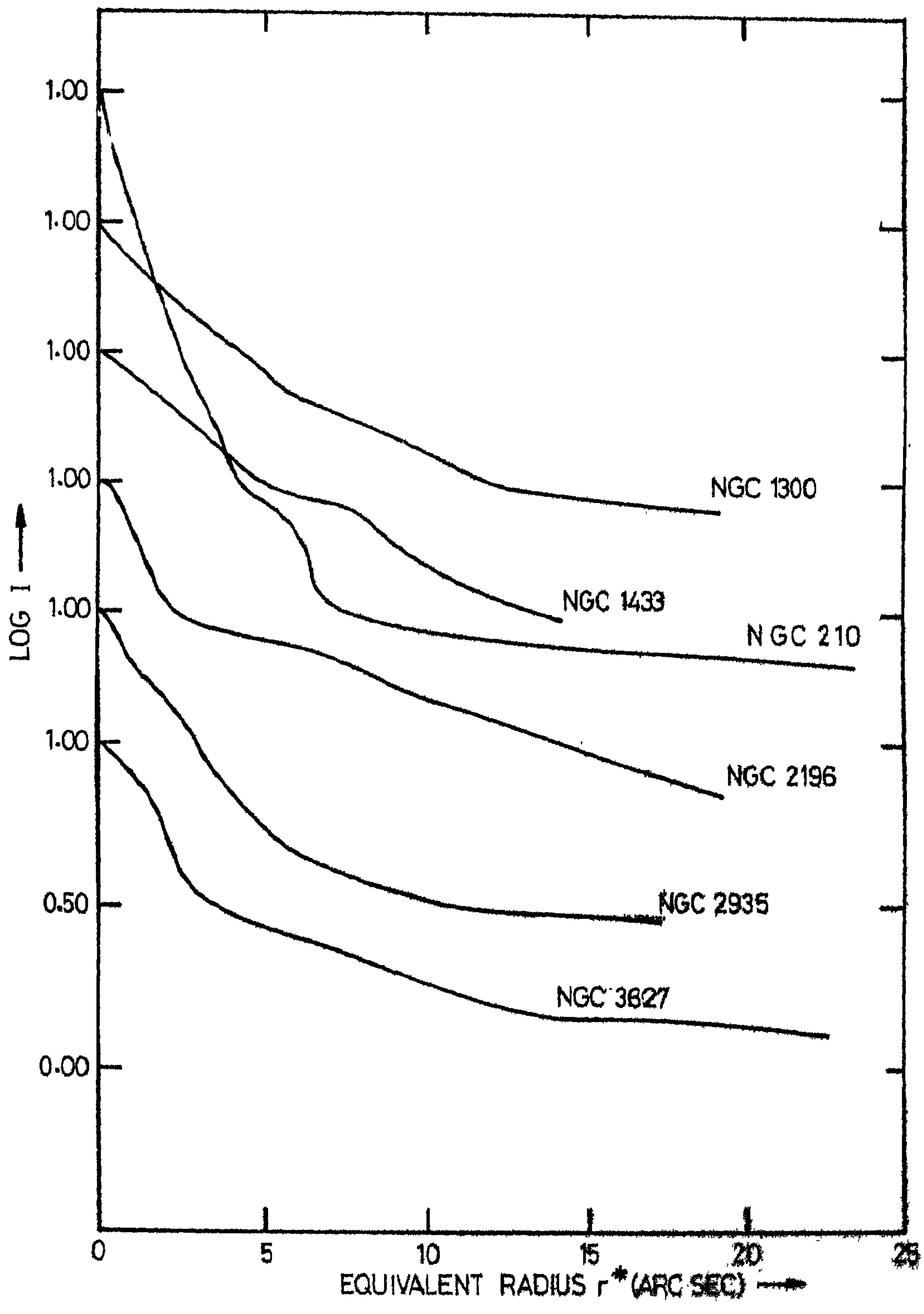

Fig. 5.28 Equivalent luminosity profiles of formations of class E

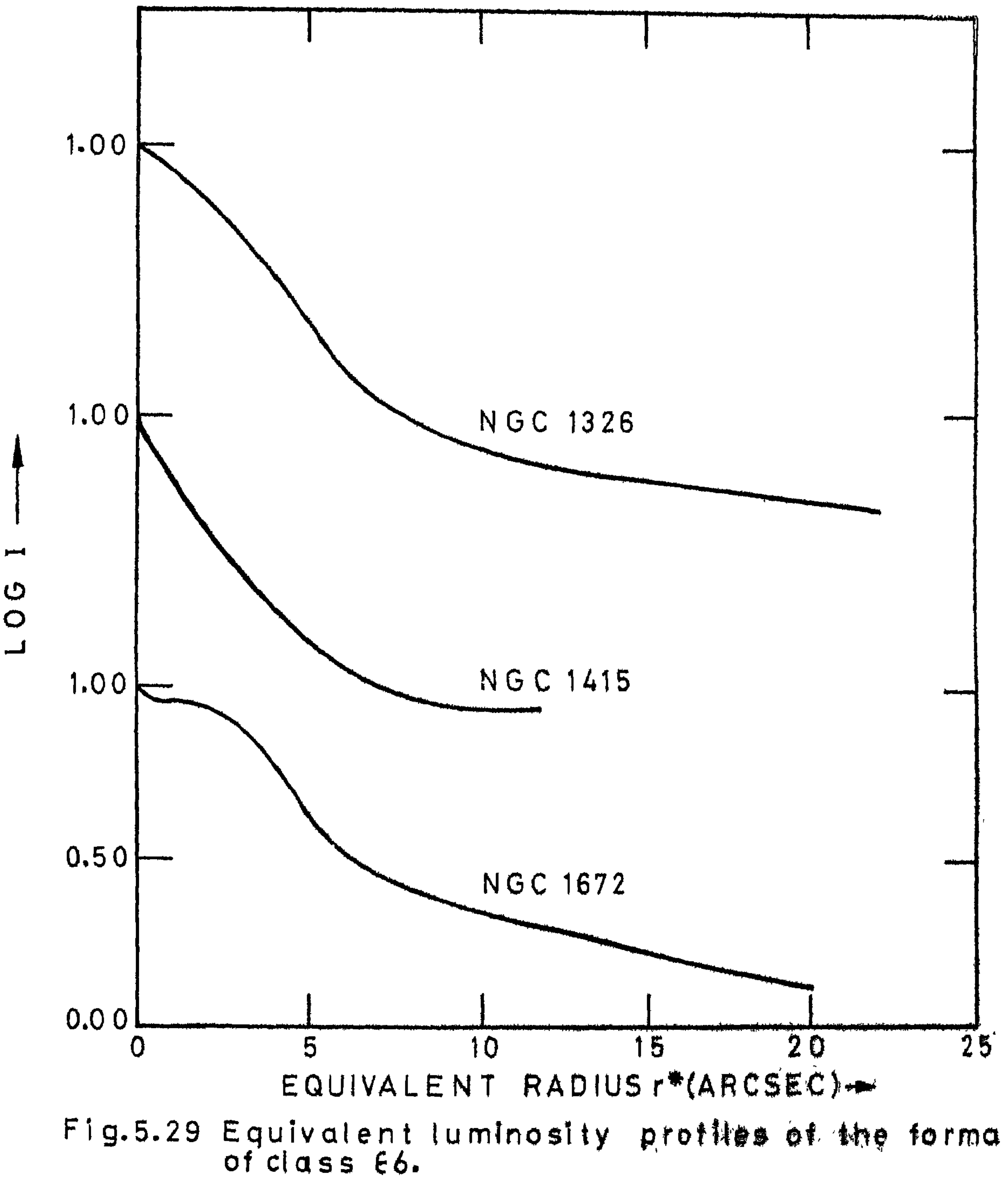

Fig.5.29 Equivalent luminosity profiles of the formations of class E6.

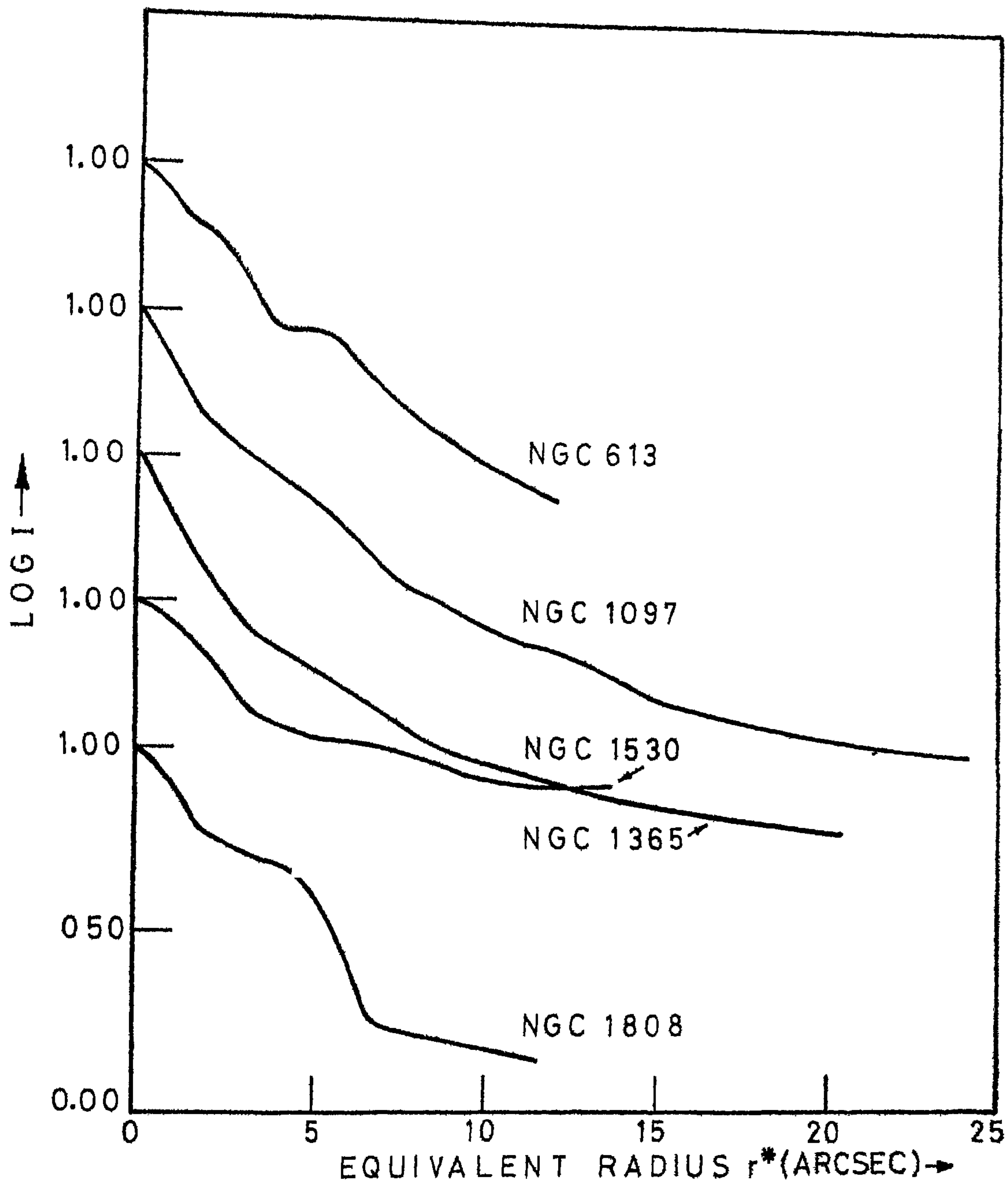

Fig.5.30 Equivalent luminosity profiles of the formations of class 6. The κ type NGC1530 is also included.

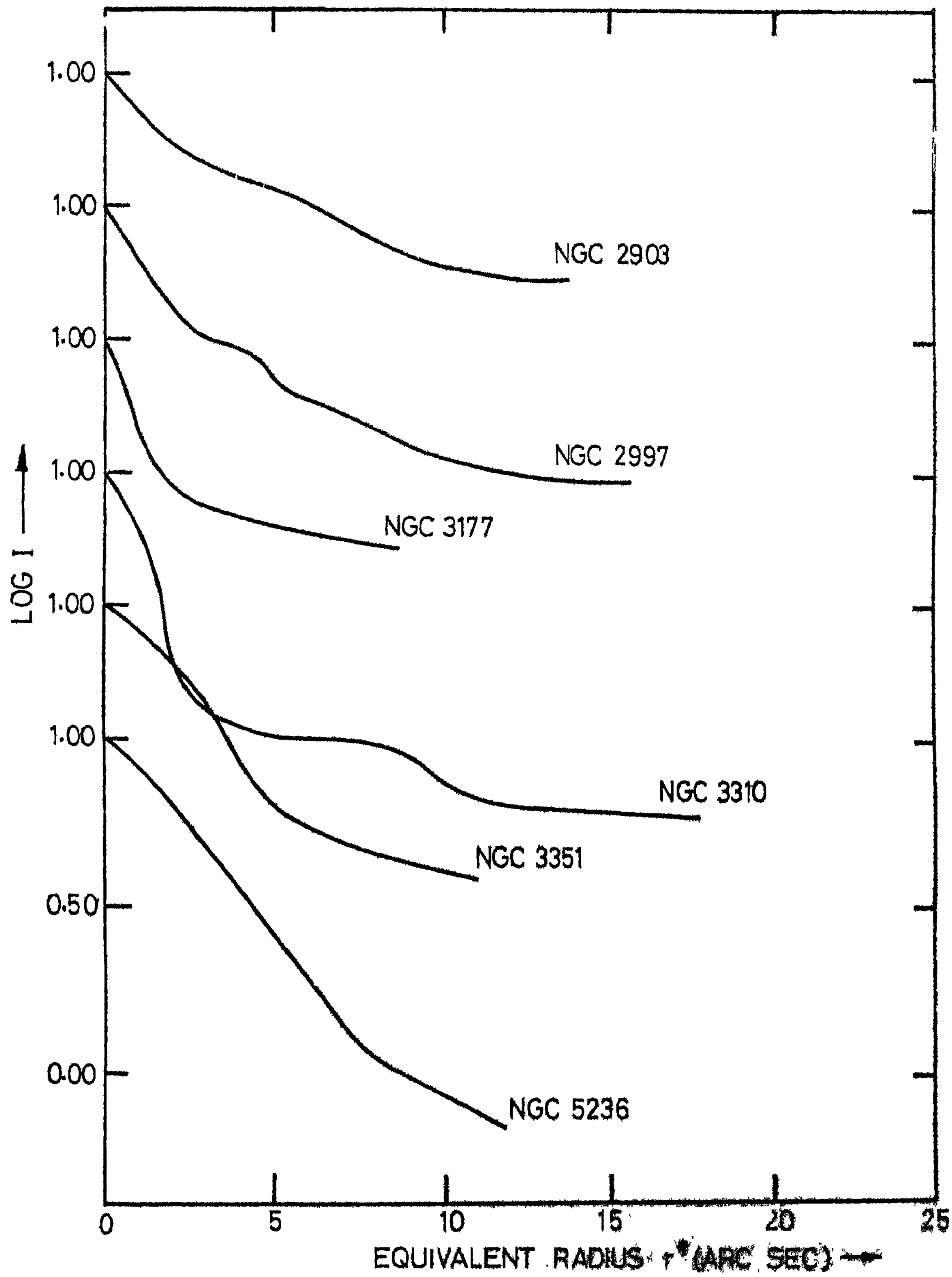

Fig. 5.30 Continued

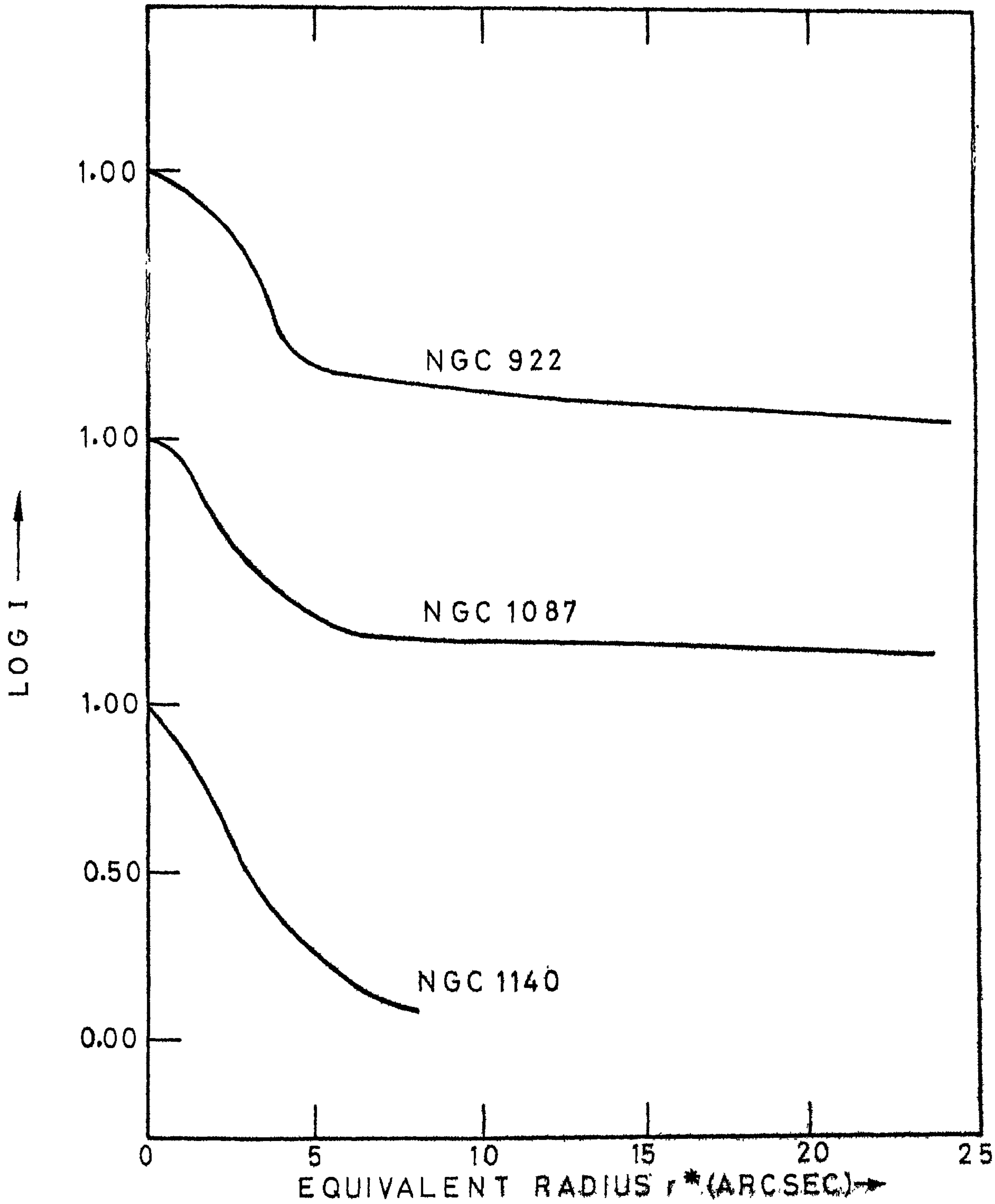

Fig. 5.31 Equivalent luminosity profiles of the formations of class 6ι.

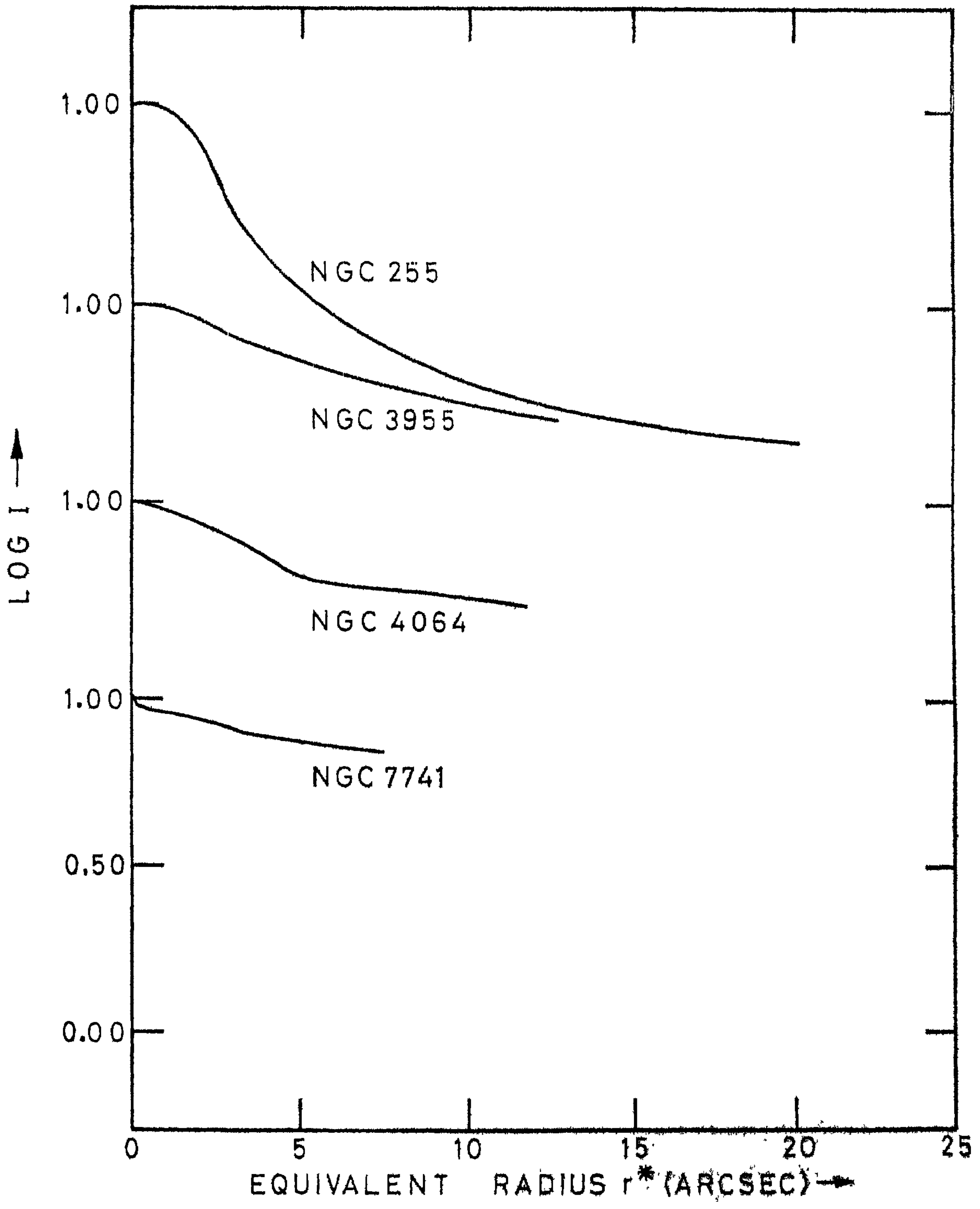

Fig. 5.32 Equivalent profiles of the formations of class t

CHAPTER 6

STRUCTURE OF THE CENTRAL REGIONS OF GALAXIES

The central regions of galaxies investigated in Chapters 4 and 5 are characterized by two distinct components: (a) a nucleus clearly visible in Class ϵ less prominent in class σ and probably absent in class η, and (b) a perinuclear formation. These two subsystems give rise to abrupt changes in the gradient of the equivalent luminosity profiles (Figures 5.28 - 5.32). The structure and the content of the two subsystems may be investigated by the study of their colours and luminosity distributions and appear distinctly different. We will examine in the following sections the colour distributions of the central regions of a few galaxies and the mean equivalent profiles of the individual classes of the perinuclear formations.

6.1 Colour Distribution in the Central Formations of Galaxies

The colour distribution proves very useful in estimating different populations and different subsystems in galaxies. With this aspect in mind we have observed one galaxy of type ϵ and five of type σ in the bands

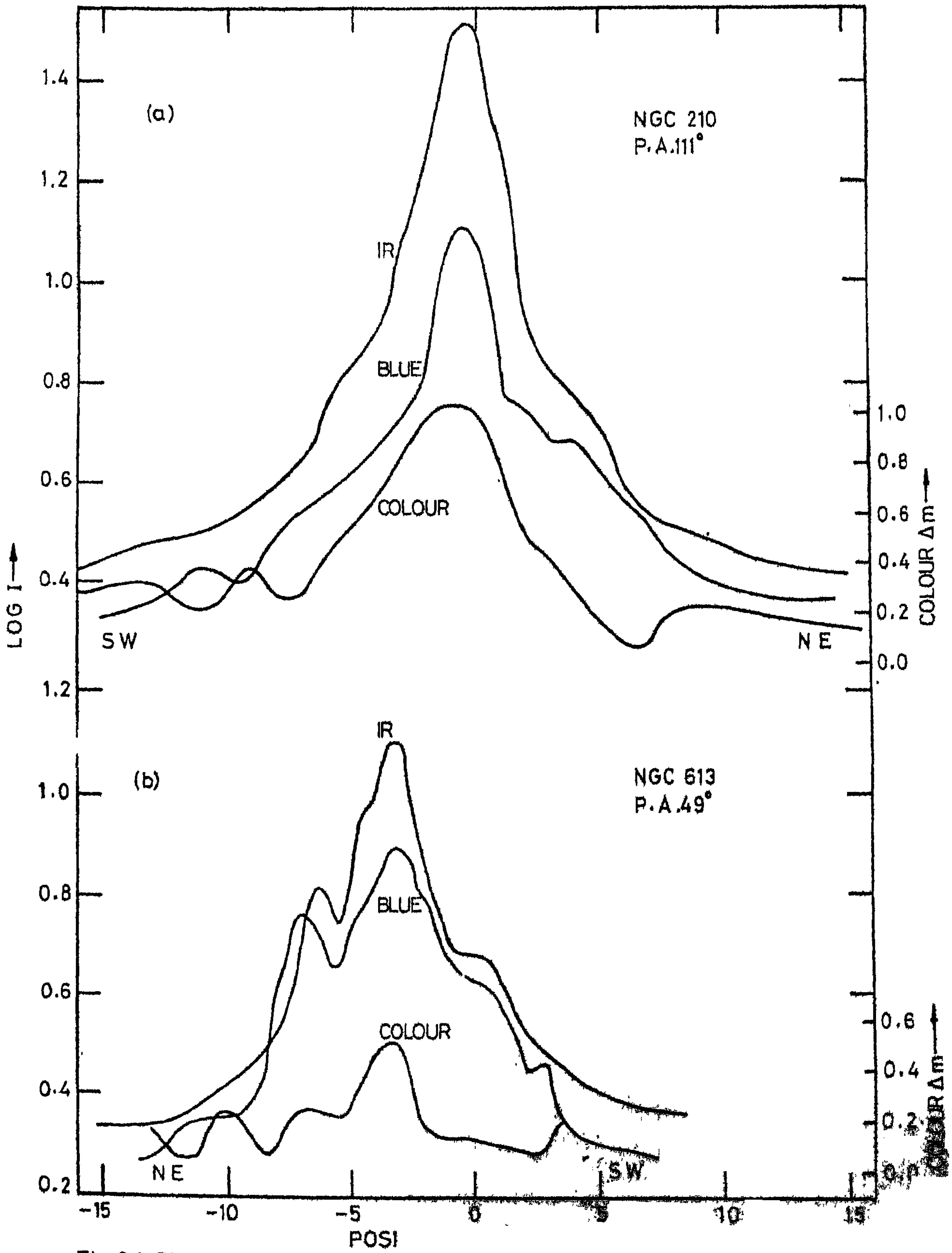

Fig.6.1 Blue and infrared profil
perinuclear formations. (a) NGC

as farthest apart as possible with the image tube camera used (λ_{eff} 4200Å and 7600Å).

The blue, infrared and the blue-infrared colour profiles of NGC 210 are shown in Figure 6.1 (a) scanned along the position angle of 21°. The nucleus of this galaxy is redder than the perinuclear formation by $0^m.8$. There is no appreciable variation in colour in the perinuclear region within a radius of 15 arcsec.

The blue, infrared and colour profiles of NGC 613 shown in Figure 6.1 (b) are also similar to the pattern exhibited by NGC 210, with the nucleus $0^m.4$ redder than the perinuclear region.

While the nucleus of NGC 1097 (Figure 6.1 c) is $0^m.43$ brighter than the outer parts of the perinuclear region, the region within 10 arcsecs of the centre is also redder. The reddest region outside of the nucleus is a diffuse emission region 6 arcsecs South-East of nucleus in the position angle of 58°.

NGC 1365 (Figure 6.1d) has a nucleus which is redder than the outer perinuclear region by $0^m.4$. The inner part has a plateau at $0^m.1$ colour with a peak of $0^m.2$ between the two hot spots 3.5 and 6.5 arcsecs North-West of the nucleus in the position angle 25°.

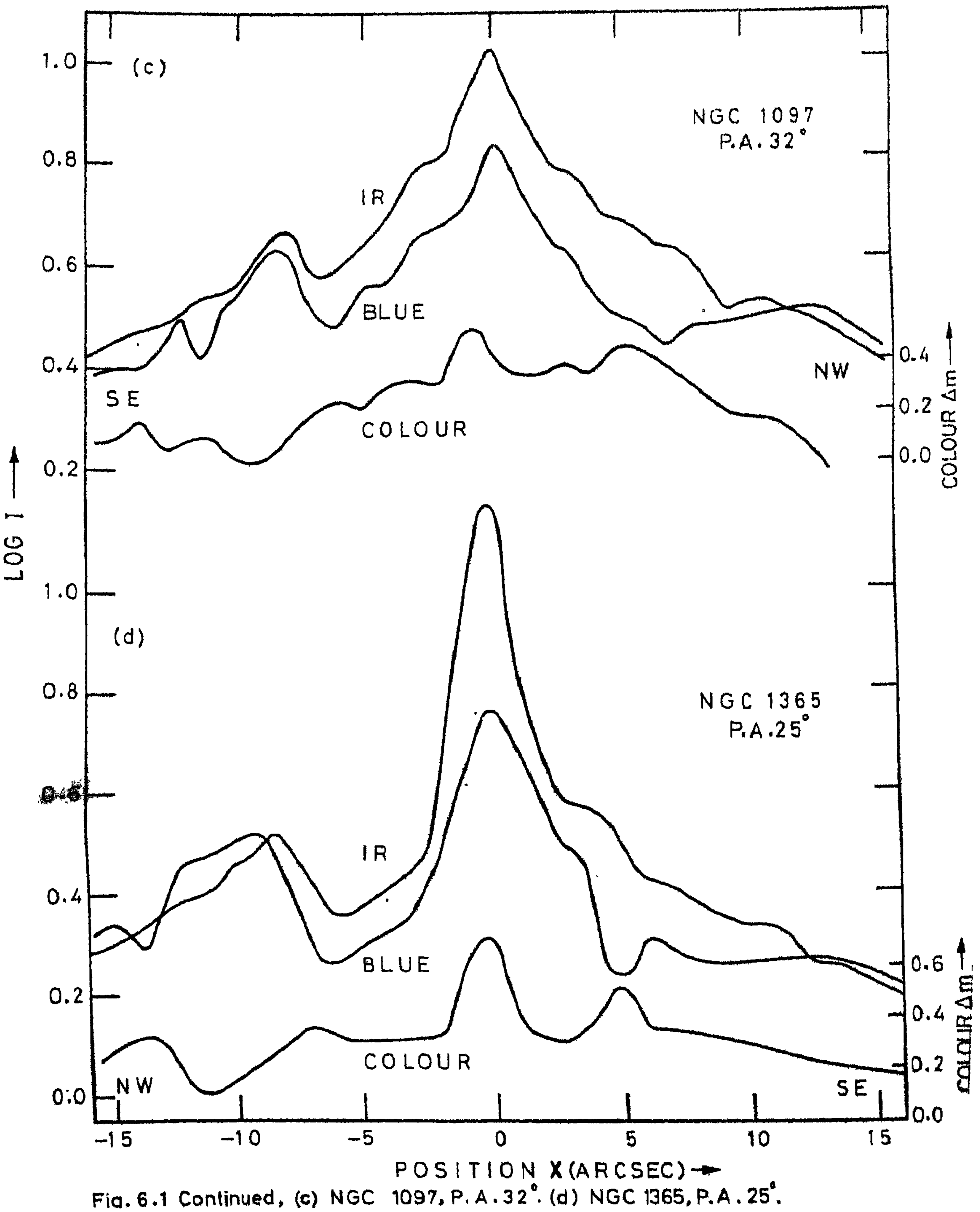

Fig. 6.1 Continued, (c) NGC 1097, P. A. 32°. (d) NGC 1365, P. A. 25°.

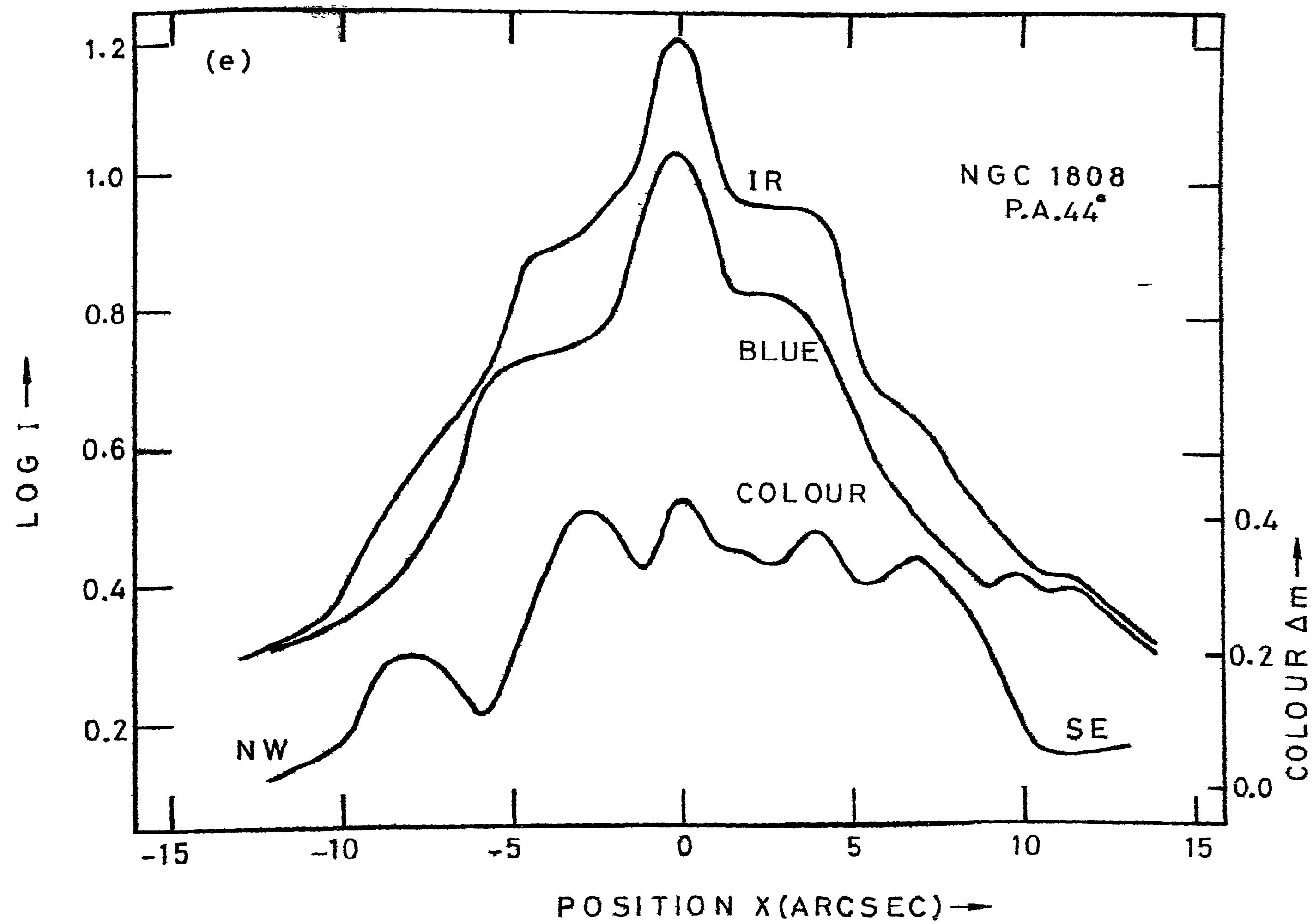

Fig. 6.1 Continued. (e) NGC 1808, P.A.44°

The perinuclear region of NGC 1808 (Figure 6.1e) is the reddest among the galaxies investigated. It is redder by more than $0^m.25$ to $0^m.30$ with individual hot spots appearing still redder. The nucleus is the reddest of all and reaches $0^m.37$ of colour. It is to be noted that large amount of interstellar dust present in this region from the large observed equivalent widths of NaID lines in this region (Burbidge et al 1968). Also, this is the reddest galaxy among the ones presented in Figure 4.7.

The photographs of NGC 2903 were scanned in two directions. The scan in P.A. 82° (Figure 6.1f) passes through the brightest hot spots at $\pm$ 4 arcsec from the nucleus. The second scan in P.A. 145° (Figure 6.1g) passes through two bright hot spots at -8 and +10 arcsecs from the nucleus. The second scan does not pass exactly through the nucleus but its closest approach is about 0.5 second of arc away from it. The nucleus is very red ($0^m.6$) relative to the perinuclear formation and it was this fact that has helped us in identifying it. An interesting feature of NGC 2903 is that there are regions that are much bluer than the average colour. One of these shown in Figure 6.1f is a hot spot at 5 arcsec to the South-east of the nucleus, which is also the brightest in both the blue and the infrared bands. The region

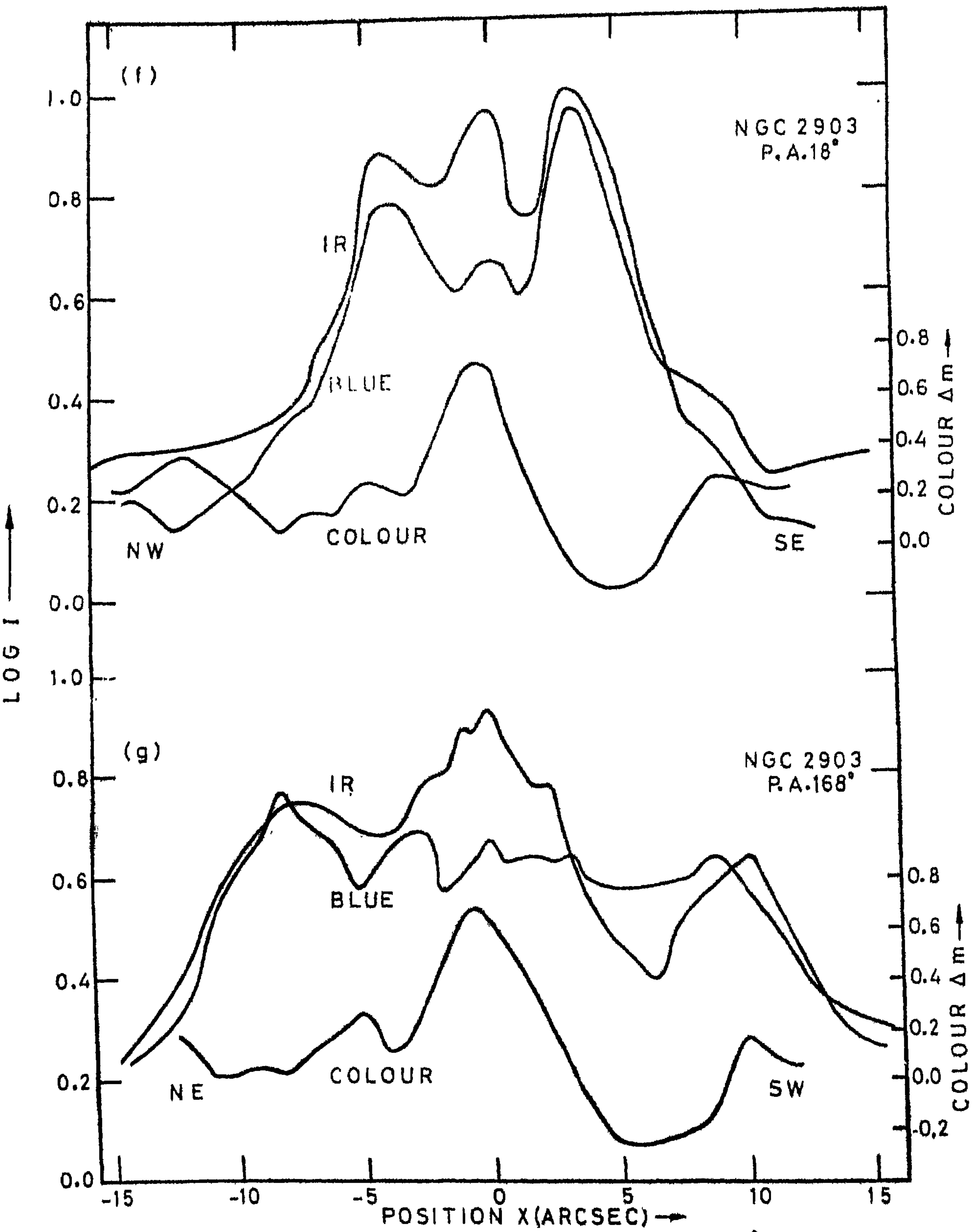

Fig. 6.1 Continued, NGC 2903 (f) P.A.18° and (g) P.A. 168°.

between the hot spot 10 arcsec to the South-West and the complex around the nucleus also appears bluer by $-0^m.3$ with respect to the average value for the peri-nuclear region. The blue hot spot of Figure 6.1f also has the same colour.

In summary, all the five galaxies investigated possess a nucleus redder than the perinuclear formation by $0^m.4$ to $0^m.8$. The latter is neutral with respect to the immediate surroundings in NGC 210, probably a common feature of $\mathcal{E}$ type formations. The hot spot complexes, on the other hand, generally appear red, with very few exceptionally blue. The reddening of the hot spots is most likely due to dust, as evidenced from the other independent observations of NGC 1808 mentioned above. It would be interesting to investigate the nature of reddening in the nuclei of these galaxies. Observations of compact radio sources congruent with several of these nuclei (de Bruyn and Willis, 1974; Van der Kruit, 1971) and definite detection of soft X-rays from NGC 1365 (Ward et al. 1978) are suggestive of mild activity in these nuclei.

6.2 Mean Profiles and the Structure of Perinuclear Formations

The majority of the profiles presented in

Figures 5.28 to 5.32 appear similar to each other and clearly show the systems of the nucleus, perinuclear formation and the main body of the galaxy. Excluding the ℓ type (NGC 3955, 4064 and 7741) formations which have a smaller gradient in luminosity, the gradients of corresponding regions of different galaxies appear similar too. It is instructive to compare the mean profiles of individual classes. It is to be noted that the r* expressed in seconds of arc corresponds to different spatial extent at different distances and hence it is necessary to convert them to constant distance to make the comparison realistic, and to check the possibility that different formations are of comparable spatial scales.

Among the galaxies for which we have obtained the luminosity profiles, only two do not have information on radial velocity. Estimating the distance to the galaxies from the radial velocity values published either in RCBG or by Sandage, 1978, we have converted the equivalent luminosity profiles to r* expressed in parsecs. The change in the luminosity gradient marking the edge of the perinuclear formation occurs between 600 and 2000 parsecs for different galaxies with a mean around one kiloparsec. There is a range of about one magnitude in the surface brightness of the perinuclear formations with respect to the nucleus. The surface brightness of the main body has a range of about 1.5 magnitudes with respect to the nucleus.

Mean profiles were obtained for individual classes (ϵ to τ). NGC 255 was excluded from the class τ , since its behaviour was non-typical of its class. It was seen that the mean profiles of the classes ϵ , $\epsilon\sigma$ and σ are very nearly the same (cf. our reservation about the class $\sigma\tau$ in Chapter 4). Hence a mean was obtained for these classes (ϵ_1). The final average profiles are listed in Table 6.1.

There are systematic differences in the central regions of the three classes of formations. With respect to the nucleus the perinuclear formations of class σ are 0.5 magnitudes fainter than the Class ϵ . The gradient in the luminosity of τ type formations is rather slow with respect to both ϵ and σ . If we assume that the mean surface brightness of the main body of different classes of galaxies is the same, the nuclear region of class σ is $0^m.4$ brighter and the perinuclear region $0^m.1$ fainter than the objects of class ϵ . On the other hand, the formations of type τ have their central brightness $0^m.8$ lower while the

Table 6.1

Mean Equivalent Luminosity Profiles for Different Classes of Perinuclear Formations.

$\log \frac{r^*}{30pc}$	Log I		
	ϵ_I	σ	ι
0.5	.93	.81	.97
0.6	.91	.76	.96
0.7	.89	.72	.96
0.8	.85	.65	.94
0.9	.82	.57	.92
1.0	.77	.52	.88
1.1	.67	.45	.86
1.2	.62	.37	.80
1.3	.51	.30	.75
1.4	.45	.26	.70
1.5	.35	.20	.69
1.7	.22	.09	
1.8	.16	.05	

perinuclear region $0^m.25$ to $0^m.5$ fainter.

The above results for the σ types should be treated with some caution. The spiral patterns generally observed in these formations have the effect of rendering the equivalent radius smaller than a physically meaningful radius like the edge of the spiral pattern. The small difference between the ϵ and σ profiles could possibly arise from this. The low surface brightness formations of class ι , however, possess a very low central concentration.

Central formations of all galaxies investigated, excluding the types ι are relatively compact and King models with the logarithm of ratio of tidal to core radius, $\log \frac{r_t}{r_o} = 0.5$ to 1.25 fit the luminosity profiles well. The perinuclear formations are similar to dwarf ellipticals at least in this aspect. Since our observations do not span a sufficient range of the main body of the galaxy, an accurate subtraction of this component was not possible. An attempt with NGC 210 gave a best fit of $\log \frac{r_t}{r_c} = 1.00$, $\log r_c = .30$ and $\log f_o = .85$ after a model of the main body with $\log \frac{r_t}{r_c} = 2.25$, $\log r_o = 0.80$ and $\log f_o = -0.70$ was subtracted. Similarly NGC 255 fitted well with a King model of $\log \frac{r_t}{r_c} = 1.00$, $\log r_c = 0.40$ and $\log f_o = 1.00$ after an exponential log I = 0.25 - 0.01315 r* was subtracted.

It may be suspected that the ℓ type formations also possess a nucleus which could be too faint to be detected. Excluding this class, all the other galaxies presented here possess a bright and very red starlike or semi-starlike nucleus and a compact perinuclear formation resembling the dwarf ellipticals in structure.

CHAPTER 7

SLITLESS SPECTROSCOPY OF GALAXIES WITH HOT SPOTS

The multiplex aspect of the photographic plate is generally reduced to a single dimension when one obtains slit spectra of emission line regions. This is especially so when the velocity dispersion or variations within the region of the object passing through the slit is lower than the resolution employed. Two dimensional aspects of emission regions can be obtained by procedures known to solar physicists for over a century. We widen the slit sufficiently to allow only the region of interest with the required degree of spectral purity and thus minimuze the interference from the continuum sources. We describe in the following one such aspect of spectroscopy with a wide slit applied to the investigation of galaxies with hot spots.

7.1 Estimation of the Velocity Field in Galaxies Employing slitless spectral image.

A spectroscopic image of a galaxy in a particular emission line is a mapped version of the monochromatic image of the galaxy in the same line. If the x-axis is chosen along the direction of dispersion, the monochromatic intensity at a position (x, y) is mapped to a position $(x + \Delta X, y)$ where Δx is given by

$$\Delta x = \beta V(x, y) \tag{7.1}$$

Here, V (x, y) is the line of sight component of the velocity at the position (x, y) and β is a constant of the spectrograph. If x is expressed in terms of seconds of arc on the sky plane, we have

$$\beta = \frac{\lambda_0}{cD} s \tag{7.2}$$

where λ_0 is the rest wavelength of the spectral line, c the velocity of light, D the reciprocal dispersion in the spectrograph and s the image scale on the plate.

We will examine a slitless spėctral image in the following, with the assumption that the velocity field consists only of rotation.

The mapping given by eq. (7.1) will have one-to-one correspondence only when

$$\frac{\Delta V}{\Delta x} \neq -\frac{1}{\beta} \tag{7.3}$$

for any two points with the same y coordinates a difference Δx in the x coordinate and a difference ΔV in the line of sight component of the rotation velocity. Since the right hand side of eq. (7.3) depends only on the spectrograph used and the negative sign puts a restriction on the direction of dispersion, it is always possible to choose a proper arrangement to assure the one-to-one correspondence.

Typically, the rotation curves of galaxies rise to a maximum from zero at the centre and then decline beyond the turnoff point. When the direction of dispersion is such that the line of nodes passes through the first quadrant, the slope $\Delta V/\Delta x$ becomes negative for the region beyond the turn-off point; when the line of nodes falls in the second quadrant, it becomes negative for the region before the turnoff point. In either case, there is only small range in β which may not fulfill the condition (7.3) for a particular rotation curve.

Thus, if one obtains a monochromatic image of a galaxy in an emission line and a slitless spectral image in the same line, it is possible to map the velocity field in the most general situation. We will examine the potentiality of the method in the next section and illustrate with preliminary results on a specific example in section 7.3.

7.2 Distortion of a slitless spectral image by the Circular rotation field in a galaxy

With the assumption that the galaxies are single inclined planes, one writes the observed velocity field as

$$V_{obs} = V_{sys} + V_{\theta} \sin i \cos\theta + V_R \sin i \sin\theta \tag{7.4}$$

Here, V_{obs} is the observed line of sight component of velocity at a point (R, θ) in the plane of the galaxy, V_{sys} the systemic radial velocity of the galaxy, V_{θ} and V_R the azimuthal and the radial components of the velocity field at the position (R, θ). The angle i is the inclination of the normal to the galaxy plane with the line of sight.

We will assume that non-circular motions are absent and write

$$V_{\theta} = \Omega R \;; \quad V_R = 0 \tag{7.5}$$

where Ω is the rotation velocity at the point R. The transformation from the plane of the galaxy (R, θ)

to the plane of the sky (r, ϕ) is given by

$$R\cos\theta = r\cos(\phi - \phi_0) \tag{7.6}$$

where ϕ_0 is the position angle of the line of nodes. Substituting equations (7.5) and (7.6) in (7.4) one obtains

$$\Delta V \equiv V_{obs} - V_{sys} = \Omega r\cos(\phi - \phi_0)\sin i \tag{7.7}$$

We define the x-axis on the slitless spectrum of the galaxy in the direction of dispersion and measure all position angles from this direction. With the y-axis at right angles to the x-axis in a right handed system, we may transform equation (7.7) to

$$\Delta V = \Omega\sin i\,(x\cos\phi_0 + y\sin\phi_0) \tag{7.8}$$

While the systemic velocity shifts the centre of the image in the direction of dispersion, ΔV distorts the image by transforming each position (x, y) to a new position (x, y) given by the transformations

$$x' = x + \Omega\beta \sin i\,(x\cos\phi_0 + y\sin\phi_0)$$
$$y' = y \qquad (7.9)$$

where β is the constant of the spectrograph given by equation (7.2). Since this mapping is one-to-one in general, one can easily establish correspondence between a monochromatic image and a spectral image to effect estimation of the velocity field. The values of Ω Sin i and ϕ_0 can be obtained as a function of the radial distance from the centre of the galaxy.

Since under the transformations (7.9) an equal intensity contour transforms into another, it is instructive to see how an area transforms with these equations. The transformation is actually an affine geometric one as it can be split into a shear,

$$x_1 = x + (\Omega\beta \sin i \sin\phi_0)y \qquad (7.10)$$

and a compression

$$x' = x_1 + (\Omega\beta \sin i \cos\phi_0)x \qquad (7.11)$$

with the ordinates unchanged. An area transforms into itself under shear while the compression changes it according to the equation

$$A' = A\,(1+\Omega\beta \sin i \cos\phi_0) \qquad (7.12)$$

(cf. Modenov and Parkhomenko, 1965), where A and A′ are the original and the transformed areas. Defining the equivalent radius r* by

$$r^* = (A/\pi)^{\frac{1}{2}} \qquad (7.13)$$

we have the relation

$$r^*_{sp} = r^*_{pg}\,(1+\Omega\beta \sin i \cos\phi_0)^{\frac{1}{2}} \qquad (7.14)$$

between the equivalent radii of the monochromatic image (r^*_{pg}) and that of the slitless spectrum (r^*_{sp}). A comparison of the two yields $\Omega \sin i \cos\phi_0$. This relation provides an easy method of obtaining the velocity field averaged over the length of a contour. However, ϕ_0 will have to be estimated independently.

FIG. 7.3 NGC 5236

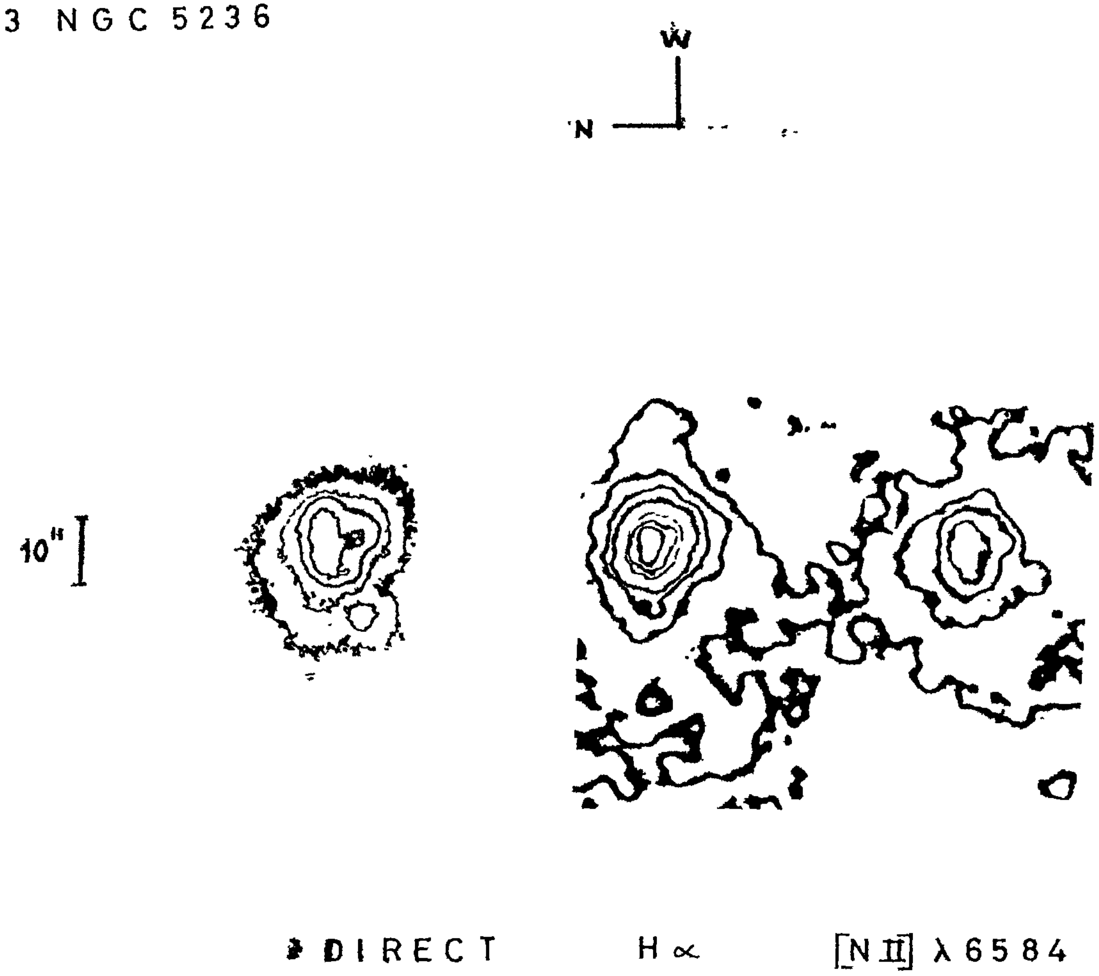

7.3 The Rotation of the Perinuclear Formation of NGC 5236

We have obtained the slitless spectral images of NGC 5236 in the emission lines of H_α and [NII] λ 6584. The spectrogram was obtained at a dispersion of 30Å mm^{-1} with the spectrograph described in Section 3.6. The slit was widened to let in only the image of the perinuclear formation and not the light from the main body of the galaxy.

The equal intensity contours presented in Figure 7.1(a) bear a striking resemblance to the contours obtained from the picture in the integrated light (Figure 5.26). The contours are reproduced in Figure 7.1 (b) to facilitate comparison.

The equivalent luminosity profiles of the images in H_α and in [NII] λ 6584 are shown in Figure 7.2. A photograph in the light of these lines and another in adjacent continuum are required for an estimation of the monochromatic luminosity distribution of the formation. These observations are planned for the future, and we will use the picture in the integrated light for the present to demonstrate the method.

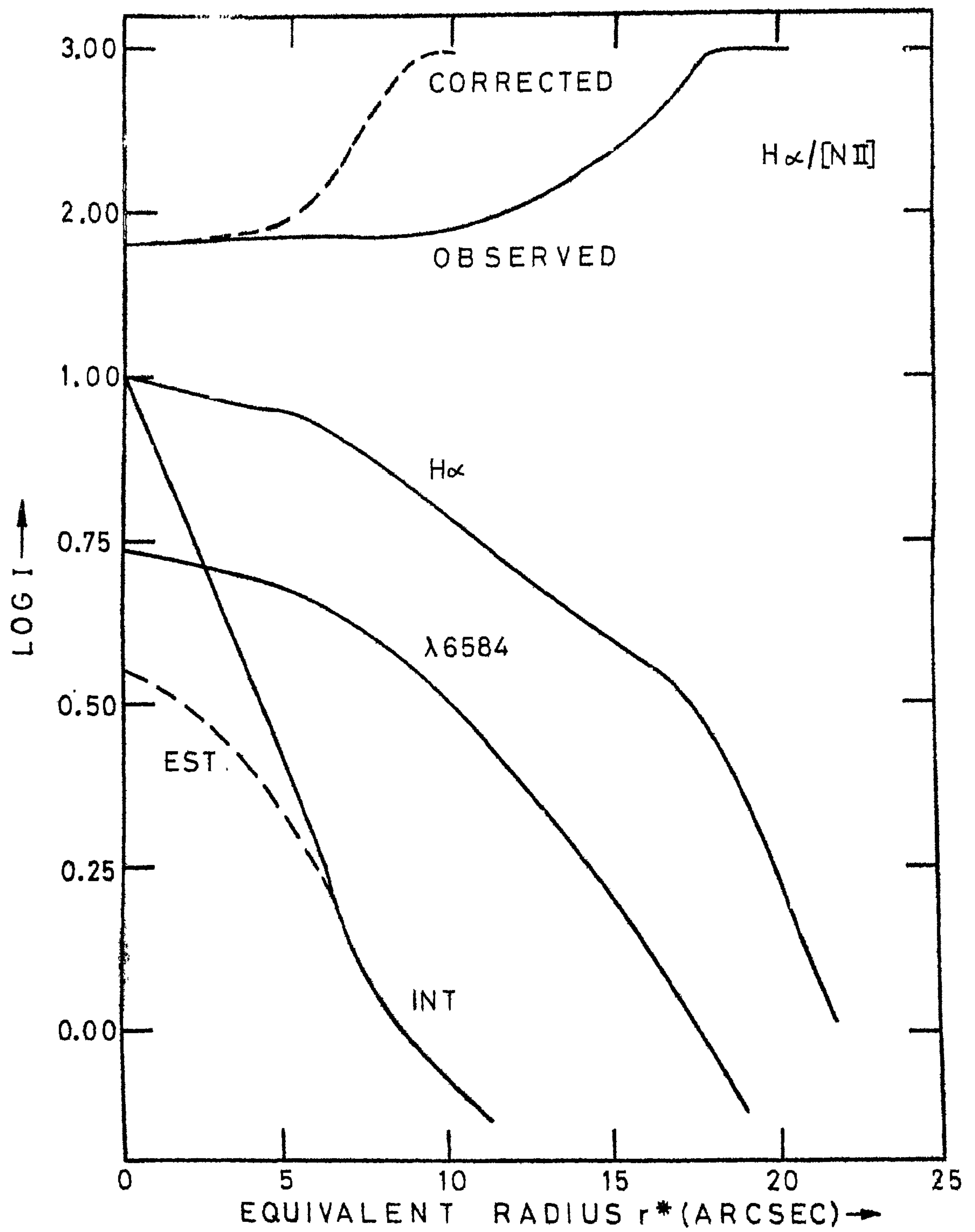

Fig. 7.1 Equivalent luminosity profiles of Hα and [N II] dispersed images of NGC 5236. Also shown are the profile in the intergrated light (INT) and the estimated profile (EST) of the undispersed monochromatic image in Hα and [N II]. Observed ratio of Hα and [N II] intensities are shown at the top, and also corrected for the distortion due to the velocity field.

The equivalent luminosity profile of the relevant region of the galaxy is also shown in Figure 7.2. The image in the integrated light is dominated by the nuclear region of high luminosity in the red. There is no evidence of such a structure in the profile of H_α. Subtracting an estimated profile of the nuclear regi from the observed profile in the integrated light we derive an approximate profile expected for the monochromatic picture in the emission lines of H_α and [NII] We were guided in this by the change of slope at a radius of $r^* = 6.5$ arcsec (Figure 7.2).

Assuming that the dynamical centre is congruent with the maximum in intensity we normalize the profiles of H_α, [NII] and the expected monochromatic one to a central intensity of 1.00. These are plotted in Figure 7.3(a) on a logarithmic scale of r^*. The difference between the abscissae of the expected monochromatic profile and the mean of the H_α and [NII] profiles gives the value of

$$\alpha \equiv \frac{1}{2}\log(1+\Omega\beta\sin i\cos\phi_0) \qquad (7.15)$$

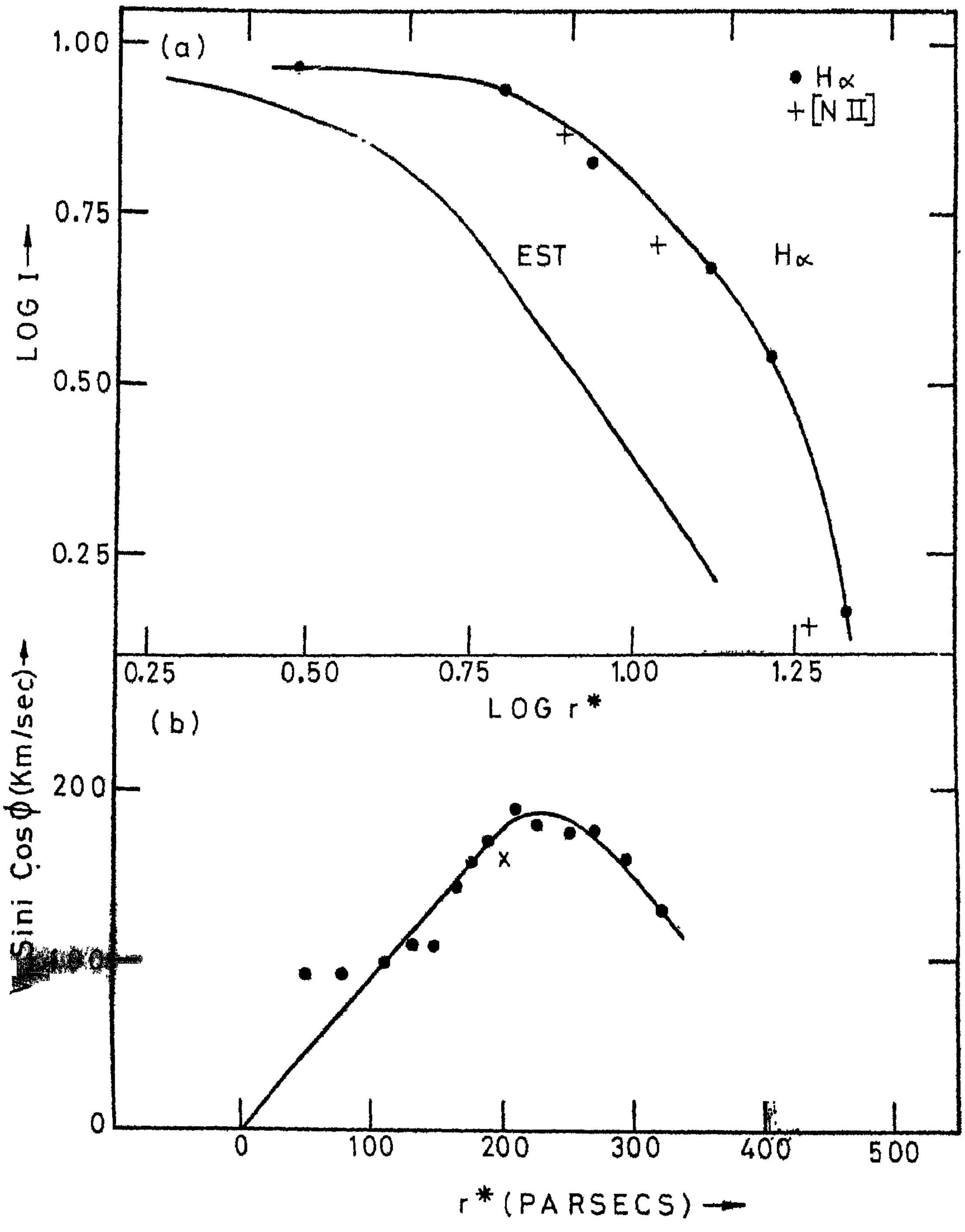

Fig.7.3 (a) The equivalent luminosity profiles of Fig. 7.2 drawn on logarithmic scale r*. (b) The rotation curve for the central region of NGC 5236 obtained as explained in the text. The cross denotes the value obtained by direct comparison of second isophote of [N II] and the direct picture.

from which $\Omega \sin i \cos\phi_0$ can be derived.

A dispersion of 30Å mm^{-1} at H_α and a scale of 200 arcsec mm^{-1} in the direction of dispersion yield a value of 6.9 kms^{-1} $arcsec^{-1}$ for β^{-1}. We adopt a distance of 5.5 Mpc for NGC 5236 based on the velocity of 275 kms^{-1} obtained by the measurement of the centres of H_α and [NII] λ 6584 lines on the spectrogram discussed (H_0 = 50 kms^{-1} Mpc^{-1}). The above value of β^{-1} then corresponds to 251 kms^{-1} kpc^{-1}. Using this value of β^{-1} we have obtained the rotation velocities as a function of the equivalent radius r*. The curve has been plotted in Figure 7.3(b), where the ordinates correspond to $\Omega r^* \sin i \cos\phi_0$. The equivalent radius r* requires a scaling factor for conversion to a physically significant distance in the plane of the galaxy. For elliptical contours due to inclined discs this factor is simply $(\cos i)^{-\frac{1}{2}}$.

We note that the second contour from the centre of λ 6584 resembles the second contour from the centre of the picture in the integrated light. Both the contours are bounded by the lines y = $\pm$ 6 arcsec. Hence, they correspond to each other. The ratio of the equivalent radii of these two contours gives r^*_{sp}/r^*_{pg} = 2.05 which corresponds to $\Omega r^* \sin i \cos\phi_0$ = 119 km/s at

$r^* = 149$ pc. This value agrees well with the curve in Figure 7.3(b).

The value of ϕ_o can be estimated easily due to the fortuitious coincidence of a hot spot 10" South-East of the centre with the y axis in the spectrum. Thus $x' = 0$ in equation (7.9), and one obtains,

$$x(1+\cos\phi_o) + y\sin\phi_o = 0$$

or

$$\tan\frac{\phi_o}{2} = -\frac{x}{y}$$

Taking into account the anamorphic reduction factor 3.35 (cf. Section 3.6) in the x direction, we obtain $\phi_o = 20°$.

The inclination i can be estimated to be 27° from the axial ratio of 1.22 tabulated in RCBG. With these values one may estimate the mass M of the perinuclear formation using the equation

$$M = \frac{aV_{max}^2}{G\alpha}$$

where a is the semi-major axis of the formation, α is a constant dependent on the true axial ratio c/a, and G the constant of gravitation. For c/a = 0.5, a = 1.418 (Burbidge et al 1964). Using a = 360 pc corresponding to r* = 240 pc and iclination $i = 27°$, we obtain a mass of $1.0 \times 10^{10}\ M_{\odot}$ for the central region of NGC 5236. This value is comparable to the mass estimates of similar formations in NGC 613, 1808 and 2903 (e.g. cf. Burbidge et al 1964).

Finally, we may calculate the ratio of $H\alpha$ / [NII] λ 6584 as a function of equivalent radius. The values so obtained are plotted against the equivalent radius corrected for the distortion due to velocity field in Figure 7.2. It is interesting to note that the ratio stays constant at a value of 1.75 for r* $\lesssim$ 5 arcsec and rises beyond to assume a value of $\sim$ 3 beyond r* = 8 arcsec. This variation agrees with the variation of $H\alpha$ /[NII] in other spiral galaxies. Burbidge and Burbidge (1962) have shown that the ratio is constant at $\sim$3 in the outer regions of a wide range of galaxies while it reaches a value of $\sim$ 1 or even $<$1 in the nuclei of several galaxies.

CHAPTER 8

CONCLUSIONS AND FUTURE PROSPECTS

The foregoing investigations show that the central regions of some spiral galaxies contain two bright substructures: (a) a starlike or semistarlike nucleus, and (b) a perinuclear formation. The galaxies listed by Sersic (1973) belong to this class of objects with possible exceptions, or transition cases of a few grouped as class ι by us (Chapter 5). While Sersic's finding lists (Sersic and Pastoriza 1965, 1967; Sersic, 1973) include sixtyfour of such galaxies, it may be possible to find an equal number of such galaxies more among bright galaxies (Table 2.2).

The nucleus is, in general, bright and red. In the case of NGC 2903, it is hardly visible in the blue, appears as a faint patch in the red (Oka et al 1974), but appears very bright in the near infrared (Figure 6.1f). Its resolved size is about 80pc x 150pc with possible extensions from the major axis. It is thus only slightly larger (cf. Figure 4.9) than the Sagittarius A complex and the HII arc in the central region of the galaxy.

Its dimensions and reddening compare well with the 60 x 170pc region of 'Super clusters' in the centre of M82 (Van den Bergh, 1971).

Around the nucleus of the galaxies investigated, light formations appear with radii ranging from about 600 parsecs to 2 kiloparsecs. The luminosity profiles of these 'perinuclear formations' indicate that they resemble dwarf ellipticals in their compactness (Section 7.2). At one extreme, the visual appearance is dominated by 'hot spots' or giant HII regions arranged in rudimentary spiral pattern which resembles the outer spiral arms in their orientation and shape (class σ, Chapter 4). From a typical example of NGC 1097 for this class, the appearance varies through less distinct hot spots (e.g. NGC 613, class σ), diffuse elliptical-like formation with emission lines (NGC 1326, Class $\epsilon\sigma$) and finally to distinct elliptical images in the case of galaxies of class ϵ (e.g. NGC 210). The luminosity distribution among these different classes of formations are not significantly different indicating that they all belong to a single class of phenomenon.

The spectroscopic information on the 'hot spots' indicates that they are giant HII regions ionized altogether by more than 10^4 O stars. The continuum energy distribution shows a high contribution from stars of spectral types earlier than F, (Osmer et al. 1974; Pastoriza, 1975). These facts point out that the perinuclear subsystems under consideration have undergone a recent burst in star formation. The statistics of galaxies with such central regions shows that they occur in only about 15% of all the spiral galaxies (Sersic and Pastoriza, 1965) suggesting that such events are only transient events in the life of a typical galaxy. One may envisage a sequence of evolution beginning from the brightest of the type σ to faintest of the types ϵ and then fading out as the stars evolve. The enrichment of heavy elements spans a large range in these formations suggesting possible recurrences of such phenomena. The correlations obtained in Chapter 2, of different classes of formations with different types of the parent galaxies arises probably due to differences in the rate of evolution.

Another spectroscopic aspect of importance is the high ratio of $H\alpha/H\beta$ and strong NaI D lines typically observed. These facts are indicative of high reddening by dust. The extreme example is NGC 1808 with $H\alpha/H\beta \sim 7$ (Osmer et al. 1974) and NaI D equivalent width of 13.2Å (Pastoriza, 1975). The U-B and B-V colours of the central region of NGC 1808 differs from the mean colours of its class of central formations in the direction of reddening in the two colour diagram (cf. the point at U-B = .18 and B-V = .88 in Figure 4.7). Our observations reveal that the central region of NGC 1808 is almost uniformly red throughout, unlike other members of its class. The latter show mainly the nucleus prominently in the colour profiles (Figure 6.1d). All the nuclei observed by us are quite probably reddened by dust. Such a concentration of dust, as also the sporadic fuelling of gas resulting in the transient bursts of star formation raise important questions on the mode of gas transport. The correlation that the bright perinuclear formations are always associated with bright nuclei appears significant.

The situation of the perinuclear formations within the typical radius of the inner Lindblad resonance (ILR) certainly has its dynamical implications. The ovoidal and barlike distortions often seen in the outer contours of the formations are supporting evidences for this fact.

The sporadic bursts of star formation in the central regions of spiral galaxies renders the central parts bright enough for detailed observations to be possible. Thus, the bright perinuclear formations provide an opportunity to examine the gravitational field in the central regions of galaxies. The structural models of ellipsoidal formations of class ϵ need to be constructed taking into account systematic variation of the position angles, ellipticities and centres of equal intensity contours. The abrupt change in the position angle of the formation and that of the main body, observed in NGC 2196 and other members of class $\mathcal{E}$ (Chapter 5) is also an important fact. The triaxial models like the one devised by Stark (1977) for the 'nuclear bulge' of M31, or possibly more complicated ones incorporating ovoidal distortions may need to be examined.

The emission lines from hot spot formations assist in mapping the velocity fields. The lack of importance of the optical thickness, and the relative ease of the measurements renders them especially valuable. The errors involved in positioning the slit need to be minimized, however, for deriving accurate velocity fields. The potential of the spectroscopic technique employing a wide slit (Chapter 7) need to be realized fully in order to achieve the best possible positioning accuracy and to minimize the observing time so as to extend such information to a large number of objects. Methods may be devised for its application to a wider range of situations.

The need for observing the nuclei and the perinuclear formations at a higher resolution, with a large space telescope need hardly be stressed. Apart from the advantages of improving the accuracy of the data, it would assist also in bridging the gap between the two extreme cases of nuclear activity as the centre of our galaxy and the nuclei of radio galaxies and quasars.

The interest in the central structures of the galaxies examined by us is certainly manifold. Apart from an interest in their own right, they would contribute much to our understanding of the central regions of galaxies that exhibit a much wider range of activity.

REFERENCES

Ambartsumian, V.A.	1958	Solvay Conf. Structure and Evolution of the Universe, R. Stoops (Editor), Brussels, p. 241
Ambartsumian, V.A.	1960	Q.J.R. astr. Soc. 1, 152
Ambartsumian, V.A.	1961	Proc. 11th Gen. Assem. Berkeley, Trans. IAU, 11B, 145.
Ambartsumian, V.A.	1965	The Structure and Evolution of Galaxies, Proc. 13th Conf. Phys., Univ. Brussels, Wiley-Interscience (1965), p. 1-12.
Ambartsumian, V.A.	1971	Nuclei of Galaxies, D.J.K. O'Connell (Editor). North-Holland Publ. Co., Amsterdam, p.9.
Ambartsumian, V.A.	1976	Stars and Galaxies from Observational Points of View Proc. 3rd European Astron. Meeting. Toilisi, p. 91
Arp, H.	1976	Astrophys. J., Lett. 207, L147
Baade, W.	1944	Astrophys. J. 100, 137
Bappu, M.K.V.	1978	Modern Techniques in Astronomical Photography. R.M. West, J.L. Heudier (Editors), Proc. ESO Workshop (1978), p. 263-271
Bappu, M.K.V., Parthasarathy, M., Sivaraman, K.R.	1974	Bull. Astron. Soc. India, 2, 35
Becklin, E.E., and Neugebauer, G.	1968	Astrophys. J. 151, 145

Bergh, S. van den	1960	Publ. David Dunlap Obs. 2, No.6
Bergh, S. van den	1971	Astron. Astrophys. 12, 474
Bohuski, T.J., Burbidge, E.M., Burbidge, G.R. and Smith, M.G.	1972	Astrophys. J. 175, 329
Bruyn, A.G., de., Willis, A.G.	1974	Astron. Astrophys. 33, 351
Burbidge, E.M.	1962	The Distribution and Motion of Interstellar Matter in Galaxies - L.Woltjer (Edr.) W.A. Benjamin, Inc., p. 123
Burbidge, E.M.	1971	Nuclei of Galaxies, D.J.K. O'Connell (Editor), North-Holland Publ. Co., Amsterdam, p. 713-739.
Burbidge, E.M., Burbidge, G.R.	1962	Astrophys. J. 135, 694
Burbidge, E.M., Burnidge, G.R.	1968	Astrophys. J. 151, 99
Byurakan	1975	Scobsch, Byurak. Obs. 47, 43
Curtis, H.D.	1918	Publ. Lic. Obs. 13, 31
Downes, D., Maxwell, A.	1966	Astrophys. J. 146, 653
Ekers, R.D.	1978	Phys. Scr. 17, 171
Freeman, K.C.	1970	Astrophys. J. 160, 811
Freeman, K.C.	1977	Galaxies, L. Martinet, M. Mayor (Editors). Geneva Obs., p. 1.
Heckman, T.M.	1978	Publ. astr. Soc. Pacific, 90, 241
Hollars, D.R., Reitsema, H.J.	1975	Publ. astr. Soc. Pacific, 86, 330

Keel, W.C., Weedman, D.W.	1978	Astr. J. 83, 1
King, I.R.	1966	Astr. J. 71, 64
Kruit, P.C. van der	1971	Astron. Astrophys. 15, 110
Lorre, J.J.	1978	Astrophys. J., Lett. 222, L99
Markarian, B.E., Lipovetskii, V.A., Sepanyan, Dzh. A.	1978	Astrophys. 13, 215
Modenov, P.S., Parkhomenko, A.S.	1965	Geometric Transformations, Vol.I. Academic Press
Morgan, W.W.	1958	Publ. astr. Soc. Pacific 70, 364
Morgan, W.W.	1959	Publ. astr. Soc. Pacific 71, 394
Morgan, W.W., Mayall, N.U.	1957	Publ. astr. Soc. Pacific 69, 291
Morgan, W.W., Walborn, N.R., Tapscott, J.W.	1971	Nuclei of Galaxies. D.J.K. O'Connell (Editor) North-Holland Publ. Co., Amsterdam, p. 27-40, 41-44
Oka, S., Wakamatsu, K., Sakka, K., Nishida, M., Jugaku, J.	1974	Publ. astr. Soc. Japan 26, 289
Oort, J.H.	1977	A Rev. Astr. Astrophys. 15, 295
Oort, J.H., Plaut, L.	1975	Astron. Astrophys. 41, 71
Osmer, P.S., Smith, M.G., Weedman, D.W.	1974	Astrophys. J. 192, 279
Pastoriza, M.G.	1975	Astrophys. Space Sci. 33, 173

Prabhu, T.P.	1978	Kodaikanal Obs. Bull. Ser. A. 2, 105
Sakka, K., Oka, S., Wakamatsu, K.	1973	Publ. astr. Soc. Japan 25, 153
Sandage, A.	1961	The Hubble Atlas of Galaxies Carnegie Inst. Washington, Publ. 618
Sandage, A.	1978	Astr. J. 83, 904
Sersic, J.L.	1968	Astr. J. 73, 892
Sersic, J.L.	1973	Publ. astr. Soc. Pacific 85, 103
Sersic, J.L., Pastoriza, M.	1965	Publ. astr. Soc. Pacific 77, 287
Sersic, J.L., Pastoriza, M.	1967	Publ. astr. Soc. Pacific 79, 152
Seyfert, C.K.	1943	Astrophys. J. 97, 28
Shields, G.A., Wheeler, J.C.	1978	Gen. Relativ. Gravitation 9, 189
Simkin, S.M.	1975	Astrophys. J. 195, 293
Stark, A.A.	1977	Astrophys. J. 213, 368
Tovmassian, H.M., Terzian, Y.	1973	Astrophys. Lett. 15, 97
Tsikoudi, V.	1977	The Univ. of Texas Publ. in Astron. No.10
Vaucouleurs, G.de	1963	Astrophys. J., Suppl. Ser. No.74, 8, 31
Vaucouleurs, G.de	1977	Evolution of Galaxies and Stellar Populations - Eds. Tinsley, B.M., Larson, R.B., Yale University Observatory.

Vaucouleurs, G. de., Vaucouleurs, A. de.	1964	Ref. Catalogue of Bright Galaxies. Univ. of Texas Press, Austin (1964)
Ward, M.J., Wilson, A.J., Penston, M.V., Elvis, M., Maccacaro, T., Tritton, K.P.	1978	Astrophys. J. 223, 788
Wolstencroft, R.D., Zealey, W.J.	1975	Mon. Not. R. astron. Soc. 173, 51
Zwicky, F.	1967	Adv. Astron. Astrophys. 5, 268.

--